A Study on the Design, Manufacture and Performance Evaluation of a 300kW-class Superconducting Induction Heater using the HTS Magnets

チョイ, ジョンゴ

Dissertation for the *Doctor of Engineering*

A Study on the Design, Manufacture and Performance Evaluation of a 300 kW-class Superconducting Induction Heater using HTS Magnets

March 2019

Department of Electrical and Electronic Engineering, Graduate school and Faculty of Information Science and Electrical Engineering, Kyushu University

Choi, Jongho

論文概要

現在の産業界において広く使用されている金属加熱炉には多くの課題がある。まず、現状の大容量金属加熱装置には旧態依然とした加熱法が採用され、入力電力に対しあまりに効率が低い。また、これら金属加熱装置は体格が大きく、広い作業スペースを必要とし、インゴットの装填・排出も手動であり安全性も低い。さらに、これら装置の運転には種々の専門的知識・技術を有する作業者が必要である。韓国では、近年、現状の産業界におけるエネルギー効率の改善と二酸化炭素の排出量削減を目指し、環境保全のために高度な技術の適用を促進する環境保全策が施行され、金属加熱装置の効率改善も喫緊の課題であった。

金屬インゴットを加熱する方式としては、從來、1）ヒータによりインゴットを直接加熱する方式、2）金屬インゴットに交流磁界を印加して渦電流を誘起させ、このジュール發熱により加熱する方式が主流であった。1）の場合の入力電力に對する加溫効率は20－30％であり、2）の場合でも交流磁界の侵入長の制約から効率はせいぜい50-60%であった。本研究では、次のような新方式の誘導加熱裝置を開發し、大幅に効率を向上させることに成功した。まず、金屬インゴットに直流磁界を印加し、金屬インゴットを機械的に回轉させて渦電流を發生させ、このジュール發熱により加熱する。この新方式では、容器、ヒータ、交流コイル等が省略され、加熱される部位が金屬インゴットに限定されることもあり、効率は90%にも向上する。しかし、實現の課題は、1000℃にも達する金屬インゴットの輻射越から超伝導マグネットをいかに低溫に保ち、安定に動作させうるかであった。

本研究で開發した加熱裝置は、C型の鐵心を高溫超伝導マグネットで勵磁し、鐵心の空隙部分に金屬インゴットに裝塡し、外部に配置したモータで機械的に回轉させ、金屬を所望の溫度まで加熱するものである。インゴットの裝塡・排出も自動で行われる。本研究では、まず直流磁界を發生させる電磁石に高溫超伝導線材を用いた超伝導マグネットを採用し、臨界溫度、および動作溫度の向上により、超伝導マグネットの熱的安定性を確保するとともに、さらなる効率向上を図った。また、超伝導線材を無絶緣とし、ターン間に高抵抗であるステンレステープ線を共巻きすることにより、マグネット勵

時時の電流パスを速やかに超伝導線材に沿った正規の電流パスに收束させるとともに、クエンチ時の他のターンへの電流分流を早期に行うことでクエンチ箇所の溫度上昇を抑制し、超伝導マグネットの燒損から保護する事にも成功している。

本論文は、300 kW級の高溫超伝導マグネットを用いた直流誘導加熱裝置の一連の開發研究をまとめたものであり、６章より成る。第1章では、本論文の背景と目的、ならびに概要について述べている。第2章では、直流誘導加熱の有限要素法による數値解析の解析手法を詳細に述べている。第3章では、300 kW級の直流誘導加熱裝置の設計について述べている。アルミニウム鋼材へ300 kWの熱量を与えるべく鐵心付き高溫超伝導マグネットの發生磁界を設定し、架台、荷役システム、およびモータスピンドルを含む裝置の仕様について述べている。また、裝置を用いて様々な金屬鋼材を加熱する際の有限要素法による溫度上昇、溫度分布等の數値解析例にも言及している。第4章では、高溫超伝導誘導加熱裝置の部品とその製造工程を紹介し、實際の加熱工程について述べている。第5章では、試作機によるアルミニウムとステンレス鋼材の加熱試驗による性能評価結果を示している。さらに、數値解析をより詳細に行い、加熱手法の改善策の提案も行っている。第6章では、本論文で得られた成果を總括するとともに、今後の課題について述べている。

ABSTRACT

In industries, there are many issues against the implementation of conventional hearting furnaces. Firstly, the current metal-hearting-furnaces with large capacity adopt an old-fashioned heating method, which is very inefficient against input power. These heating furnaces are large in size, which require a large work space. The furnaces have low-safety because ingots are loaded and discharged manually. In addition, engineers with various skills are required to operate the furnaces. In Korea, in recent years, the government executed an environmental protection policy in order to improve energy efficiency and reduce CO2 emissions. Therefore, improvement in the efficiency of the metal heating furnaces is an urgent task.

Conventional metal hearting methods are: (1) directly heating an ingot by a heater, (2) inducing an eddy current by apply an alternating magnetic field to an ingot and hearting by the Joule heart. In the case of (1), heating efficiency for input power is 20-30%. In the case of (2), heating efficiency is 50-60% due to the restriction of penetration length. In this study, we developed new type of induction heater furnace as below and succeeded in greatly improving the efficiency. A DC magnetic field is applied to a metal ingot and the metal ingot is mechanically rotated to generate an eddy current. In this new method, container, heater, AC coil are omitted and only the metal ingot is heated. In the result, efficiency improves to 90%. However, the realization challenge was how to keep the superconducting magnet at low temperature and operate stably from the radiation ingress of the metal ingot reaching 1000℃.

The heating device has a C-shaped iron core which is excited with a high-temperature superconducting magnet. The metal ingot is loaded in the gap portion of the iron core and mechanically rotated by a motor. Loading and discharging of ingots is also done automatically. The superconducting magnet using a high-temperature superconducting wire is adopted for generating a DC magnetic field. By improving the critical temperature and operating temperature, the thermal stability of the superconducting magnet was secured and further

efficiency improvement was attempted. By making the superconducting wire with no-insulation and co-winding a high resistance stainless steel tape wire, the current path at the time of magnet excitation is promptly converged to the correct current path along the superconducting wire. This method suppresses the temperature rise at the quenching part by performing the current diversion to the other turns at the early stage during quench.

This the doctoral dissertation is a series of development studies of 300 kW-class DC induction heating equipment using high-temperature superconducting magnets and consists of 6 chapters. In chapter 1, the background, purpose and the outline of this paper were explained. In chapter 2, the numerical analysis method for DC induction heating by the finite element method is described in detail. In chapter 3, the design of 300 kW-class DC induction heater device is described. The magnetic field generated by the high-temperature superconducting magnet with iron core was set so as to give a heat quantity of 300 kW to the aluminum billet. The specifications of the supporting stand, the loading/unloading system, and the motor spindle are described. Numerical analysis examples of temperature rise, temperature distribution, etc. by the finite element method when heating various metal billet using this equipment are also explained. In chapter 4, parts of the high-temperature superconductive induction heating device and its manufacturing process and the actual heating process are introduced. In chapter 5, performance evaluation results by heating test of aluminum and stainless steel billet by prototype machine are shown. In addition, numerical analysis is carried out in more detail, and proposals for improvement of heating method are also being made. In chapter 6, the results obtained in this paper are summarized and discuss future issues.

CONTENTS

CHAPTERS

LIST OF FIGURES

LIST OF TABLES

CHAPTER 1

INTRODUCTION

1.1 Industrial demands of the development on a Superconducting induction heater (SIH)

In industries, there are many issues against the implementation of conventional heaters. First, the government recently executed an environmental protection policy that requires industries to use better technologies against low efficiency and CO_2 emissions, etc. Second, industries use old and inefficient technologies for heating metals with large capacity and low efficiency. Also, the work space is sometimes large, dirty, dangerous, and dull. Finally, engineers with various skills are required to operate advanced heating furnaces.

Induction heating provides fast, efficient, contact-less heating of conductive materials. Due to its advantages over classical heating techniques, such as flame or resistance heating in traditional ovens or furnaces as shown in Fig. 1.1(a), it is becoming one of the preferred heating technologies in industrial [1], domestic [2], medical [3], and other applications in Fig. 1.1(b).

(a)

(b)

Fig. 1.1 (a) Traditional oven for forging process; (b) Induction heater for heating long metal billets; (c) Gas or electric furnaces for hot rooling of steel plates (photos by google image)

Induction heating technology is utilized with processing units in industrial fields such as induction hardening, preheating, soldering, and melting. These are available for the preheating processing of metal billets to produce parts for airplanes, automobiles, and electric power machinery.

(a)

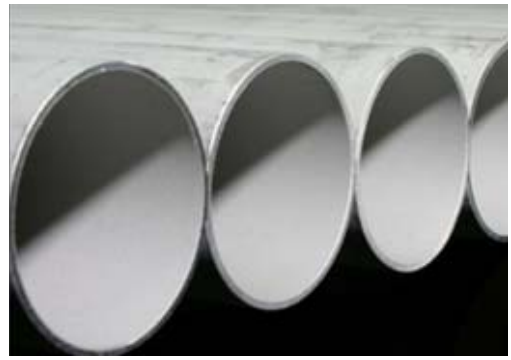

(b)

Fig. 1.2 (a) Extrusion process for stainless steel pipes and tubes; (b) An example of extrusion parts, pipes and tubes for plants (photos from SeAH CSS homepage;www.seahss.co.kr)

As shown in Fig. 1.2 (a) and (b), the stainless steel (STS) extrusion companies produce the STS seamless tube and pipes to endure a high temperature and pressure for thermal and nuclear plants. The STS billets are heated up to 1300 Celsius degree for the extrusion by using induction heaters. Also, the other extrusion companies are producing copper or brass tubes and pipes for heat exchangers or water supply system or cooling water circulation system as shown in Fig. 1.3.

Fig. 1.3 An example of extrusion parts, copper tube for a heat exchanger (photos from google images)

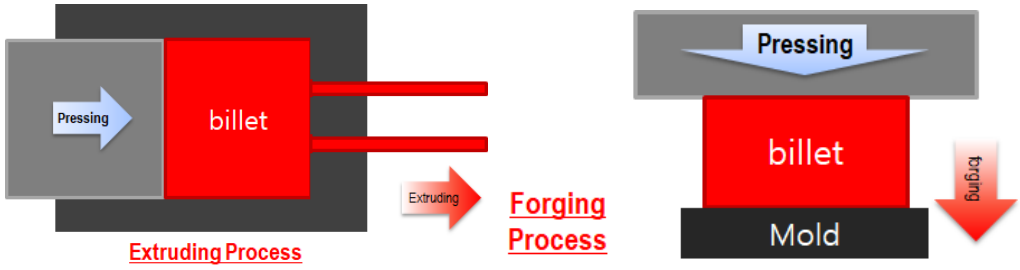

(a) (b)

Fig. 1.4 There are two process for production parts such as automobiles, airplanes and ships etc, (a) extrusion process; (b) forging process

In the metal industries, they use AC induction heater with copper coils in Fig. 1.5(a) to preheat Titanium and stainless steel as well as copper billets in extrusion and forging process which describe in Fig 1.4(a) and (b),

respectively. These metals are indirectly heating up to almost melting temperature. In addition, an electric furnace with heat elements in Fig. 1.6 as well as a gas furnace with burners in Fig. 1.5(b) are mainly used to preheat carbon steels in forging and heat treatment industries. Steel is directly or indirectly heated up to the specific temperatures by process in the atmosphere. It requires huge energy consumption, continuously.

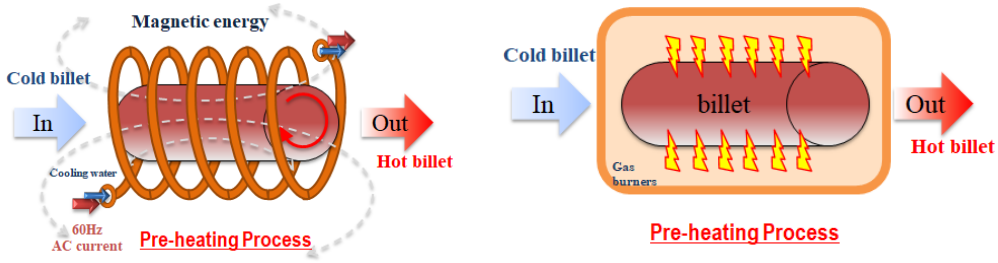

(a) (b)

Fig. 1.5 Two types of heating process mainly are for heating aluminium, (a) induction heater; (b) gas burner

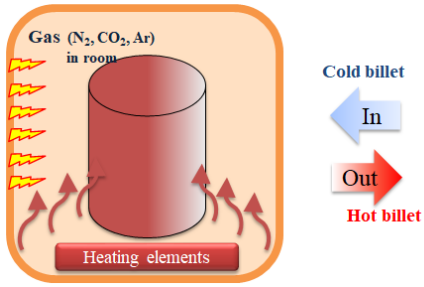

Fig. 1.6 Gas furnace and electric furnace for heating steel and titanium metals

1.2 Operational characteristic analysis among the industrial furnaces including a SIH

Large-scale induction furnaces for non-ferrous metal billets operating at a power net frequency have an energy efficiency of only 50–60% owing to the energy loss caused by the copper coils used to generate the magnetic fields [4-6]. The efficiency improvement of these induction furnaces have been

hampered by physical limits [7-10]. A novel DC induction heating method using high temperature superconducting (HTS) magnets has been suggested as a method for achieving higher energy efficiency [11-20]. The author called it as the superconducting induction heater (SIH).

a SIH is a preheating machine for the extrusion and forging processes. An SIH is applicable to heat all the current conducting materials including nonferrous metals and ferrous metals, such as aluminum, copper and brass, magnesium, titanium alloys, stainless steel and ferrous carbon steel. A magnetic field is generated by the superconducting magnet as shown in Fig. 1.7. An SIH is available to get best product quality after the extrusion and forging process.

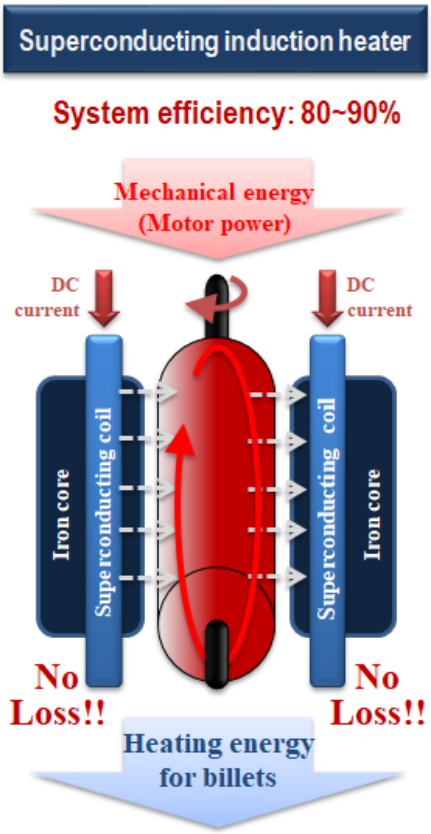

Fig. 1.7 A conceptual diagram of a SIH for heating various metal billet

1.2.1 The efficiency characteristics of the industrial furnaces

The industrial furnaces has individual efficiency characteristics. First, an atmosphere furnace has poor energy efficiency for heating metals as shown in Fig. 1.8. Only 20 ~ 40% heating power of the total input power uses to heat the metal. The rest of the energy is radiative and conductive and convective losses including rail loss. Second, a conventional induction heater has 50 ~ 60% system efficiency as shown in Fig. 1.9. The most energy loss is a copper loss to excite coils. To decrease the temperature of the copper coil, the water cooling system was equipped, necessarily. And the other are transformers, power control and measurement system, and utilities losses.

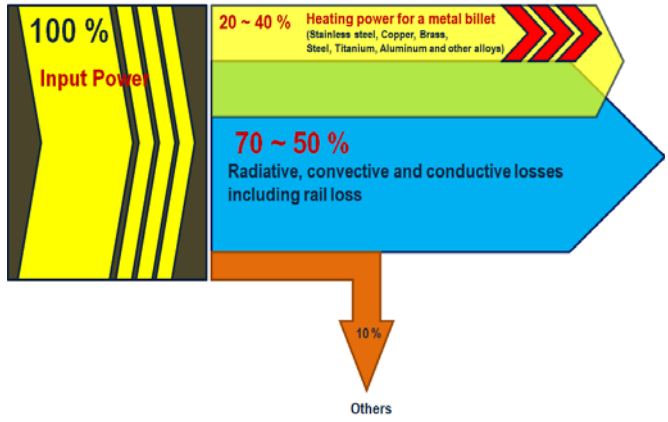

Fig. 1.8 An efficiency characteristic of an atmosphere furnace

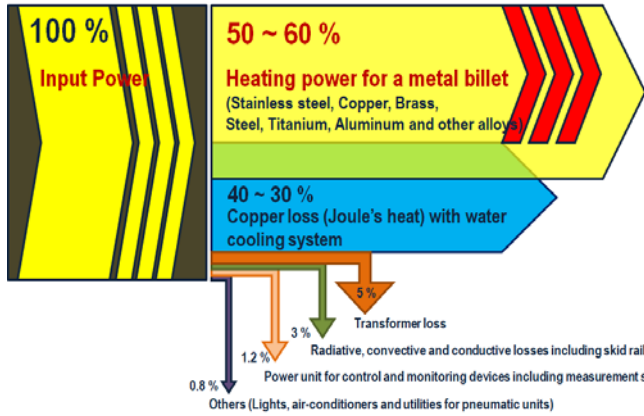

Fig. 1.9 An efficiency characteristic of a conventional induction heater (Low frequency; 50~60Hz)

A SIH leads to an energy efficiency of approximately 80–90% in a large capacity heating system as depicted in Fig. 1.10 [21-26]. No copper loss exists in superconducting magnets to generate magnetic field. The most of the total loss are the induction motor and inveter operation losses including a power source for operating cryogenic cooling system with chiller.

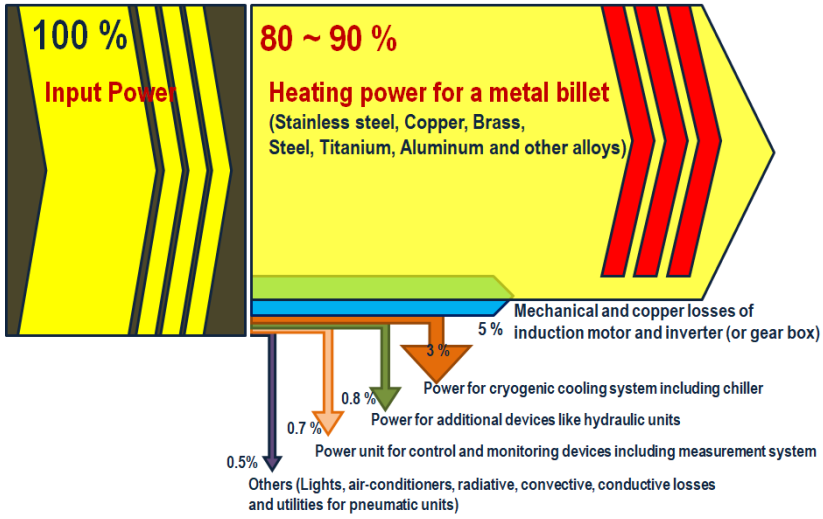

Fig. 1.10 An efficiency characteristic of a SIH

In the efficiency characteristics analysis as summarized in Fig. 1.11, the atmosphere furnace should supply input power to almost 5 times and the AC induction heater should supply input power to almost 2 times, if the heating power for a metal billet up to the target temperature without any loss is 100%. However, a SIH should supply input power to 1.1 times and it could save 389% of the input power of the atmosphere furnace.

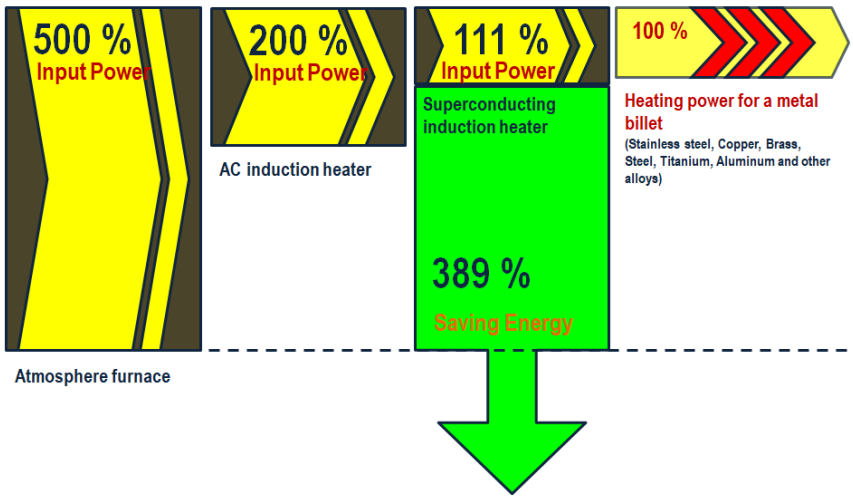

Fig. 1.11 A comparison of efficiency characteristics among three types of heating furnaces

1.2.2 The heating quality characteristics of a SIH

The uniformity of the temperature between the metal billet's surface and center in an extrusion and forging products is a very important factor to improve product quality. The temperature deviation of the metal billet during heating process is dependent on the frequency and resistivity and permeability of the metal. Metals have a different relative resistivity and it's a metal nature characteristic. The frequency in a SIH was controlled by rotating speed. A copper and aluminum with low resistivity are thinner penetration depth, but stainless and Titanium with high resistivity are thicker penetration depth, when the rotational speed is the same.

We can calculate the penetration depth of the metal billet using the rotating speed for a given resistivity, angular frequency, and permeability. The penetration depth in the rotating billet can be calculated as given in the equation (1.1):

$$\delta = \sqrt{\frac{2\rho}{\omega\mu}} \tag{1.1}$$

ρ: *Resistivity*
ω: Angular frequency
μ: permeability

The penetration depth is related to the quality of the metal billet with temperature distribution. The deviation between the inner and outer temperatures of the billet should be below 2 K in the forging and extrusion process.

As depicted in Table 1.1, the penetration depths of various metal billet were calculated according to the frequency. The penetration depths of a copper and aluminum billets at the frequency of 60 Hz are 11.8 mm and 14.5 mm, respectively. The penetration depths of a STS and titanium billets are 65 mm and 93 mm, respectively. In the case of low rotational speed, 600 rpm, the penetration depths of the aluminum and STS billets are calculated to 35.6 mm and 159.2 mm, respectively. Actually, the STS billet has lower thermal conductivity than that of the aluminium billet and the temperature deviation between the center and surface of the STS billet is bigger than that of the aluminum billet. To improve the heating quality, the metal billets with low thermal conductivity such as a STS and titanium and brass billet heats up at a low rotational speed [27-30].

There are 2-dimensional temperature distribution of the metal billets with different rotational speeds and magnetization characteristics as shown in Fig. 1.12. In the case of the same rotational speed of 3,600 rpm, the metal billet with magnetization characteristic has very low penetration depth.

Table 1.1 The penetration depths of various metal billets according to the frequency or rotational speed

Metal types	Freq. [Hz(rpm)]	Penetration Depth (mm)
Copper	60 (3,600)	11.8
	20 (1,200)	16.7
	10 (600)	28.9
	5 (300)	40.9
Aluminum	60	14.5
	20	25.2
	10	35.6
	5	50.3
Stainless steel	60	65
	10	159.2
Titanium	60	93
	10	227
	5	322

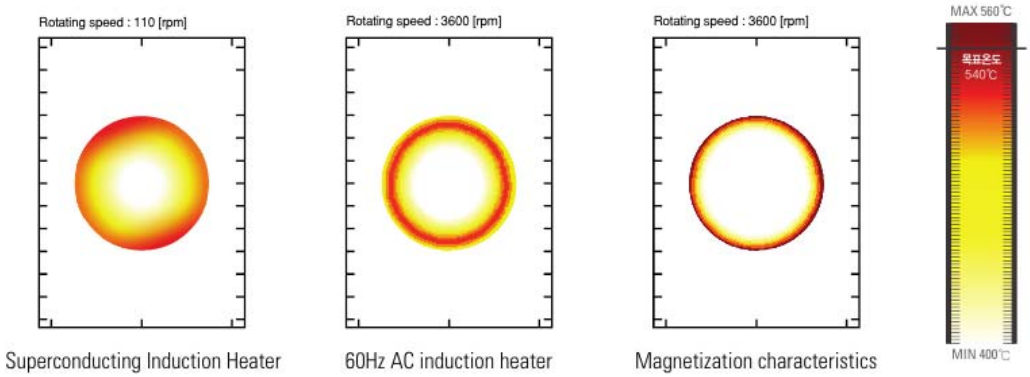

Fig. 1.12 2-dimensional temperature distribution by the frequency and magnetization characteristic in the surface of the metal billet in simulation results

As shown in Fig. 1.13, 3-dimensional temperature distributions of the aluminum billets with three different rotational speeds were analyzed. The temperature deviation of the aluminum billet heated at 5 Hz is lower value than that of the 60 Hz.

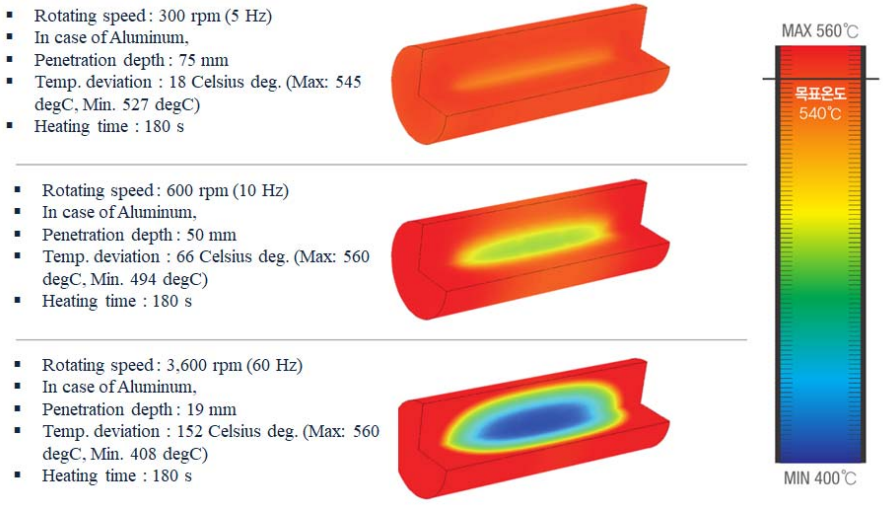

Fig. 1.13 3-dimensional temperature distribution by three different frequencies of the aluminum billet

1.2.3 The product quality improvement of a SIH

The extrusion plant for the aluminum billet requires the temperature control system along the longitudinal direction of the metal billet as shown in Fig. 1.14(a) and (b). It improve the extrusion product quality.

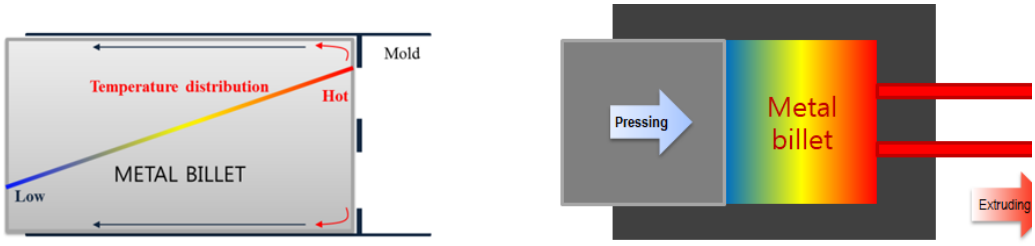

(a) (b)

Fig. 1.14 3-dimensional Temperature distribution by the frequency in the surface of the aluminum billet in simulation results

As shown in Fig. 1.15, a SIH has the function to control the magnetic field along the longitudinal direction of the metal billet. It's called as a magnetic displacement control unit. It controls the magnetic field along the longitudinal

direction of the metal billet by exchanging the iron yoke with different angle for 0 to 5 degree as shown in Fig. 1.16 and then, the temperature of the billet was controlled, when the heating with a rotation occurs. The extrusion product quality was improved with a high extrusion performance.

Fig. 1.15 10 kW SIH heating results for the magnetic control along the longitudinal direction.

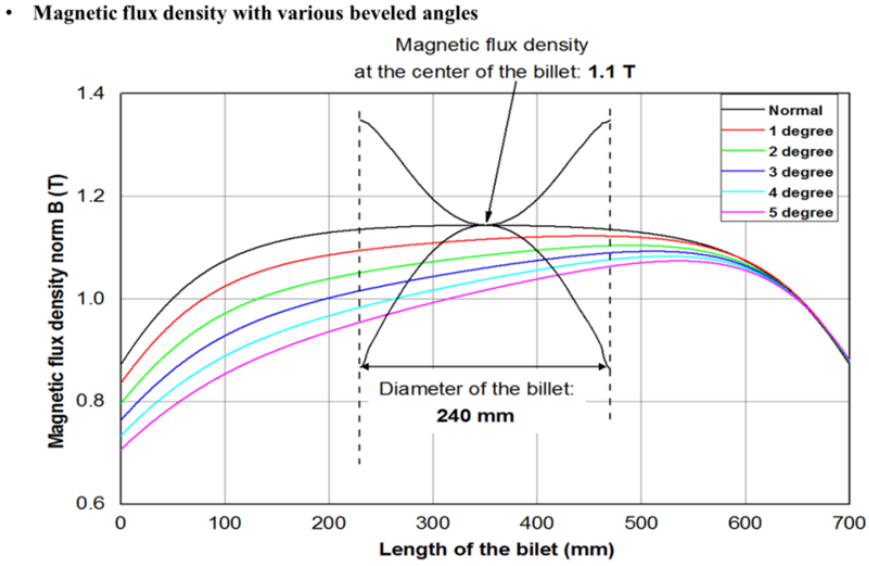

Fig. 1.16 The magnetic fields controlled by angle of the iron yoke shape from 0 degree to 5 degree from the electromagnetic simulation.

1.2.4 Available for heating various size of the metal billet with a SIH

A conventional induction heater has each coil to heat different diameters of the metal billet and need a big space for keeping each copper coil as shown in Fig. 1.17. It makes the initial machine cost increase and the maintenance expense during the operation occurs continuously.

Fig. 1.17 Conventional induction heater has each coil against a diameter of the metal billet and needs a big space for storage of various copper coils

However, a SIH has a gripping system with changeable jigs on different diameters of the metal billets. In addition, the hydraulic moving system is installed and operated for different lengths of the metal billets as shown in Fig. 1.18. So, a SIH is available to heat various size billets in aspect of diameters and lengths.

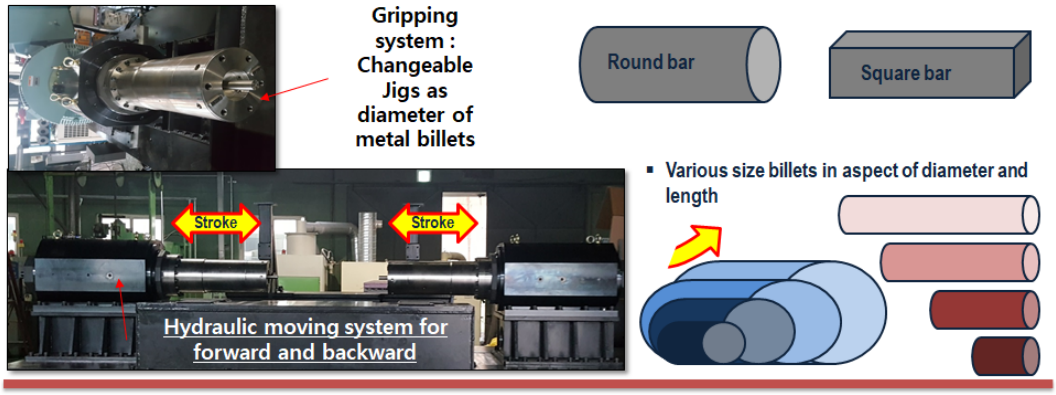

Fig. 1.18 A SIH is available to heat various size billets in aspect of diameter and length by using changeable jigs of gripping system and hydraulic moving system

1.2.5 Maintenance components with a SIH

A SIH was compared to and a conventional induction heater in aspect of maintenance components as shown in Fig. 1.19. The major maintenance components of a conventional induction heater are copper coils, parts of lager cooling water circulation system, insulation materials and switching devices, an IGBT and thyrister with capacitors. They can cause sudden faults or damages and there are many kinds of parts with high cost. The other hands, a SIH uses the superconducting coil permanently and major components are mechanical seals for cryo-cooler and bearings of spindle units. These components are required to periodic replacement and do not cause the sudden damages or faults. So, a SIH can minimize the expense of the maintenance and repair during the operation.

Fig. 1.19 A comparison of major maintenance components between SIH and a conventional induction heater

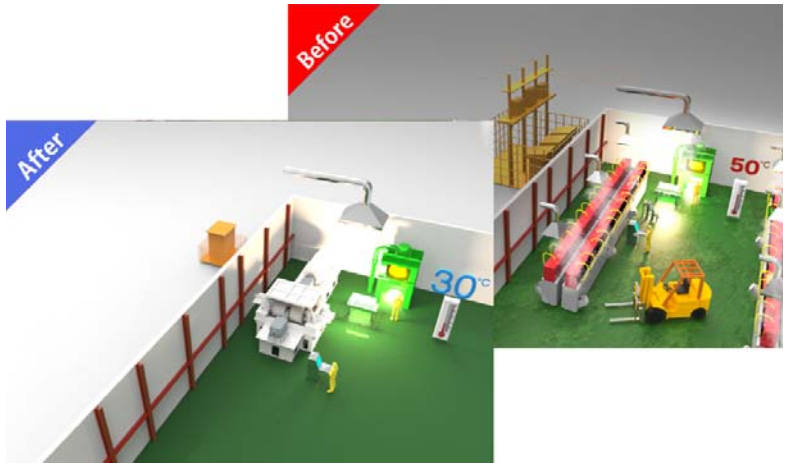

Fig. 1.20 These pictures show the change of the factory environments through the comparison between the before and after the installation of a SIH

1.2.6 Eco-friendly automation manufacturing system

The installation and operation environments of a SIH are compared to those of the conventional atmosphere furnaces as shown in Fig. 1.20. A SIH decreases not only the capacity of an electric power facility for heater operation, but also the room temperature of the working place in industries. And a SIH minimizes the installation space and CO_2 emissions during the heating operation. A SIH is possible to automate the total manufacturing process without any fork lift and operator.

1.3 Economic Feasibility Study of a SIH

In 2014, Changwon National University and TECHSTEEL initiated a project to develop a 300 kW-class SIH with HTS magnets that aims to achieve 90% energy efficiency within 3 years. Thus, the authors purpose to commercialize the SIH through the project. Prior to launching the SIH, the economic feasibility has to be verified. We studied economic feasibility of the SIH in comparison with two different types of conventional heating furnaces such as an atmosphere furnace (ATF) and AC induction furnace (AIF). To minimize

electricity fee, net present value (NPV), internal rate of return (IRR) and pay-back period (PBP) methods were used [31]-[39]. All indicators such as system efficiency, operation time, heating capacity, inflation rate and incidental cost were considered to evaluate the investment returns of the SIH.

Detailed investigations and analysis were conducted on 300 kW-class SIH in connection with atmosphere and AC induction furnaces. The evaluation results were discussed in detail. The analysis results were be available to the commercialization of the SIH.

Preconditions including operation parameters were determined for the equivalent comparison on three different types of the heating furnaces. The total investment cost was estimated reflecting major items such as the system efficiency, heating capacity, electricity fee, inflation rate, and incidental cost. The direct benefit on the investment was calculated focusing on saving the electricity fee. This analysis was performed concerning the 300 kW SIH.

Table 1.2 Basic requirements for the 300 kw heating furnaces

Parameters	Value
System capacity	300 kW
Billet type	Aluminum billet
Diameter of the billet	236 mm (9")
Length of the billet	700 mm
Initial temperature	20℃
Target temperature	540℃
Heat capacity at 540℃	1257 J/kg·K
Density at 25℃	2700 kg/m^3
Resistivity at 540℃	8.93E-8 Ω·m
Required energy for a billet	53.6 MJ
Operation hour in a day	20 hours
Operation day in a month	25 days
Operation hours in a year	6000 hours
Electric rate	US¢ 7.7/kWh
Target production in a month	9000 PCS
Total energy required in a month	482 GJ

1.3.1 Cost assesment of the SIH

To analyze the economic feasibility, the basic requirement of 300 kW-class heating furnaces were defined in advance as shown in Table 1.2. The billet is made of aluminum with a diameter of 236 mm for the 300 kW-class system capacities. The length of the billet is 700 mm. The unit price of the electricity fee is US¢ 7.7/kWh and the furnace operates 25 days in a month.

Annual operating expenditure (AOE) and total investment cost (TIC) were calculated by the equation (1.2) and (1.3). The meanings of the abbreviations are given below.

$$AOE = ICC \times \frac{AIR(1+AIR)^{SLT}}{(1+AIR)^{(SLT-1)}} + OPEX \tag{1.2}$$

$$TIC = ICC + \frac{EF(1+AIR_{EF})^{(SLT-1)}}{AIR_{EF}} + \frac{MOC(1+AIR_{MOC})^{(SLT-1)}}{AIR_{MOC}} \tag{1.3}$$

ICC: Initial capital cost
AIR: Annual interest rate
SLT: Service life time
OPEX=EUF+MOC: Operating expenditure
EF: Electricity fee
MOC: Maintenance and operation cost
AIR_{EF}:Annual interest rate for EF
AIR_{MOC}:Annual interest rate for MOC

As given in Table 1.3, TIC of the 300 kW high temperature superconducting induction furnace (HIF) during the service life time of 20 years were calculated at US$ 6.2 M. However, the TIC cost of the 300 kW and 1.4 MW ATF was estimated at US$ 4.4 and US$ 21.2 M. The total investment cost of the HIF is much lower than that of the ATF and AIF. AOE was calculated according to the increment of the machine cost. In 300 kW HIF, the AOE was estimated at US$ 0.25 M. It is lower than those of two different heating furnaces. These AOE curves of the HIF, ATF and AIF were shown in Fig. 1.21 for the 300 kW-class.

Table 1.3 Direct benefits estimation for the three different types of the 300 kW heating furnaces

Parameters	ATF's value	AIF's value	HIF's value
Machine cost	US$ 0.48 M	US$ 0.88 M	US$ 1.2 M
System capacity	1,400 kW	600 kW	300 kW
Efficiency	20%	50%	90%
Machine operating rate	95.7%	89.3%	99.2%
Service life time	20 years	20 years	20 years
Electric fee in a month	US$ 51,704	US$ 20,682	US$ 11,490
Electric fee in a year	US$ 0.62 M	US$ 0.25 M	US$ 0.14 M
Operation and maintenance rate of the cost	1% (US$ 4,784)	3.3% (US$ 27,216)	1% (US$ 12,371)
Corporation discount rate	5%	5%	5%
Incidental expense	US$ 41,237	US$ 41,237	US$ 41,237
Inflation rate	2.5%	2.5%	2.5%
Operating expense in the first fiscal year	US$ 0.63 M	US$ 0.28 M	US$ 0.15 M
Annual capital expenditure	US$ 41693	US$ 69488	US$ 0.10 M
Annual operating expenditure (AOE)	US$ 0.67 M	US$ 0.35 M	US$ 0.25 M
Total investment cost	US$ 21 M	US$ 9.8 M	US$ 6.2 M

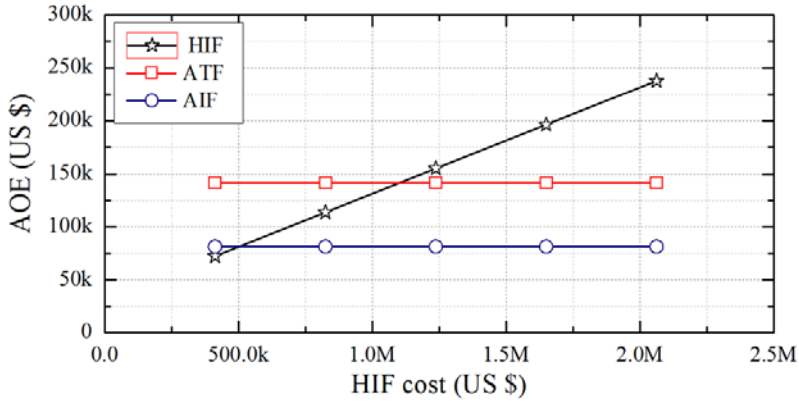

Fig. 1.21 Annual operating expenditures on the three different types of the heating furnaces of the 300 kW

1.3.2 Economic Analysis and Results

First, the corporate discount rate represents the required rate of return to make a business acquisition worth. Especially, the corporation discount rate was used to evaluate the profitability on the company investment business and calculate the NPV. Meanwhile, IRR was calculated for the minimum expected profitability under the break-even condition and compared to the corporation

discount rate. And then, PBP was deduced in order to evaluate how faster the investment cost can return.

$$NPV=\sum_{t=0}^{n}\frac{NB_t}{(1+\gamma)^t},\ (\mathrm{n}=0,\ 1,\ 2,\ 3,\ \cdots,\ 20) \tag{1.4}$$

$$IRR=\gamma,\quad if\ NPV=\sum_{t=1}^{n}\frac{NB_t}{(1+\gamma)^t}=0\ (\mathrm{n}=1,\ 2,\ 3\ \cdots,\ 20) \tag{1.5}$$

$$PBP=n,\quad if\ \sum_{t=0}^{n}NB_t\geq 0\ \ (\mathrm{n}=0,\ \ 1,\ \ 2,\ \ 3\ \cdots,\ \ 20) \tag{1.6}$$

Net present value (NPV) internal rate of returns (IRR) and pay-back period (PBP) were defined by the equation (1.4), the equation (1.5), and the equation (1.6) respectively, where, NB_t and means net benefit at t year and corporate discount rate, respectively. If NPV is positive, it means that the investment would be effective. In the case of the 300 kW-class HIF, the NPV on ATF and AIF were evaluated as the positive values after 3 years and 12 years, respectively.

IRR means the benefit rate of the investment. If this value is positive, it means that the investment is effective after passing the break-even point. IRR of the 300 kW HIF against the ATF was calculated at about 6% after 3 years. The IRR against the AIF was calculated as 6 % after 12 years. These results were the same as the NPV analysis results. The higher is the system capacity for the HIF, the more effective is the investment.

The PBP was depicted in Fig. 1.22. The PBP was deduced as three years and three months in the case of changing the 600 kW AIF to the 300 kW HIF, which has the machine cost of US$ 1.24 M as shown in Fig. 1.21.

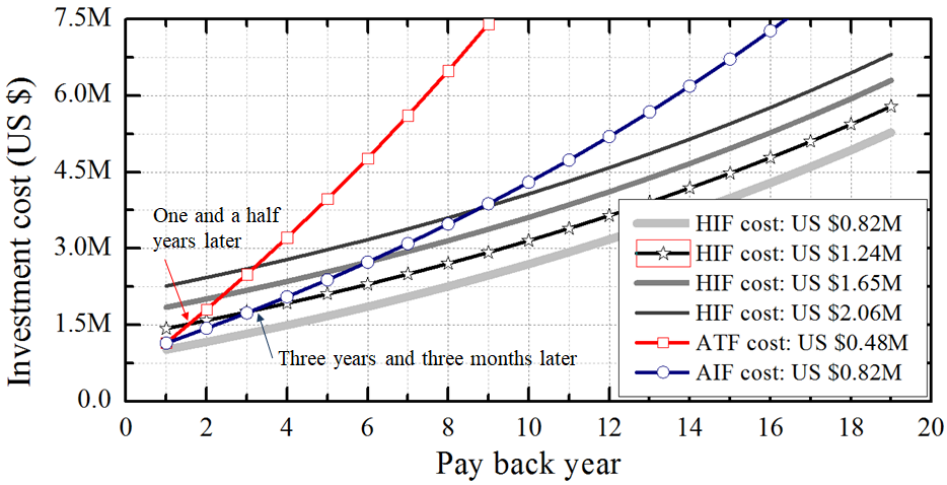

Fig. 1.22 Annual operating expenditures on the three different types of the heating furnaces of the 300 kW

The NPV had positive value in the 300 kW-class HIF for both cases of changing the ATF and AIF based on the corporate discount rate of 6%. The IRR was getting higher as the service life time of the HIF increased. It means that the investment return rate of the HIF with larger capacity over 300 kW is very high. The PBP of 300 kW HIF, which has the machine cost of US$ 1.24 M, was achieved at below three years and three months after substituting it for the AIF. The analysis results are used for the investment decision process of the HIF.

1.4 Objectives and contributions of this study

In metal production infrastructure industries, there are many issues against the conventional heating furnaces to produce metal products by forging and extruding and melting etc.

An environmental protection policy to achieve a energy savings and CO_2 zero-emissions is now required world wide. Also, the metal industries use old and inefficient technologies for heating metals with large capacity and low efficiency. The workplace is dirty, dangerous, and dull. Finally, they need engineers with various skills to apply advanced technologies to their production

system.

As one of the solutions to resolve these issues, the SIH should be developed through HTS magnets. These technologies should be developed and would yield many positive contributions to metal processing industries as shown in Fig. 1.23.

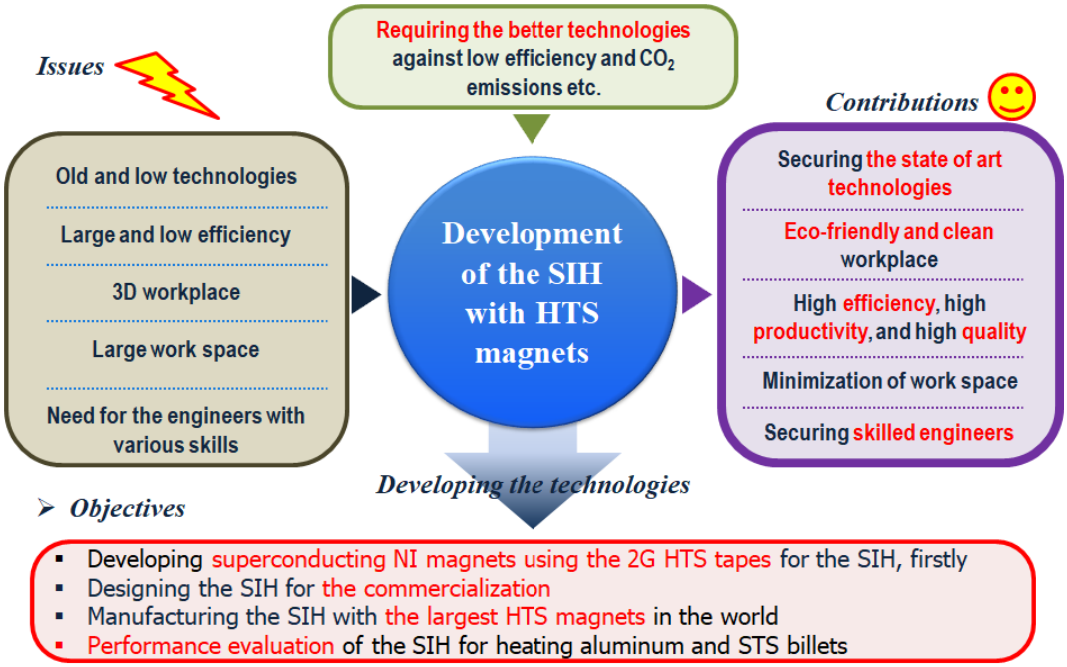

Fig. 1.23 Objectives and contributions of developing the SIH with HTS magnets

CHAPTER 2

NUMERICAL DESIGN OF A SUPERCONDUCTING INDUCTION HEATER

Establishing the numerical equations for engineering these systems is very important. To design the direct current (DC) induction heater with HTS magnets, a numerical design should be performed. However, it is not easy to calculate exactly the amount of the induced current inside of the metal billet, because of many kinds of variables, such as resistivity, heat conductivity, temperature, heat capacity, mass, diameter and length of the metal billet, frequency, magnetic field, thermal conductive, and convective, and radiative, heat fluxes and so on. To acquire the relationships for the various parameters of the DC induction heating process, the theoretical relationships of the dependent variables first need to be proposed in this dissertation.

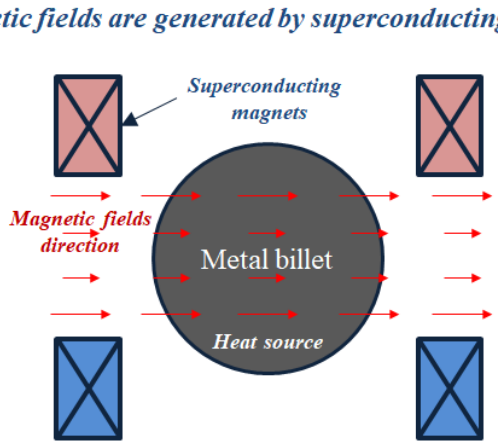

Fig. 2.1 A conceptual diagram of the metal rotating type - DC induction heating with superconducting DC magnets

In DC induction heating, three different energy transfer relationships are existed. The DC induction heater largely consisted of three devices—the DC magnet to generate a magnetic field, the metal billet to be heated up, and the rotating mechanical power to get a heating power source. The heat energy inside of the metal billet is considered by the electrical energy inside of the billet which is induced by the rotating mechanical power. The billet temperature increases.

The induced current inside the metal billet flows along the longitudinal direction in the case of the DC induction heating as shown in Fig. 2.2. If the magnitude of the induced current is dependent on the magnetic field strength on the metal billet. The higher magnetic field, the larger induced current inside the metal billet. The other hands, if the uniform magnetic field keeps on the longitudinal direction of the metal billet, the billet is heated up with uniform temperature distribution.

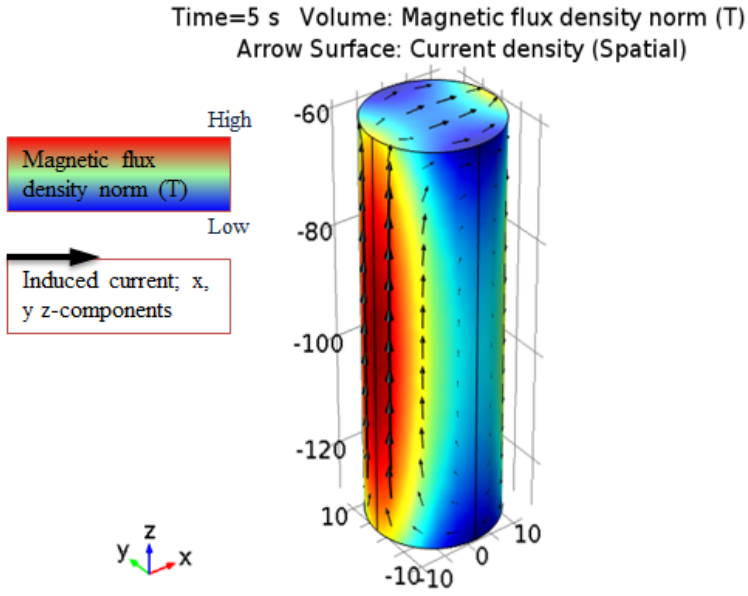

Fig. 2.2 3-dimensional FEM model for the magnet rotating type - DC induction heating

2.1 Theoretical DC induction heating principle

In general, the resistive heating of the metal billet was calculated as the equation (2.1).

$$P_w = k \cdot T_m \times rpm = R_w \cdot I_{ind}^2 \tag{2.1}$$

From the equations (2.2–2.6), a resistive heating power is equal to the output power of the rotating motor derived from the product of the mechanical torque and rotating speed [48-49]. The magnitude of the mechanical torque, which decreases as the rotational speed increases, is calculated by the vector product of the position vectors and the force applied, which depends on the cross product of the induced current density and the magnetic flux density.

$$T_e = \int \tau_i dV \tag{2.2}$$

$$\tau_i = r \times F \tag{2.3}$$

$$F = J \times B \tag{2.4}$$

$$I \frac{d\omega}{dt} = T_e - T_m \tag{2.5}$$

$$T_e = T_m \tag{2.6}$$

- $\mathbf{R_w}$: *Resistance of the metal billet [Ω]*
- $\mathbf{I_{ind}}$: *Induced current [A]*
- **F** : *Lorentz force[N/m^3]*
- **J** : *Current density[A/m^2]*
- **B** : *Magnetic flux density[T]*
- T_e : *Electric torque [N·m]*
- T_m: *Mechanical torque [N·m]*
- τ_i : *A unit torque [N·m]*
- **r** : *A rotational position vector in a geometry [m]*
- **I** : *inertia moment*
- **ω** : *Angular velocity [rad/s]*
- **rpm** : *revolutions per minute*

Thus, as the applied magnetic field increases, greater resistive heating power is output. HTS magnets can easily generate a high magnetic field without any loss.

2.2 Electro-magnetic relations

To define the electromagnetic relations for DC induction heating, the Maxwell's equations should be calculated. Under certain circumstances it can be helpful to formulate the problems in terms of the magnetic vector potential **A** as in equation (2.9). By using the magnetic vector potential **A**, Maxwell's equations are rewritten as equations (2.7–2.8) and termed Ampere's Law. These equations are available for the induced current inside of the metal billet. From equation (2.7), the magnetic field is going to be converted to the magnetic flux density with permeability. The equations (2.10) and (2.11) are related to the boundary condition and the magnetic insulation for the electromagnetic analysis, respectively [50-55].

Resistive heating power input to the billet is proportional to the Joule's heat. The Joule's heat is calculated as the product of the square of the induced current. The resistance of the current loop within the billet varies only with skin depth and depends on the angular velocity of the billet, if a radius of the meta billet is constant. The induced current is deduced from the impedance of the induced voltage inside of the billet. The induced voltage is calculated from the time-varying magnetic flux linkages and is proportional to the angular velocity, the number of coil turns, and the induced current as shown in equation (2.12) [56].

$$\sigma \frac{\partial \mathbf{A}}{\partial t} + \nabla \times \mathbf{H} = J_e \tag{2.7}$$

$$\sigma \frac{\partial \mathbf{A}}{\partial t} + \nabla \times \left(\frac{\mathbf{B}}{\mu_0 \mu_r} \right) - \sigma \mathbf{v} \times \mathbf{B} = J_e \tag{2.8}$$

$$\mathbf{B} = \nabla \times \mathbf{A} \tag{2.9}$$

$$\mathbf{n} \times \mathbf{A} = 0 \tag{2.10}$$

$$\mathbf{n} \cdot \mathbf{B} = 0 \tag{2.11}$$

$$J_e = \frac{N I_{coil}}{A} e_{coil} \tag{2.12}$$

- *Electric field intensity* **E**
- *Magnetic field intensity* **H**
- *Magnetic vector potential* **A**
- *Magnetic flux density* **B**
- *An externally generated current density* **J**
- *A geometry moving with velocity* **v**
- *Electric charge density* **ρ**
- *Electric conductivity* **σ**
- *Permeability of air* μ_0
- *Relative permeability* μ_r

As shown in Fig. 2.5, the magnetic flux density inside of the billet was expressed with color distribution according to time through the finite elements method (FEM) to calculate the induction heating power of the metal billet. The red color represents high magnetic flux density and its direction is the red arrows. The blue color represents low magnetic flux density. The center of the billet has a very low magnetic flux density because of the vector summation of the magnetic fields by the induced current inside the billet. The iron cores between two DC magnets was installed and concentrates the magnetic flux density to the center of the metal billet. The magnetic flux density inside the iron cores located between the DC magnets is the highest point. The stream

lines under the stationary state express the magnetic field of the SIH with iron cores on the air as shown in Fig. 2.6.

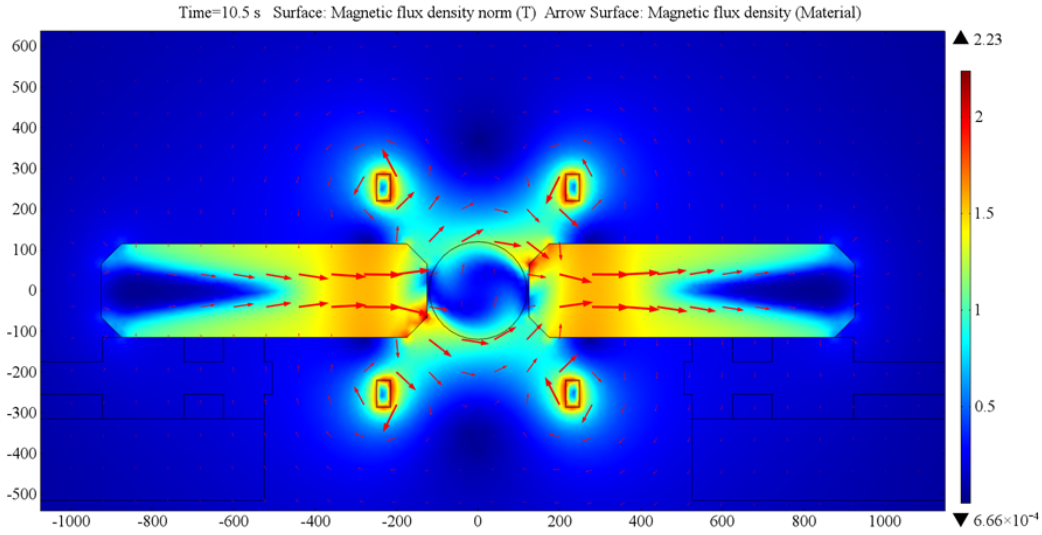

Fig. 2.5 2-dimensional electromagnetic FEM model for the DC induction heating; time-dependent solution

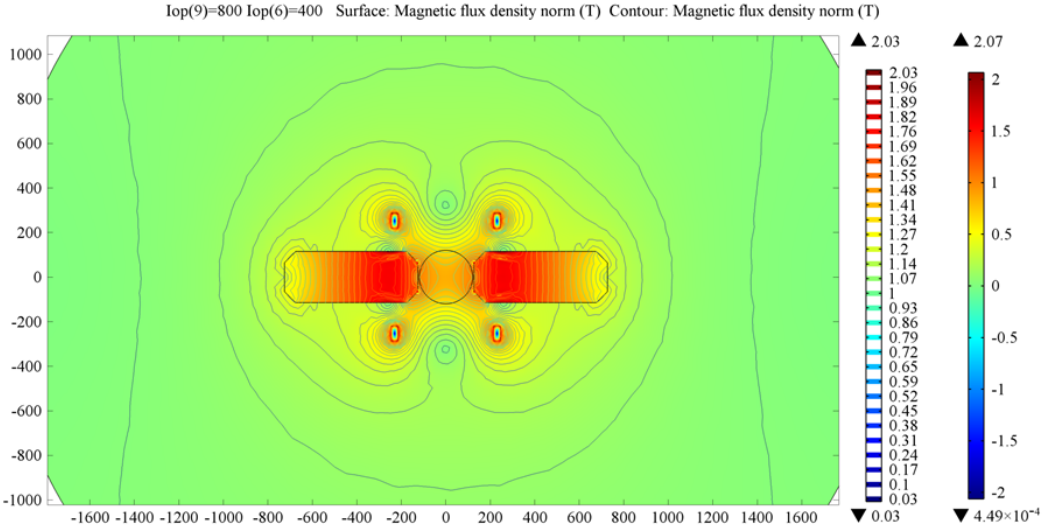

Fig. 2.6 2-dimensional electromagnetic FEM model for the DC induction heating; stationary solution

2.3 Heat transfer relations

Heat transfer is defined as the movement of energy due to a difference in temperature. There are three mechanism such as conduction, convection and radiation [57-74]. First, thermal conduction generally occurs between solid bodies in contact. A temperature increment is generated the interface between the two surfaces in contact. This phenomenon is referred to be a result of a thermal contact resistance existing between the contacting surfaces. Interfacial thermal resistance is a measure of an interface's resistance to thermal flow. This thermal resistance differs from contact resistance between two materials with thermal properties.

During heating operation with temperatures changes in time within an metal billet, the thermal energy flow is termed transient conduction. They may also occur with temperature changes inside a metal billet, as a result of a heat source or sink.

Second, the convection heat transfer comprises one mechanism. In addition to energy transfer due to specific diffusion, energy is transferred by motion of the fluid like air. Two types of convective heat transfer are distinguished as free or natural convection and forced convection. A fluid like an air moves due to variations of thermal temperature. In the absence of an internal source, when the fluid is in contact with a hot surface, the hotter volume transfers heat towards the cooler volume of that fluid. Familiar examples are the upward flow of air due to a fire or hot metal billet and the circulation of water in a pot that is heated from below. The other forced convection occurs when a fluid is forced to flow over the surface by an internal source such as fans.

Thermal radiation is also one of the fundamental mechanisms of heat transfer. The characteristics of thermal radiation depend on various properties of the surface including its temperature. If the radiating body and its surface are in thermodynamic equilibrium and the surface has perfect absorptivity at all wavelengths, it is characterized as a black body. A black body is also a perfect emitter. The radiation of such perfect emitters is called black-body

radiation. The ratio of any body's emission relative to that of a black body is the body's emissivity, so that a black body has an emissivity of unity.

As shown in Fig. 2.7, the temperature inside of the billet was expressed with color distribution according to time through the multi-physics FEM model by calculating the electromagnetic and heat transfer equations for DC induction heating of the metal billet.

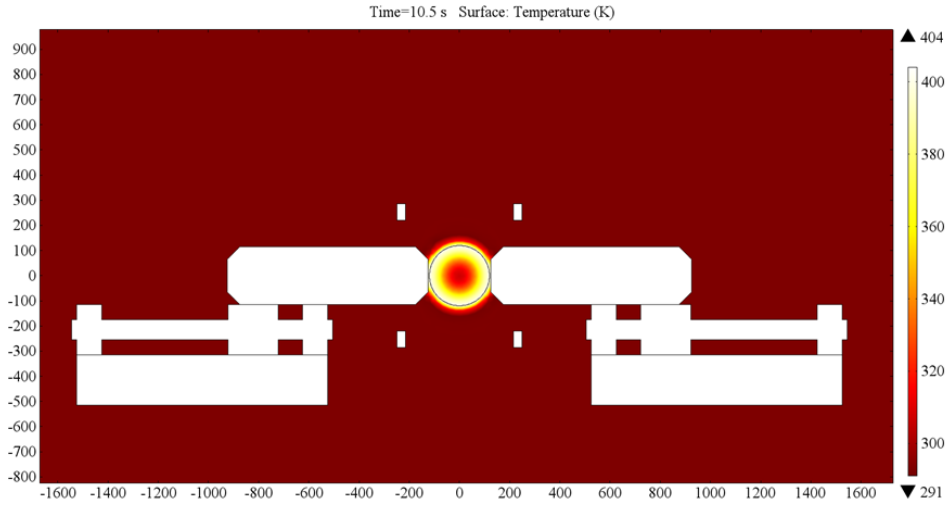

Fig. 2.7 2-dimensional multi-physics FEM model (electromagnetic and heat transfer) for the DC induction heating; time-dependent solution

2.2.1 Heat conduction, convection and radiation considerations

The heat transfer in solids is calculated using the heat equation (2.18). Inside the billet, the heat is conducted to the center of the billet. As shown in equation (2.19), the thermal insulation condition is referred. For a steady-state problem, the temperature does not change with time and the first term disappears. The equation includes the following material properties: density, heat capacity, and thermal conductivity. It also includes the velocity field, $\boldsymbol{u}$ and a heat source (or sink), $\boldsymbol{Q}$.

$$\rho C_p \frac{\partial T}{\partial t} + \rho C_p \boldsymbol{u} \cdot \nabla T = \nabla \cdot (k \nabla T) + \boldsymbol{Q} \tag{2.18}$$

$$-\mathbf{n} \cdot (-\boldsymbol{k}\boldsymbol{\nabla}\boldsymbol{T}) = \mathbf{0} \tag{2.19}$$

$$-\mathbf{n} \cdot (-\boldsymbol{k}\boldsymbol{\nabla}\boldsymbol{T}) = \boldsymbol{q_0} \tag{2.20}$$

$$-\mathbf{n} \cdot (-\boldsymbol{k}\boldsymbol{\nabla}\boldsymbol{T}) = \boldsymbol{\varepsilon}(\boldsymbol{G} - \boldsymbol{e_b}(\boldsymbol{T})) \tag{2.21}$$

$$(\mathbf{1} - \boldsymbol{\varepsilon})\boldsymbol{G} = \boldsymbol{j} - \boldsymbol{\varepsilon}\boldsymbol{e_b}(\boldsymbol{T})) \tag{2.22}$$

$$\boldsymbol{e_b}(\boldsymbol{T}) = \boldsymbol{n^2}\boldsymbol{\sigma}\boldsymbol{T^4} \tag{2.23}$$

$$\boldsymbol{G} = \boldsymbol{G_m}(\boldsymbol{j}) + \boldsymbol{G_{amb}} + \boldsymbol{G_{ext}} \tag{2.24}$$

$$\boldsymbol{G_{amb}} = \boldsymbol{F_{amb}}\boldsymbol{e_b}(\boldsymbol{T_{amb}}) \tag{2.25}$$

- *Density(kg/m^3):* $\boldsymbol{\rho}$
- *Heat capacity(J/(kg·K):* $\boldsymbol{C_p}$
- *Thermal conductivity(W/mK):* $\boldsymbol{k}$
- *Velocity field(m/s):* $\boldsymbol{u}$
- ***Normal vector of the boundary:*** $\mathbf{n}$
- *Heat source(W):* $\boldsymbol{Q}$
- ***Irradiation(or incoming radiative heat flux): G (W/m^2)***
- ***Ambient irradiation: G_{amb} (W/m^2)***
- ***Radiosity(or total outgoing radiative heat flux): G (W/m^2)***
- ***Ambient temperature: T_{amb}***
- ***Surface emissivity: ε***
- ***The transparent media refractive index: n***
- ***Mutual irradiation: G_m***
- ***Irradiation from external radiation source: G_{ext}***
- ***Ambient view factor: F_{amb} ($0 \leq F_{amb} \geq 1$)***

As the temperature of the non-ferrous metal billet increases under the heating process, its physical properties, such as resistivity, thermal capacity, and thermal

conductivity, change. Outside of the billet, thermal exchange occurs on the boundary of the billet, where the heat is transferred to the air through thermal convection.

The convective heat flux condition as shown in the equation (2.20) is adapted to cases in which an isothermal domain is considered solid and is adjacent to a fluid. Convection occurs at the interface with a specified heat transfer coefficient.

Surface-to-ambient radiation as shown in the equation (2.21) to (2.25) assumes the following: (1) the ambient surroundings in view of the surface have a constant temperature and (2) the ambient surroundings behave as a blackbody. This is interpreted to mean that the emissivity and absorptivity are equal to 1, and the reflectivity is 0.

2.4 Structural mechanics relations

The Solid mechanics (solid) interface is intended for general structural analysis of 3D, 2D, or axisymmetric bodies. In 2D, plane stress or plane strain assumptions can be used. The solid mechanics interface is based on solving Navier's equations, and results such as displacements, stresses, and strains are computed [75-76].

The linear elastic material is the default material, which adds a linear elastic equation for the displacements and the elastic material properties can be defined.

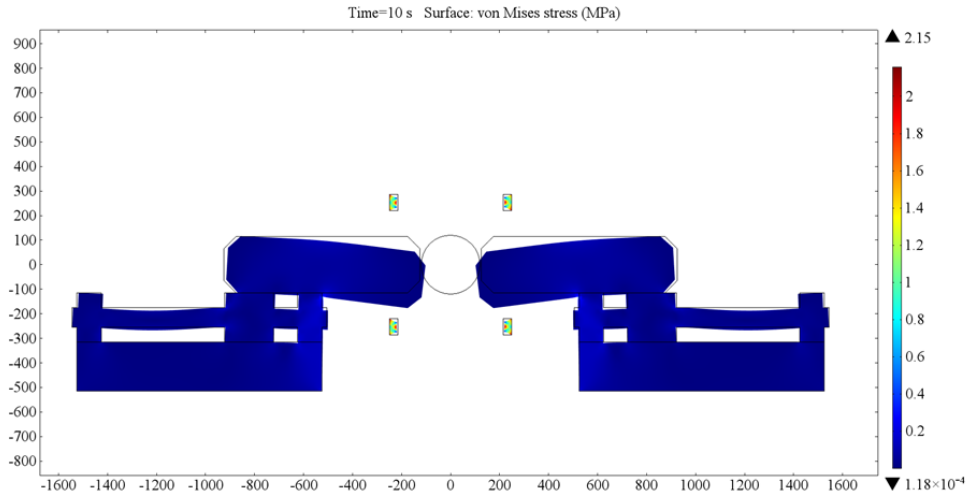

Fig. 2.8 2-dimensional multi-physics FEM model (electromagnetic, structural mechanics and heat transfer) for the DC induction heating; time-dependent solution

As shown in Fig. 2.8, the Von mises stress of the SIH with structure to support the HTS magnet and iron cores was expressed with color distribution according to time through the multi-physics FEM model by calculating the electromagnetic and solid structural equations for DC induction heating of the metal billet.

The solid mechanics relations are calculated using the governing equation (2.26) to (2.29). The body loads in the multi-physic model of the electromagnetics and solid mechanics are calculated to the Lorentz forces from the electromagnetic equation as shown in the equation (2.30) to (2.31). For a steady-state problem, the velocity field does not change with time like the equation (2.32) and the first term disappears. The equation includes the following material properties: density, heat capacity, Poisson's ratio and Youngs modulus. It also includes the velocity field, u and a volume force $\boldsymbol{Fv}$.

$$\rho \frac{\partial^2 u}{\partial t^2} - \nabla \cdot \sigma = \boldsymbol{F}v \tag{2.26}$$

$$\rho \frac{\partial^2 u}{\partial t^2} = \nabla \cdot s + \boldsymbol{F}v \tag{2.27}$$

$$s = S_0 + C : (\varepsilon - \varepsilon_0 - \varepsilon_{inel}) \tag{2.28}$$

$$\varepsilon = \frac{1}{2}(\nabla u + (\nabla u)^T) \tag{2.29}$$

$$\rho \frac{\partial^2 u}{\partial t^2} - \nabla \cdot \sigma = \boldsymbol{F}v \tag{2.30}$$

$$\boldsymbol{F}v = Lorentz\ force\ in\ Electro - magnetics \tag{2.31}$$

$$\boldsymbol{u} = 0 \tag{2.32}$$

- *Density(kg/m³)* $\boldsymbol{\rho}$
- *Heat capacity(J/(kg·K))* $\boldsymbol{C_p}$
- *Thermal conductivity(W/mK)* $\boldsymbol{k}$
- *Velocity field(m/s)* $\boldsymbol{u}$
- *Heat source(W)* $\boldsymbol{Q}$
- ***Yong's modulus:*** $\boldsymbol{E}$
- ***Poisson's ratio:*** $\boldsymbol{v}$
- ***Volume force:*** $\boldsymbol{Fv}$
- ***Von Mises Stress:*** $\boldsymbol{\sigma}$
- ***Strain:*** $\boldsymbol{\varepsilon}$
- ***Thermal strain:*** $\boldsymbol{\varepsilon_{th}}$
- ***Coefficient of thermal expansion:*** $\boldsymbol{\alpha}$
- ***Strain reference termperature:*** $\boldsymbol{T_{ref}}$

The numerical analysis for the SIH design was performed with the multi-physics FEM models development, When the metal billet rotates with a

mechanical torque, the supporting system for the SIH gets the volume force and the stress and strain of the supporting structure are analysed at the same time. The von Mises stress for the supporter of the HTS magnets was calculated through the FEM model as shown in Fig. 2.9.

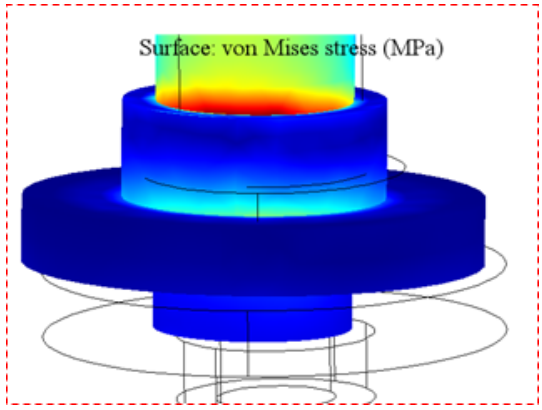

Fig. 2.9 Von Mises stress was calculated through the solid mechanics analysis

2.5 Multi-physics considerations of three theoretical relations

The multi-physics consideration for the SIH numerical analysis should be performed. The three theoretical relations such as an electro-magnetics, a heat transfer and solid mechanics physics models are calculated at the same time.

The temperature change generates the stress by thermal expansion, Also, the material properties like a heat capacity and thermal conductivity and density were changed, too. The SIH was operated under the cryogenic conditions and the the all physics parameters are not normal state.

As shown in the equation (2.33), the Joule's heat of the electro-magnetics model is acted as the source of the heat transfer model. The default coefficient of thermal expansion uses values from material. A value or expression for the strain reference temperature is entered, which is the reference temperature that

defines the change in temperature together with the actual temperature of the heat transfer physic model as shown in the equation (2.34) to (2.36).

In this section, the physics involved in the multi-physics coupling were defined as shown in Fig. 2.10. The electro-magnetics, heat transfer and solid mechanics include all applicable physics interfaces.

$$\rho C_p \frac{\partial T}{\partial t} + \rho C_p \boldsymbol{u} \cdot \nabla T = \nabla \cdot (k \nabla T) + \boldsymbol{Q_e} \tag{2.33}$$

$$\varepsilon_{th} = \alpha (T - T_{ref}) \tag{2.34}$$

$$J_{th} = (1 + \alpha (T - T_{ref}))^3, \tag{2.35}$$

$$F_e = F \int_{th}^{1/3} \tag{2.36}$$

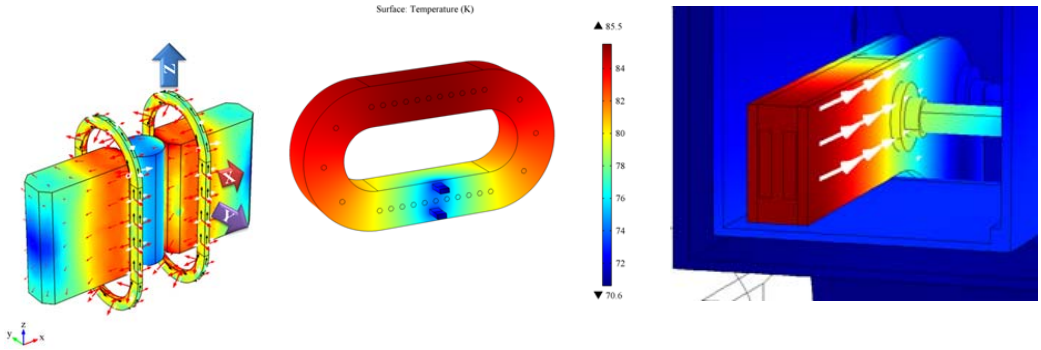

(a) (b) (c)

Fig. 2.10 There are three FEM models for the SIH; (a) The electro-magnetics, (b) heat transfer and; (c) solid mechanics

CHAPTER 3

DESIGN OF A 300 KW-CLASS SIH WITH HTS MAGNETS

3.1 Design of the SIH with HTS magnets with iron cores

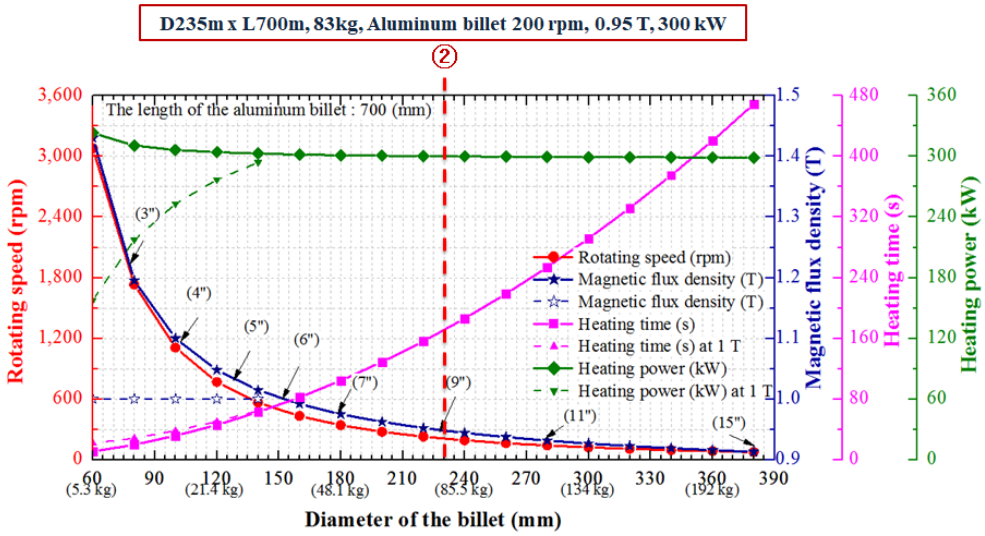

Fig. 3.1 The magnetic flux densities at the target position of the developed electromagnetic FEM model for a SIH according the excitation current

Here, the SIH with HTS magnet with iron cores was designed. In order to get the 300 kW-class heating power, the magnetic flux density at the center of the billet should be decided. The target billet is aluminum billet and its diameter is 9 inch. Its length is 700 mm and its weight is 83 kg. The magnetic field at the center of the aluminum billet is 0.95 T and the rotating

speed is 300 rpm. At that time, the heating power is estimated to 300 kW and heating time is expected to 180 seconds as shown in Fig. 3.1.

As shown in Fig. 3.2, the magnetic flux densities at the target position of the aluminum billet were simulated according to the excitation current using the developed electromagnetic FEM model for the SIH. The 1.1 T the magnetic flux density at the center of the billet was deduced through the FEM simulation. The target excitation current will be 440 A.

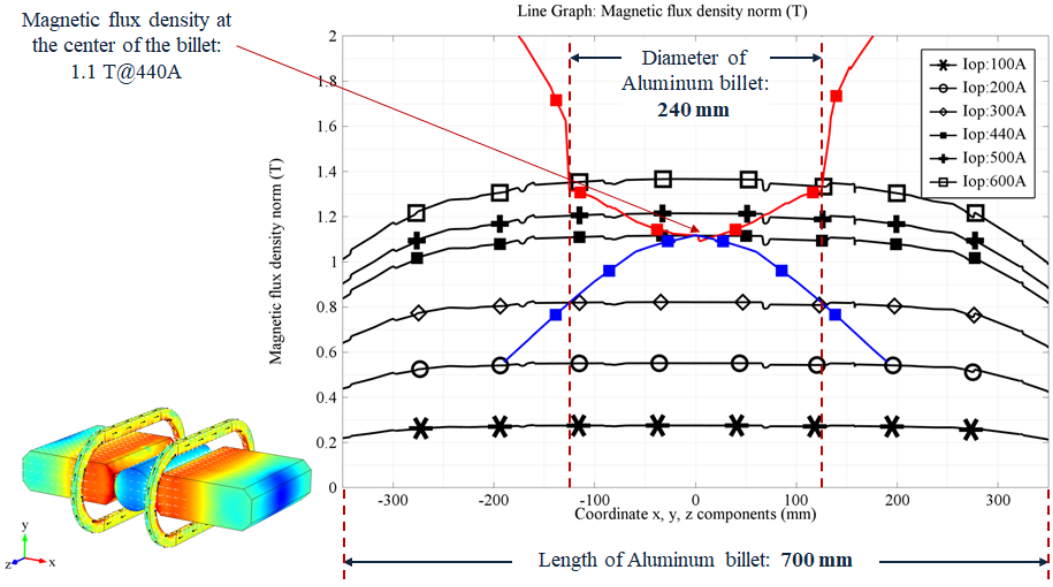

Fig. 3.2 The magnetic flux densities at the target position of the developed electromagnetic FEM model for a SIH according the excitation current

And then, the electromagnetic FEM model for the SIH was composed of two iron cores by considering the magnetization characteristic. In the real SIH, the iron cores are installed on the supporting base with the ferromagnetic materials. The FEM model was developed by considering the base with the ferromagnetic material as shown in Fig. 3.3. The simulation results were presented in Fig. 3.4. The magnetic flux density at the center of the billet increased to 1.33 T because of minimizing the magnetic field leakage.

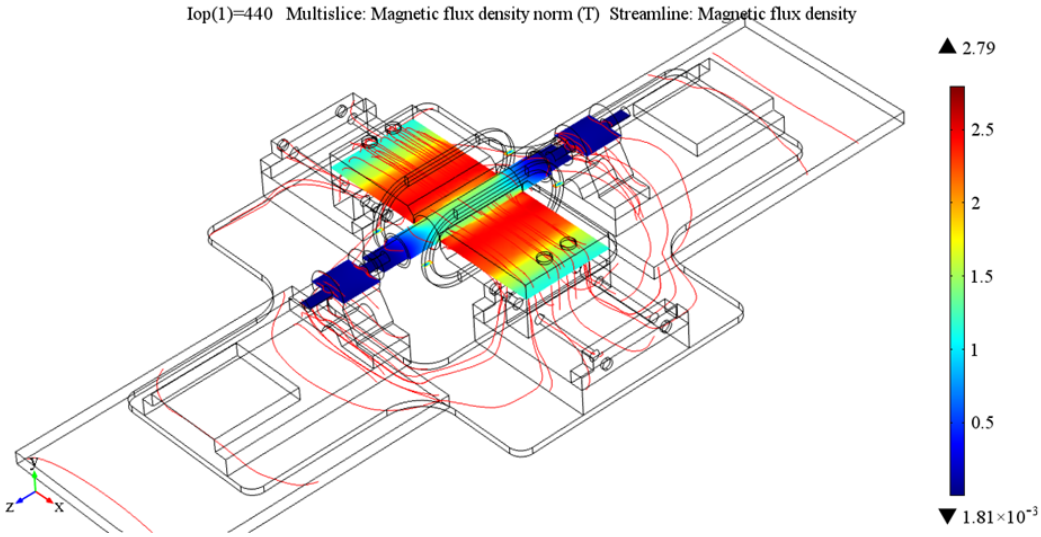

Fig. 3.3 The magnetic flux density streamlines of the entire SIH considering the ferrous supporting and rotating units

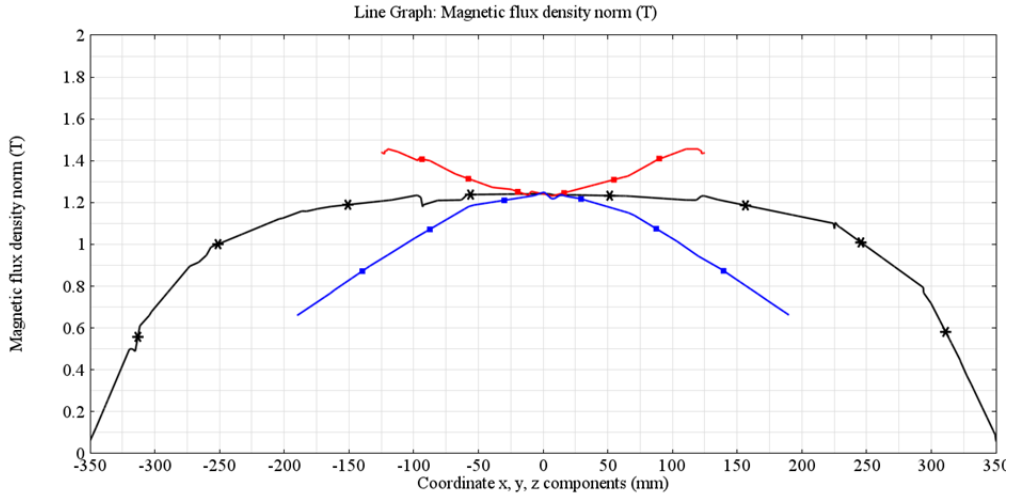

Fig. 3.4 The magnetic flux density at the metal billet position of a SIH considering the ferrous supporting materials

The spindle unit is designed with the ferrous material, in general. The spindle unit which consists of two parts, spindle body and gripping jig, will be installed between two HTS magnets and the magnetic field affects the gripping

jig. As shown in Fig. 3.5, the magnetic field at the target position will be changed and decreased, if the gripping jig was made of the ferromagnetic material. The magnetic field at the edge of the billet decreased to 0.1 T as shown in Table 3.1. It means the gripping jig of the spindle unit will be made of non-ferrous magnetic material like a stainless steel. All rotational metal are heated up under the magnetic field. The gripping jig will be heated and it should be minimized.

The target magnetic flux density at the center of the billet were increased about 21 %. The supporting base and the body of the spindle unit will be fabricated of the ferromagnetic materials and the gripping jig is fabricated with a stainless steel.

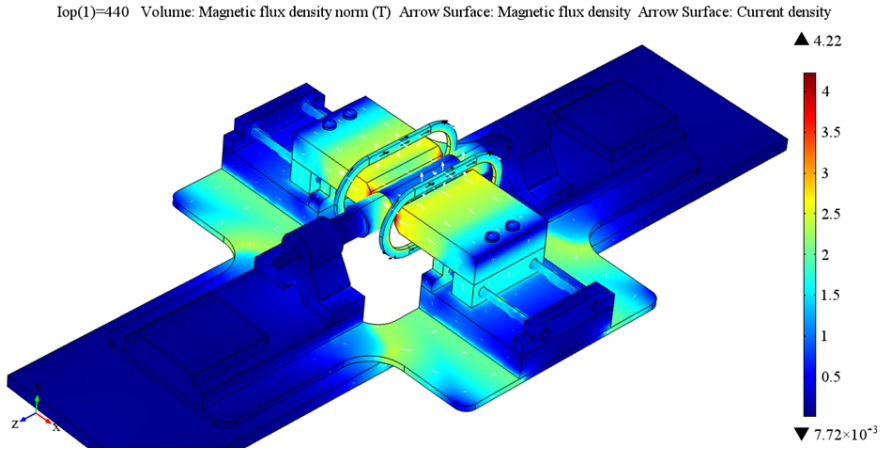

Fig. 3.5 The magnetic flux density distributions of the entire SIH considering the ferrous supporting and gripping units

Table 3.1 Analysis table of the magnetic flux densities of a SIH without or with the ferrous supporting metals and gripping unit

No.	Item	B_{edge}	B_{center}
1	The electromagnetic FEM simulation results for the SIH with HTS magnets and two iron cores	0.83 (T)	1.1 (T)
2	**With only supporting base made of ferromagnetic material**	**0.99 (T)**	**1.33 (T)**
3	With the supporting base and a rotating body of spindle unit made of ferromagnetic materials	0.98 (T)	1.31 (T)
4	With the supporting base, the spindle body and gripping jig all made of ferromagnetic materials	**0.1 (T)**	1.2 (T)

3.2 Design of the spindle unit

The spindle unit is designed by considering a high torque and low-speed rotation, in particular, focused on gripping method and jig shape for the metal billet. The gap between the HTS magnets is narrow and not enough space to install a gripping device. The closer two HTS magnets, the higher magnetic field we can get at the target position of the metal billet.

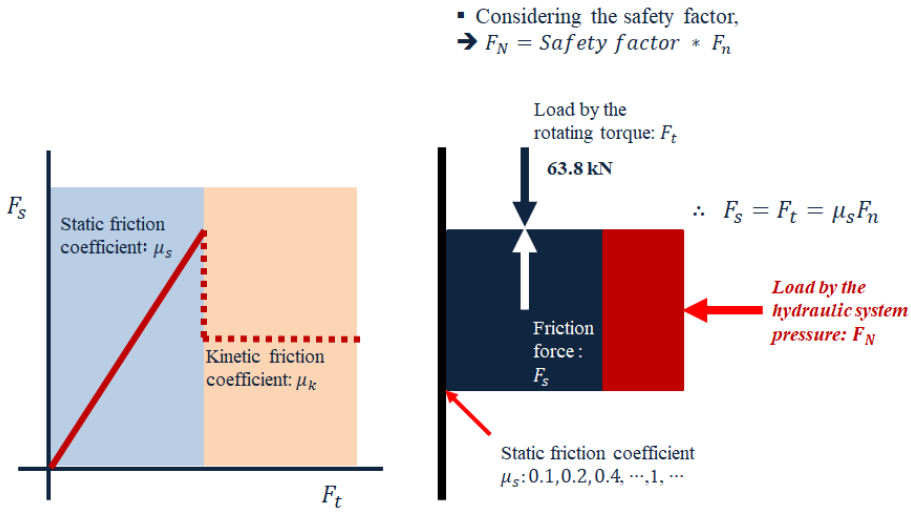

Fig. 3.6 An practical example for the friction force calculation of a SIH to grip the metal billet

The load by the hydraulic system pressure to grip the metal billet is calculated by the friction force calculation equation (3.1) and (3.2) as described in Fig. 3.6. The load by the rotating torque is calculated by the mechanical power equation. The friction force F_s should be always as high as the load F_t by the rotating torque. The load by the hydraulic system pressure F_N should be selected properly by considering a safe factor.

$$F_N = Safe\ factor \times F_n \tag{3.1}$$

$$F_s = F_t = \mu_s F_n \tag{3.2}$$

· Static friction coefficient: μ_s

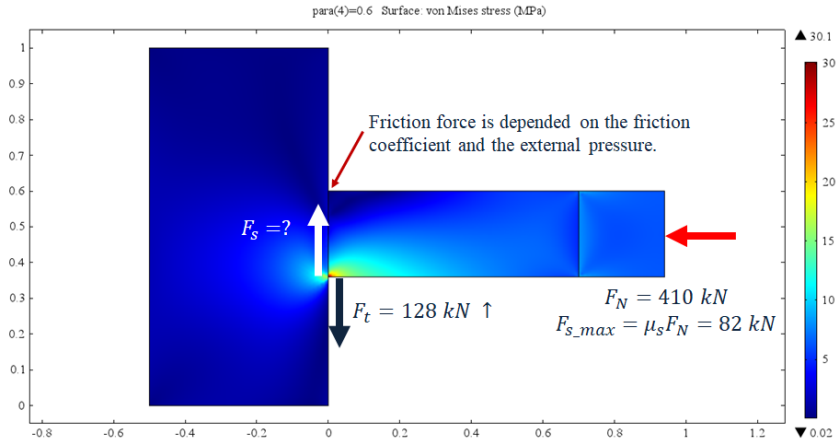

Fig. 3.7 An FEM simulation model for the friction force calculation of a SIH to grip the metal billet

A simple FEM model was developed to simulate the friction force to grip the metal billet. As shown in Fig. 3.7, If the F_t is higher than F_s, the model occurs the displacement. It means that the spindle unit doesn't grip the metal billet. So, The load F_N by the hydraulic system pressure is increased to get higher friction force between a gripper jig and the metal billet. The simulation results of the friction force calculation model for the spindle unit were presented in Fig. 3.8.

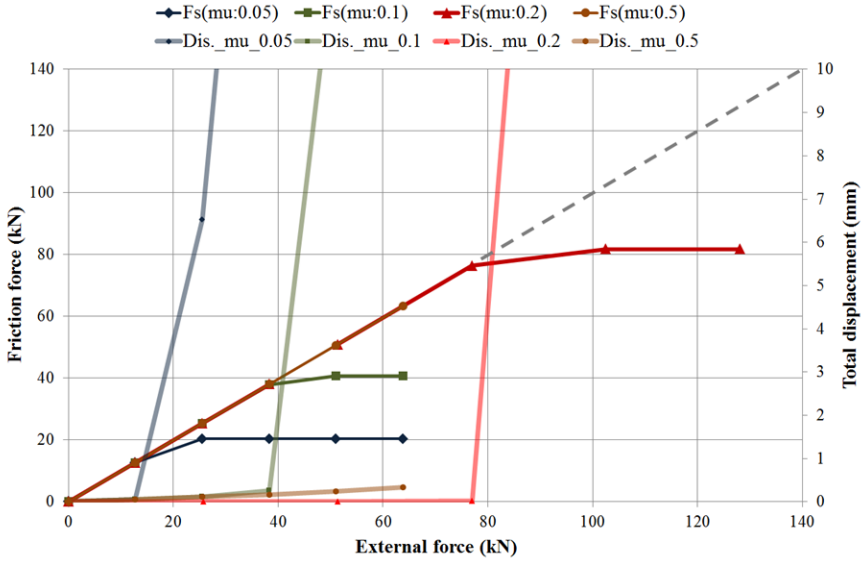

Fig. 3.8 The friction force curves of the FEM simulation results of a SIH gripper according to the external force increment

3.3 Specifications of a 300 kW-class SIH with HTS magnets

The 300 kW SIH was configured with three systems, a magnetic field generation system, rotating system, and loading and unloading system. A magnetic field generation system includes the HTS magnets, operating equipment, excitation and measurement devices. The rotating system has an induction motor, spindle unit to grip a metal billet and electrical devices for rotation. The loading and unloading system is important issue for total productivity improvement in coincidence with the process flow of customer's manufacturing line. Also, the detailed specifications of the SIH were described in this section.

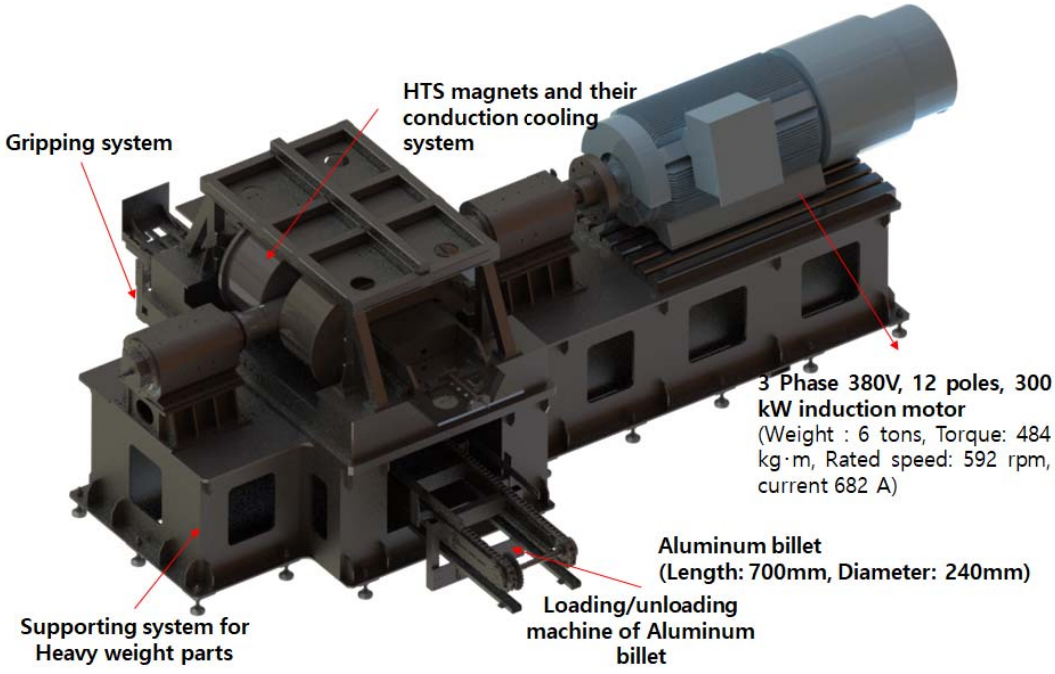

Fig. 3.9 3-dimensional design of a 300 kW-class superconduction induction heater

The three dimensional design of the SIH was shown in Fig. 3.9. The two HTS magnets and their conduction cooling system were designed to generate 1 T at the center between two HTS magnets with iron core. To achieve the heating power of a 300 kW-class for the aluminum billet, the 300 kW induction motor was selected for the order and has 12 poles to rotate the rated speed of 592 rpm. The rated rotating speed was decided to get uniform temperature deviation between the center and surface of the aluminum billet. And then, the spindle unit was designed to grip the aluminum billet without any slip. The spindle unit should keep the gripping force to endure a high torque of 500 kg·m of the aluminum billet. The hydraulic unit was installed to press the aluminum billet. To support all the devices including HTS magnets, the induction motor, and spindle units, the base was designed. Also, the base is a role of the magnetic path between two magnets to minimize the leakage magnetic field. The loading and unloading system were finally designed to load and unload the aluminum billet automatically. And then, the internal structure was indicated in Fig. 3.10.

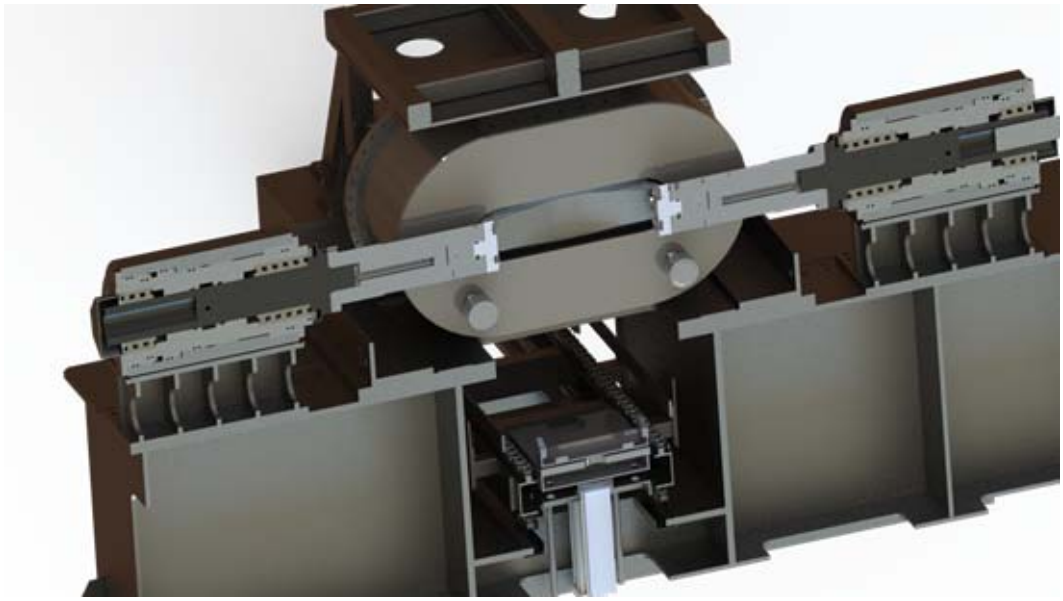

Fig. 3.10 3-dimensional internal structure design of a 300 kW-class SIH

As shown in Table 3.2, the SIH was designed for the 300 kW heating power capacities for Aluminum billet. This heater is possible to heat various metal billet including a stainless steel, copper and brass billet. The heater has 90 % of the energy efficiency. It means the total energy loss including the power to the magnet cooling, motor loss, hydraulic pump power and other electric power has 10 % in the case of the 300 kW SIH.

Table 3.2 Specifications of the 300 kW SIH

Parameter	Value
Heating Capacity	300 kW-class
System efficiency	~ 90%
Excitation current for the magnet	≤650 A @ 10 K (measured value)
Superconducting magnet type	HTS magnet, metal insulation, racetrack, a double pancake, iron cored type, stainless steel tape co-wound
Heating billet type	Aluminum billet, copper and stainless steel billets
Billet size	Max. Dia. 240mm x Max. length 700 mm
Maximum magnetic field at the center of the billet	1.3 T
Inductance of the magnets	1.6 H
Induction motor type	3 Phase 380V, 12 poles
Rotational speed	592 rpm
Total SIH size	Length 7.4m X Height 2.9m X Width 4.7m
Total SIH weight	45 tons

The excitation current to the magnets was tested to 650 A at 10 K. The minimum time to excite the magnets is 44 minutes up to 440 A with 0.1 A/s ramping rate. The excitation current of the 440 A generates 1 T of the magnetic flux density and it is a setting value to heat the aluminum billet to achieve a 300 kW heating power. To heat a stainless steel billet with a 300 kW heating power, the excitation current is set to 520 A. The maximum

inductance is measured to 1.6 H at the excitation current of 50 A. Two iron cores are installed with the HTS magnets and has magnetization characteristics. It makes a non-linear charging characteristics of the magnetic field .

The SIH has a controllable rotating speed range from 300 rpm to 600 rpm. It uses a induction motor made by HYOSUNG, Korea. The total machine size is as follow; length 7.4 m, height 2.9 m, and width 4.7 m. The maximum heating temperature is dependent on the metal billet

A 300 kW SIH is available to heat maximum temperature of 1,100 Celsius degree of the metal billet, but the heating time is dependent on the metal types. They have different material characteristics such as heat capacity, density, and relative resistivity. In the case of aluminium billet, it takes 180 seconds to heat 540 Celsius degree, whereas it takes 360 seconds for a stainless steel billet to heat up to 850 Celsius degree.

3.4 Simulation analysis of the SIH according to various metal billets

To heat a metal billet in the experiment, the heating simulation should be performed in advance to confirm the characteristics of temperature distribution, heating power and time..

3.4.1 Heating simulation results for a copper billet

The copper billet size is the outer diameter of 178 mm and the length of 700 mm and the mass, electric conductivity, heat capacity and thermal conductivity of the billet are dependent to the billet temperature. The surface of the billet has convective heat loss and the value was set to 100 $W/m^2 \cdot K$ of the forced heat flux. The rotating speed of the SIH is 600 rpm and the heating power is demanded to max. 450 kW. The temperature distribution and temperature curves at the several positions of the copper billet for 200 s were presented as shown in Fig. 3.11 (a) and (b). The temperature of the copper billet reached 1,080 Celsius degree. The next process is an extrusion and the final product is

a copper tube and bus bar etc

- Billet Size : OD178 x L700 mm, 171 kg
- Heating Condition : Heating sequence for 300 s (Heating: 200s, Holding: 100s), forced convection of 100 W/m^2·K
- Rotating Frequency : 600 rpm (10 Hz)
- Manetic field at the center of the metal billet : 0.81 T
- Heating Capacity : Max. 450 kW

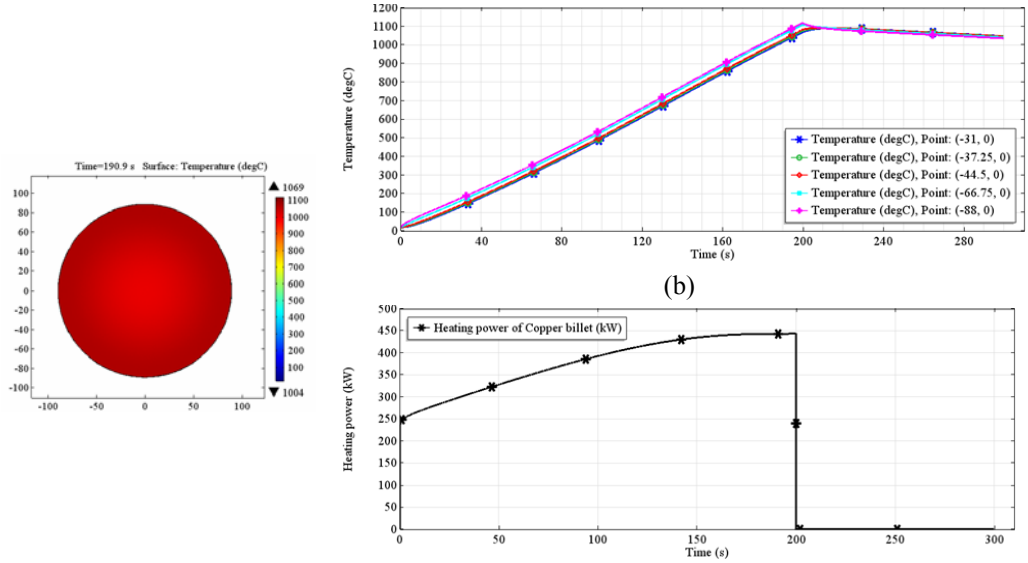

(a) (b) (c)

Fig. 3.11 (a) Temperature distributions of copper billet at the heating time of 190.9 seconds; (b) Temperature characteristic curve according to the heating time; (c) the input heating power curve for heating process of a copper billet

3.4.2 Heating simulation results for a brass billet

The brass billet size is the outer diameter of 178 mm and the length of 700 mm and the mass, electric conductivity, heat capacity and thermal conductivity of the billet changes to the billet temperature increment. The surface of the billet has convective heat loss and the value was set to 100 W/m2·K of the forced heat flux. The rotating speed of the SIH is 600 rpm and the heating power is demanded to max. 330 kW. The temperature distribution and temperature curves at the several positions of the copper billet for 160 s were presented as shown in Fig. 3.12 (a) and (b). The temperature of the brass billet reached to average 820 Celsius degree. The next process is an extrusion and the final product is a brass tube and so on.

- Billet Size : OD178 x L700 mm, 148 kg
- Heating Condition : Heating sequence for 260 s (Heating: 160s, Holding: 100s), forced convection of 100 W/m^2·K
- Rotating Frequency : 600 rpm (10 Hz)
- Magnetic field at the center of the metal billet: 0.72 T
- Heating Capacity : Max. 330 kW

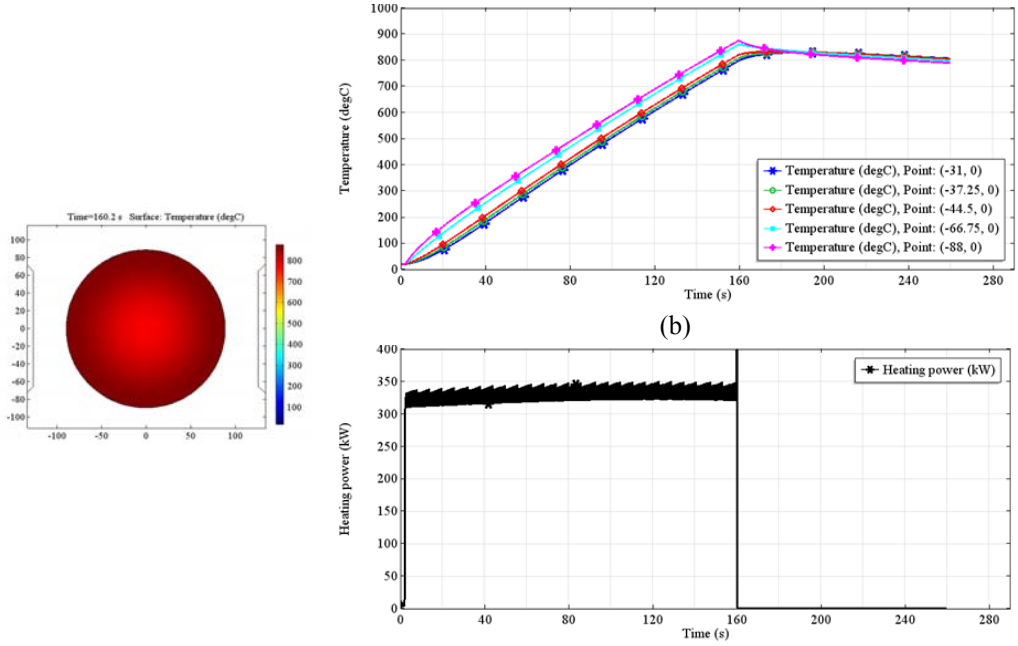

Fig. 3.12 (a) Temperature distributions of brass billet at the heating time of 160.2 seconds; (b) Temperature characteristic curve according to the heating time; (c) the input heating power curve for heating process of a brass billet

3.4.3 Heating simulation results for an aluminum billet

The aluminum billet size is the outer diameter of 178 mm, and the length of 700 mm and the mass, electric conductivity, heat capacity and thermal conductivity of the billet changes to the billet temperature increment. The surface of the billet has convective heat loss and the value was set to 100 W/m^2·K of the forced heat flux. The rotating speed of the SIH is 600 rpm and the heating power is demanded to average 300 kW. The temperature distribution and temperature curves at the several positions of the aluminum billet for 200 s were presented as shown in Fig. 3.13 (a) and (b). The temperature of the aluminum billet reached to average 480 Celsius degree for

the holding time of 20 s. The next process is an extrusion and the final product is a aluminum profiles or pipe and so on

- Billet Size : OD178 x L700 mm, 48 kg
- Heating Condition : Heating sequence for 200 s (Heating: 90s, Holding: 110s), forced convection of 100 W/m^2·K
- Rotating Frequency : 600 rpm (10 Hz)
- Magnetic flux density at the center of the metal billet : 0.72 T
- Heating Capacity : Average 300 kW

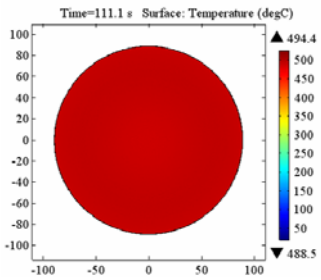

(a)

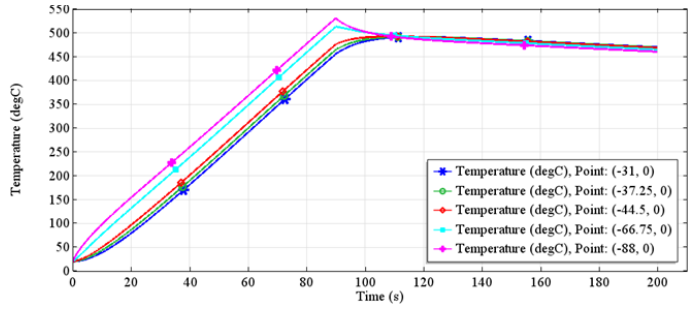

(b)

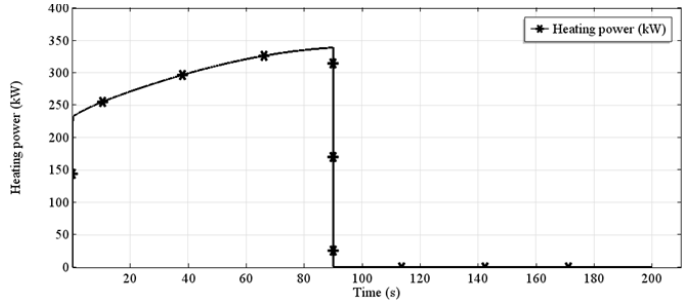

(c)

Fig. 3.13 (a) Temperature distributions of aluminum billet at the heating time of 111.1 seconds; (b) Temperature characteristic curve according to the heating time; (c) the input heating power curve for heating process of a aluminum billet

3.4.4 Heating simulation results for a STS billet

The STS billet size is the outer diameter of 178 mm, the inner diameter of 60 mm and the length of 700 mm and the mass, electric conductivity, heat capacity and thermal conductivity of the billet changes to the billet temperature increment. The surface of the billet has convective heat loss and the value was set to 100 W/m^2·K of the forced heat flux. The rotating speed of the SIH is 1,200 rpm and the heating power is demanded to max. 1,100 kW. The temperature distribution and temperature curves at the several positions of the

STS billet for 200 s were presented as shown in Fig. 3.14 (a) and (b). The temperature of the STS billet reached to average 961.5 Celsius degree for the holding time of 100 s. The next process is an extrusion and the final product is a stainless seamless tube or pipe and so on.

- Billet Size : OD178 x L700 mm, ID60mm Hole, 134 kg
- Heating Condition : Heating sequence for 200 s (Heating: 100s, Holding: 100s), forced convection of 100 $W/m^2 \cdot K$
- Rotating Frequency : 1,200 rpm (20 Hz)
- Magnetic flux density at the center of the metal billet: 1.31 T
- Heating Capacity : Max. 1,100 kW

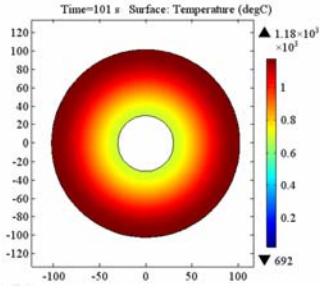

(a)

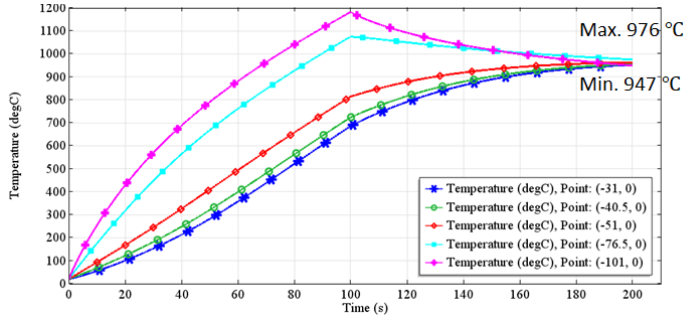

(b)

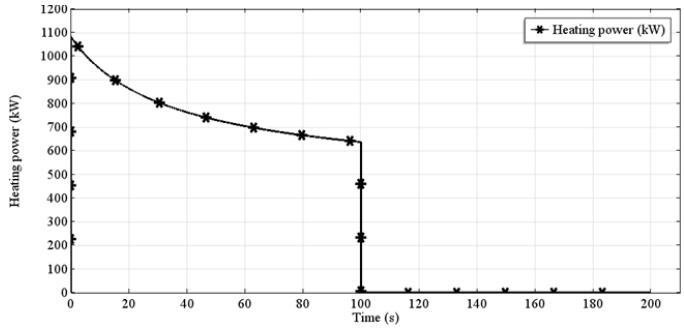

(c)

Fig. 3.14 (a) Temperature distributions of stainless steel billet at the heating time of 101 seconds; (b) Temperature characteristic curve according to the heating time; (c) the input heating power curve for heating process of a STS billet

CHAPTER 4

MANUFACTURE OF THE SIH

This SIH consists of three systems mainly. First, the HTS magnets with iron cores and their conduction cooling system generate the uniform and strong magnetic flux density. It includes additional devices such as DC power supplier for the excitation, cryo-coolers with compressors and chiller with water circulation for them. The magnetic flux density to get a 300 kW heating power is 1 T and it is possible to generate 1.3 T. Second, the spindle unit makes a heat for various metal billets. It includes the 300 kW induction motor with a 450 kW class inverter, gripping devices to rotate the metal billets and a hydraulic supply unit. Third, the loading and unloading system including the supporting base supplies the metal billet and drawing the heated metal billet to the next process.

4.1 Manufacture process

In this section, the manufacturing process of the SIH is introduced in detail. The supporting base, which is made of the ferromagnetic material, was installed as shown in Fig. 4.1, firstly. Two spindle units with hydraulic system of the SIH was installed and adjusted by checking the concentric arrangement of them as shown in Fig. 4.2. This unit is rotating system to heat metal billet as heat energy source. Two hydraulic spindle units hold the metal billet and keep it rotate possible with holding pads. Holding pads retain appropriated friction with the force as strong as the rotating torque during the rotation. In addition, it measures the length of the metal billet prior to the heating process and check whether the product is well gripped. The induction motor rotates the metal billet mechanically and the induced current is generated inside the billet,

electrically. The heating energy is transferred to the metal billet. The 300 kW-class induction motor was fixed on the base and connected to one of the spindle unit with a coupling. The HTS magnets connected in parallel was set up to the base by fixing the supporters as shown in Fig. 4.3.

As a core unit of the SIH, it generates the uniform magnetic field through the metal billet. The HTS magnets with iron cores are located in parallel as shown in Fig. 4.4. The operation of the magnets is very reliable, because they adapted the metal insulation method and the cooling temperature of the magnet was kept stable during the excitation process.

Fig. 4.1 The supporting base installation of a SIH

Fig. 4.2 The installation of the rotational motor and the spindle unit with hydraulic system of a SIH

Fig. 4.3 The installation of two HTS magnets of the SIH

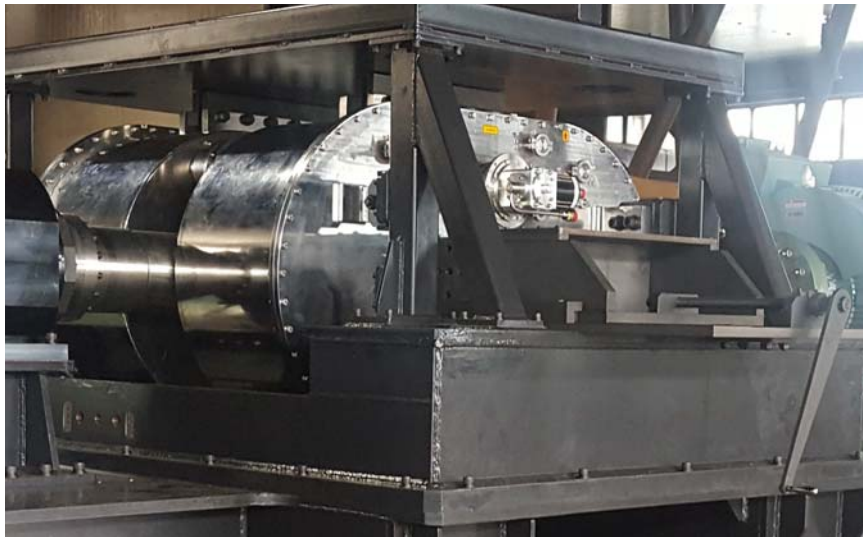

Fig. 4.4 The installation of two iron cores for the HTS magnets

The next component is loading and unloading system. The loading and unloading system functions to locate the metal billet at the specific position for rotation after loading, and then the billet is unloaded through a conveyor unit after heating was completed as shown in Fig. 4.5. These loading and unloading units are changeable to customer requirement conditions

Fig. 4.5 The installation of loading and unloading units of a SIH

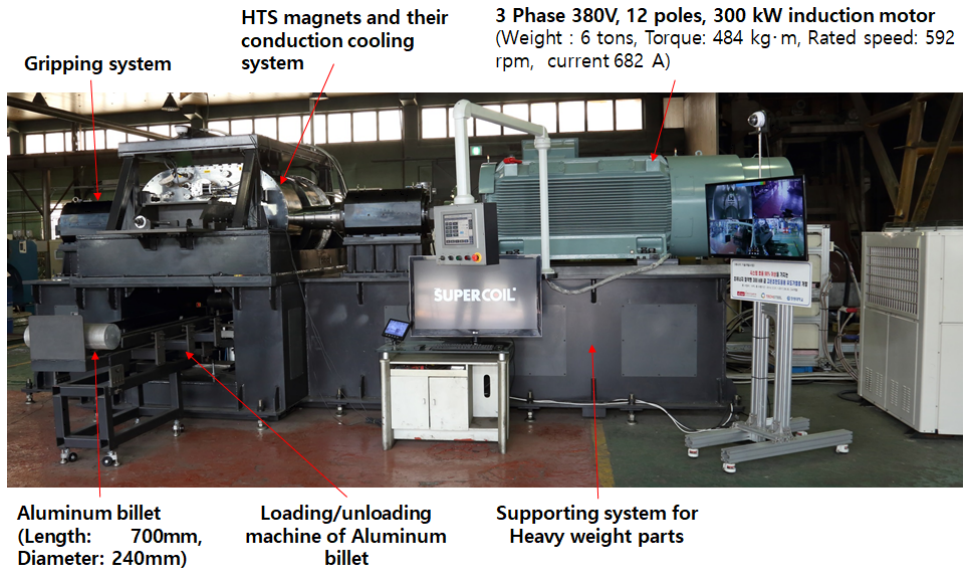

Fig. 4.6 The entire machine view of a SIH

As shown in Fig. 4.6, the entire machine was assembled all. The HTS magnets, spindle unit, induction motor and supporting base including loading and unloading machine for the metal billet were composed. The monitoring system was installed with four recordable cameras, four non-recordable cameras and the measurement system.

4.2 Composition and explanations of the SIH

The SIH is composed with the several devices as described in the previous section. The machine configuration as shown in Fig. 4.7 introduces the system composition. The monitoring and operation system of the SIH control the SIH with HTS magnets and rotating motor including loading and unloading system.

In this section, the all components are described in detail. These are components list of the SIH; HTS Magnets with iron cores including a cryogenic conduction cooling system, the spindle units with hydraulic pump system and induction motor.

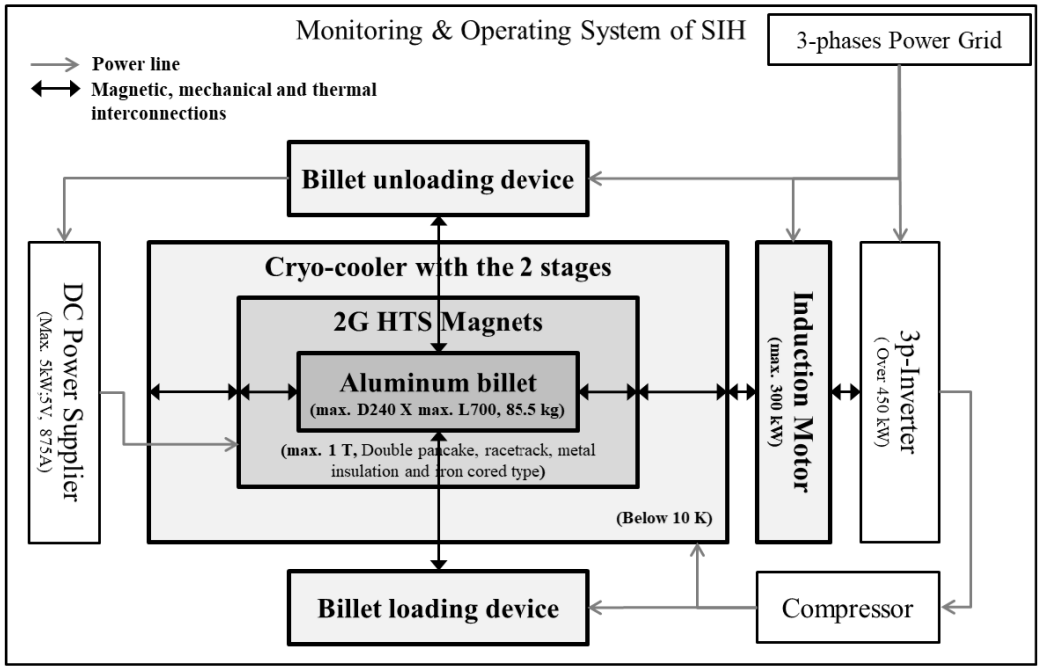

Fig. 4.7 The machine configuration of the SIH

4.2.1 The HTS magnets with iron cores

The first component is the HTS magnets with iron cores to generate the magnetic field. As a core unit of SIH, the HTS magnets, a pair two magnet with opposite polarity, is located in parallel at the both side of metal to be heated, of which the location is adjusted. They adapted the metal insulation

method and the cooling temperature of the magnet was kept stable under 10 K during the excitation process. The iron cores are located in the center of the HTS magnet to concentrate the magnetic field and fixed on the ferromagnetic base, solidly. The HTS magnets was operated under the conduction cooling system, which is made of a vacuum chamber and a cryo-cooler including several feed-throughs.

Fig. 4.8 The HTS magnets with iron cores

4.2.2 The spindle unit with a hydraulic pump system

Two spindle units with a hydraulic pump system are provided to hold and rotate the metal billet desired to heat as shown in Fig. 4.9 (a) and (b). The spindle units take care of holding and rotating the product, and prevent the slip of the metal billet with holding pads while retaining appropriated friction between the metal billet and holding pads during the heating process. In addition, the spindle units can measure and check the length of the metal billet whether the metal billet has a proper length to heat or not.

Two spindle units individually are operated with the proper pressure for

holding of product. The larger diameter of billet, the bigger force is required to hold the billet. When the diameter of billet is relatively small, the less force is required. The maximum pressure of the hydraulic pump units were designed to meet various products.

(a) (b)

Fig. 4.9 (a) The spindle unit with a gripper operated by (b) the hydraulic pump system

Fig. 4.10 The induction motor for rotating the metal billet using spindle unit

4.2.3 The induction motor for rotating the metal billet

The induction motor is a core equipment for heating the metal billet located under the uniform magnetic field. The electric power capacity of the induction

motor is directly converted to the heating power capacity of the metal billet. To shorten the heating time, the power capacity of the induction motor should be increased. The low speed and high torque condition makes the billet minimize the temperature deviation between the center and surface of the billet. The numbers of motor poles are related with the rotation speed. The induction motor for the 300 kW SIH was selected to 12 poles to achieve the rated speed of 592 rpm.

4.2.4 The loading and unloading unit for the metal billet

The loading and unloading system functions to locate the metal billet at the specific position for rotation after loading, and then the billet is unloaded through a conveyor unit after heating was completed as shown in Fig. 4.11.

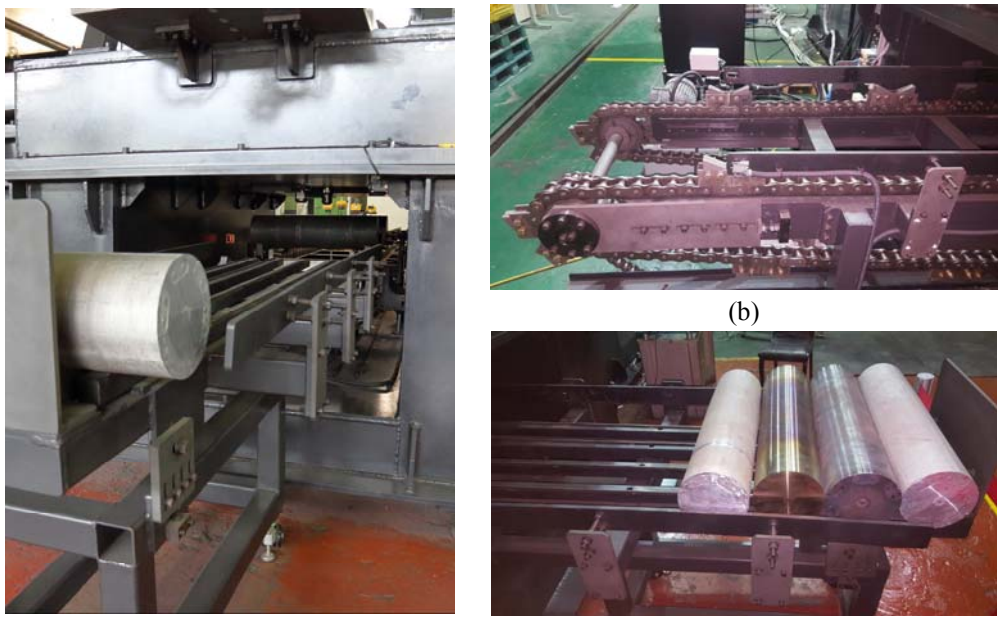

(a) (b) (c)

Fig. 4.11 (a) A view of the automatical loading and unloading unit for the metal billet; (b) a loading position of the metal billet with a conveyor system; (c) an unloading position of the metal billets

4.2.5 The main electric power supply system and operational panel

The main electric power supply system was composed for operation of the SIH as shown in Fig. 4.12. All the electric power sources including the inverter to control the induction motor are connected to the main system to measure the efficiency of the SIH. The power for the HTS magnets operation was supplied from the main power supply system. The watt-hour meter was set to the receiving point of the electric power supply line and measured in the real time. The operational panel is possible to control the SIH including loading and unloading process, gripping process, rotating process and emergency process and so on.

(a) (b) (c)

Fig. 4.12 (a) Electric box; (b) 450 kW-class inverter module; (c) Control panel for operation of the SIH

4.2.6 The measuring and monitoring system of the SIH

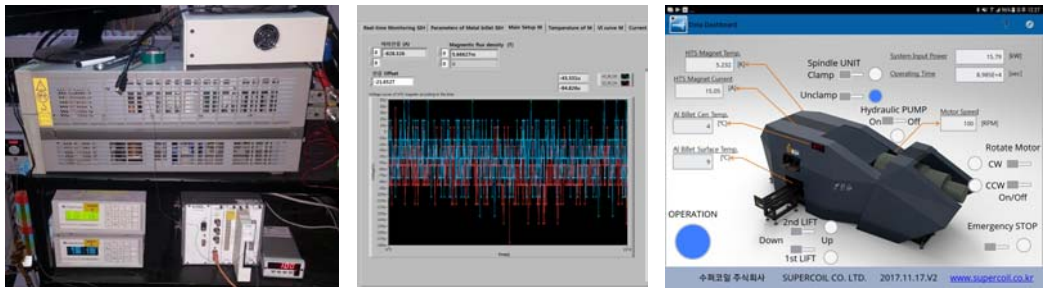

(a) (b) (c)

Fig. 4.13 (a) Measuring system for the HTS magnets; (b) Monitoring system for the HTS magnets; (c) Real-time monitoring and control system of the SIH

The measurng and monitoring system of the SIH is composed of two parts, such as the excitation system of the HTS magnets and the monitoring and control system of the SIH. The excitation system configuration consists of DC power supply, DC current controller, temperature monitors, signal measuring instruments and the monitoring system as shown in Fig. 4.13(a) and (b). The monitoring and control system of the SIH consists of the PLC, the main server computer and a Tablet PC for the remote control as shown in Fig. 4.13(c).

4.2.7 Video monitoring and recording system

The SIH is provided with the video monitoring and recording system to check and confirm the operation status on a real time basis. The operation movies are stored and checked in the real-time with remote control. The SIH are continuously operated with the real-time camera installed by each process as shown in Figs. 4.14 and 4.15.

Fig. 4.14 Real-time video monitoring and recording system for the SIH operation

Fig. 4.15 Operation monitoring units by each process, loading, heating and unloading processes

4.3 Heating operational process of the SIH

The SIH is operated with the heating operation process as shown in Fig. 4.16. First, the metal billet is loaded through the conveyor system. And then, the up-down cylinder unit locates the metal billet to the specific position under the uniform magnetic field. Third, the spindle unit grips the metal billet with hydraulic press process and the induction motor rotates the spindle unit with the metal billet. The rotating process takes 86% of total heating process cycle time as shown in Fig. 4.17. This is the main heating process. After the heating process, the heated metal billet was unloaded.

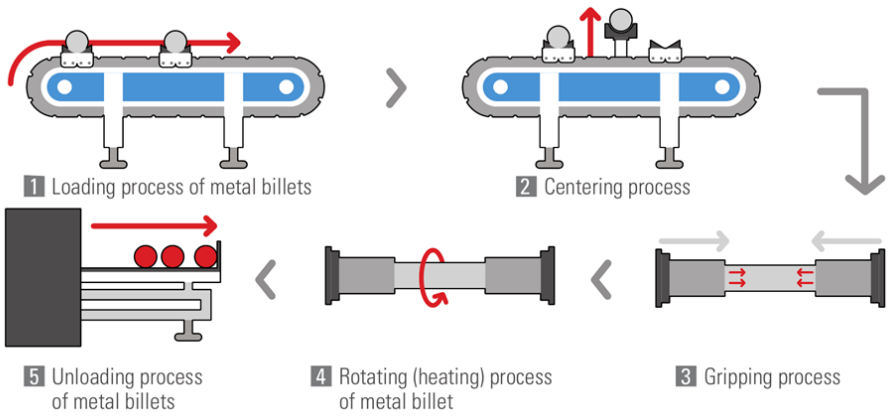

Fig. 4.16 The operation process of a SIH

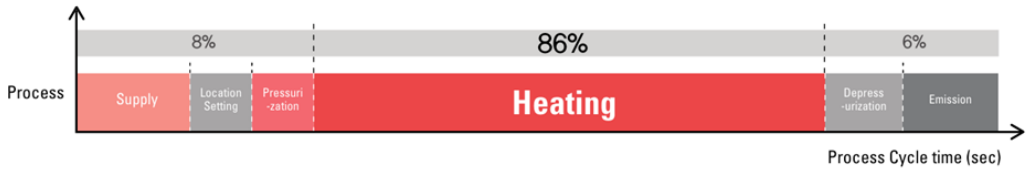

Fig. 4.17 The heating sequence of a SIH

The rotating process, which is called the heating process, is described in Fig. 4.18. The rotational speed increases at the starting section. In the main heating section, the metal billet keeps the rated speed and the induction motor maximizes the heating power. At that time, the temperature of the metal billet almost reached the target temperature and the rotating speed decreases to minimize the temperature deviation between the center and surface of the billet. If the temperature reached the target temperature, the induction motor is stopped and the heating process is terminated.

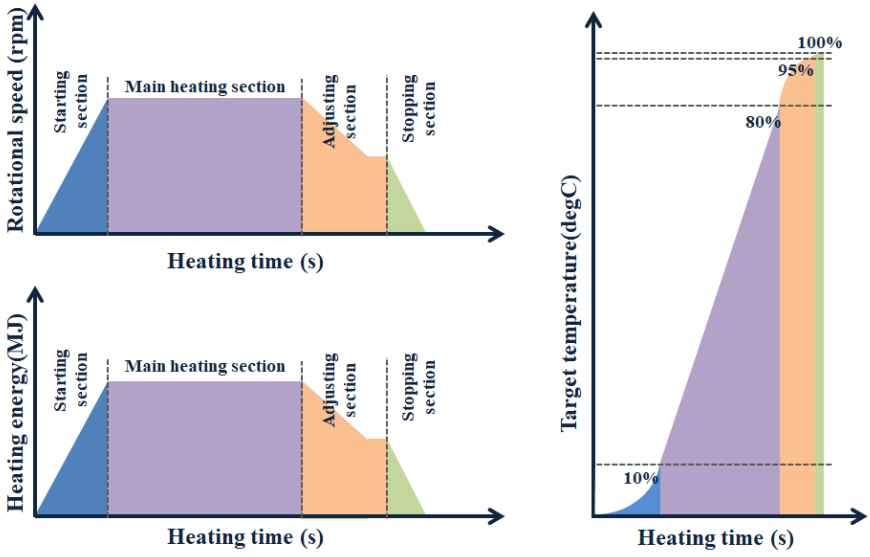

Fig. 4.18 Rotational speed, heating energy and temperature graphs in heating sequence in detailed

CHAPTER 5

PERFORMANCE ANALYSIS AND EVALUATION OF the SIH

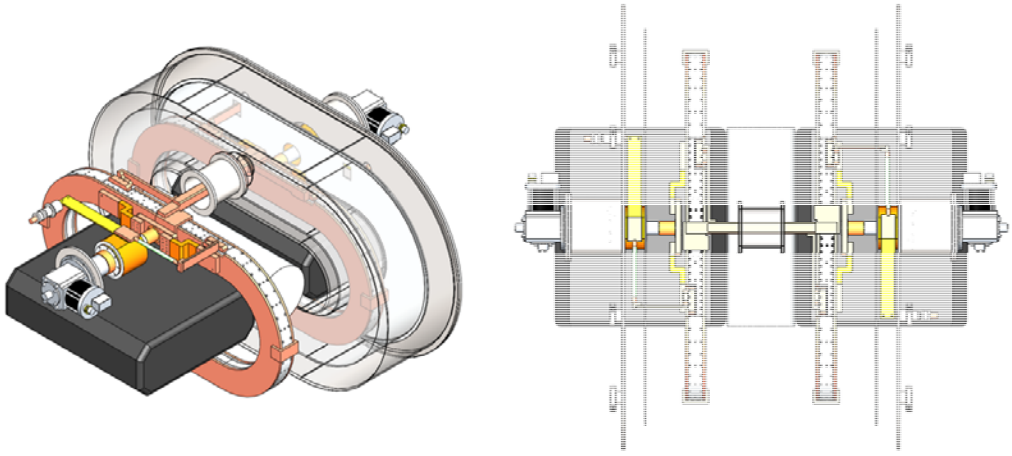

(a) (b)

Fig. 5.1 Design of the HTS magnets with iron cores; (a) 3D view of the HTS magnets; (b) A plane view of the HTS magnets

5.1 Basic performance of the HTS magnets

To design the cryostat of the HTS magnets for the 300-kW-class SIH, the cryogen-free conduction cooling method was applied using the 2nd stage Gifford-McMahon (GM) cryo-cooler as shown in Fig. 5.1. This cryo-cooler was used because of its small size, simple operation, and high reliability. The HTS magnets consisted of two double pancake coils (DPC) with an iron core and

metal insulation [77-80]. Table 5.1 shows the basic design specifications of the HTS magnets. A 12 mm-wide HTS tape was used, and the magnet was wound with 300 turns. In this section, we presented the 2nd stage cryostat performance test results for the conduction cooled-type cryostat for the HTS magnets.

Table 5.1 Basic design specifications of the HTS magnets

Parameter	Value
HTS tape maker	SuNam, Korea
HTS tape (Width × Thickness)	W12.1 (±0.1) mm × T100 (±15) μm
SUS tape (Width × Thickness)	W12 mm × T100 μm
Minimum critical current (@77 K)	≥600 A (copper laminated)
Substrate material	Stainless steel
HTS magnet type	MI, racetrack, double pancake, iron-cored type
Size (Radius × Length)	R220 mm × L625 mm
Number of turns	300
Total length of the HTS tape	3,407 m
Estimated critical current at 30 K (I_c)	520 A
Operating current (I_{op})	440 A (Iop/Ic=0.85)

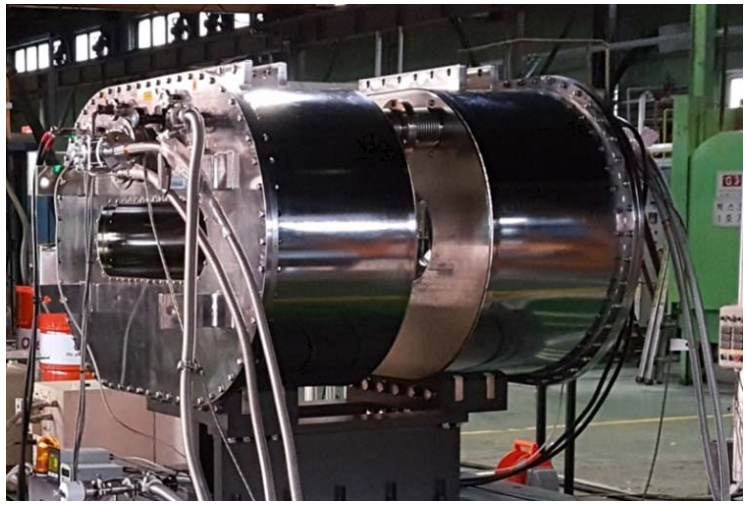

Fig. 5.2 The real fabrication of the HTS magnets with the conduction cooling method using the second stage cyro-coolers

5.1.1 Conduction cooling test and results

The HTS magnets with the conduction cooling method using the second stage cyro-coolers were fabricated as shown in Fig. 5.2 [81-85]. To perform the cooling test with no load condition, the system utilities including the compressors, chiller and cooling pipes were installed. The measurement devices including temperature monitor and data acquisition unit were set beside cryostat. And then, the cooling was proceeded with no load condition. The results were shown in Fig. 5.3. The total cooling time took 2 days and 14 hours. The temperature at the 1st stage of cryo-cooler was saturated at 42.3 K. Temperatures of the 2nd stage was cooled down and saturated at 5.2 K.

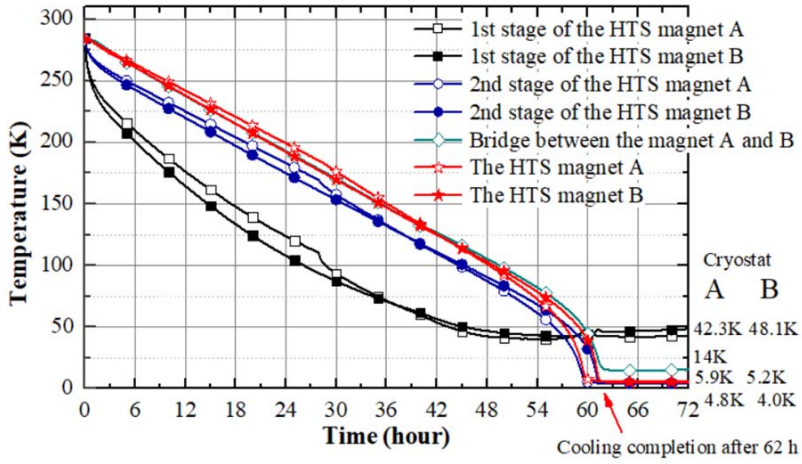

Fig. 5.3 Temperature curves of the superconducting magnets on the cooling down process

The warm-up was proceeded without any heater power. The results were shown in Fig. 5.4. The totally warm-up time took almost 14 days.

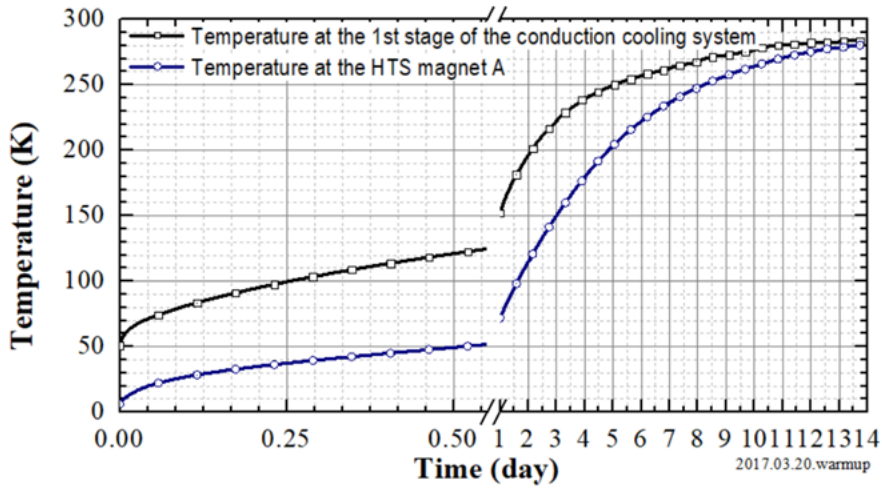

Fig. 5.4 Temperature curves of the superconducting magnets on the warm-up process

5.1.2 Cooling performance results during long-term operation

The cooling power for the cryogenic conduction cooling system was measured to almost 15 kW and the chiller power to water circulation system for two compressors was measured to about 10 kW as shown in Fig. 5.5. The chiller was operated periodically. The temperatures of the 1st stage and the 2nd stage were monitored for 74 hours as shown in Fig. 5.6. The temperature at the 1st stage of the conduction cooling system was changed periodically by the room temperature of the day and night in the winter. The temperature variation between the max. temperature and the min. temperature was analyzed to about 1 K. Also, The 2nd stage temperature was changed to the surrounding temperature of the cryostat, too. But the temperature variation is below 0.1 K. The radiation heat invasion affects little the 2nd stage temperature. As shown in Fig. 5.7, the temperatures of the 1st stage and the 2nd stage of the cryogenic cooling system were measured for 11 days.

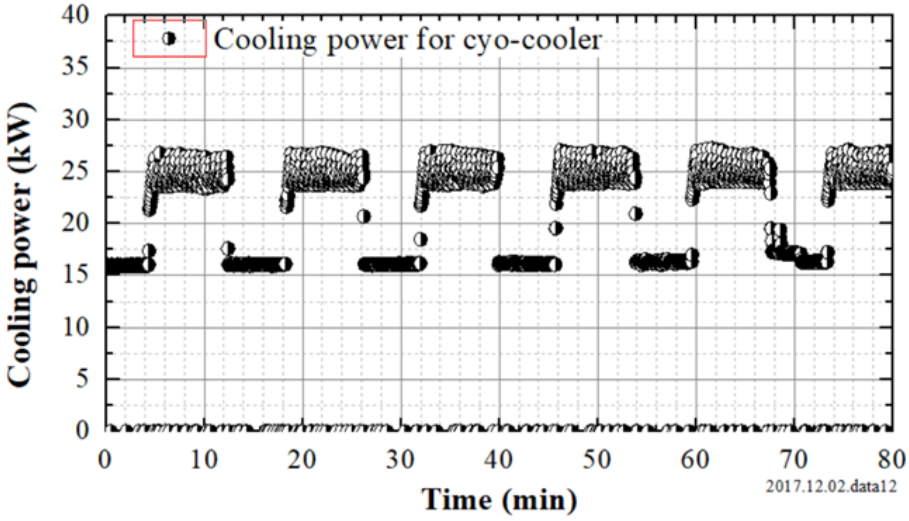

Fig. 5.5 A dissipation power curve for cooling the superconducting magnets

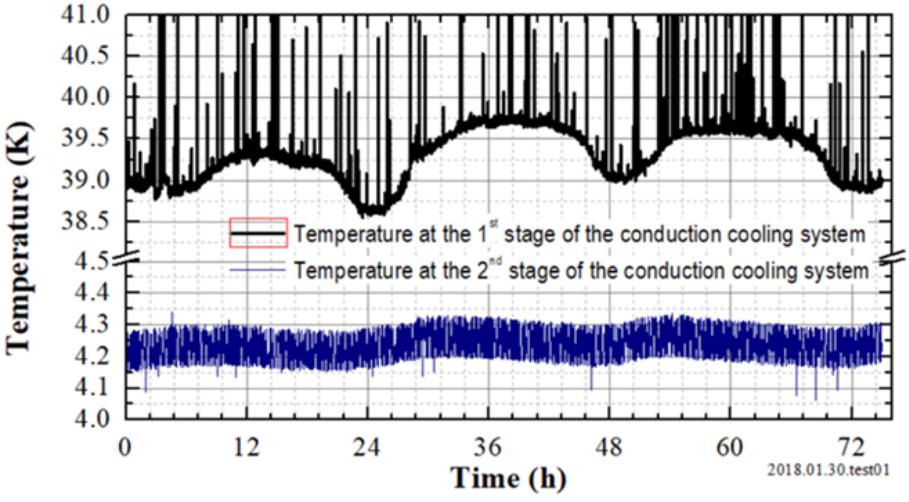

Fig. 5.6 The temperatures of the 1st stage and the 2nd stage monitored for 74 hours

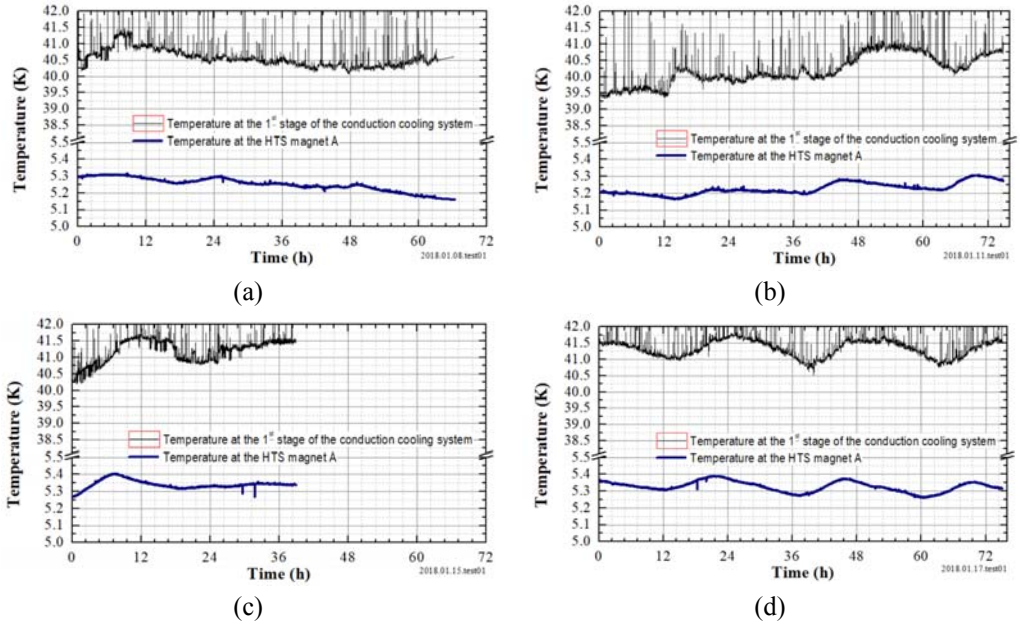

Fig. 5.7 The temperatures of the 1st stage and the magnet A of the cryogenic cooling system for long-term operation

5.1.3 Excitation test and results

First, the HTS magnet excitation test was performed without iron cores. One of two HTS magnets, HTS magnet A, was estimated to have an inductance of 528 mH without an iron core. An characteristic resistance of the non-insulated HTS magnets is a parallel resistance to the magnet, and is calculated by the rate of the inductance divided by the time constant. The characteristic resistance was calculated to 23.6 mΩ. Therefore the time constant to the charge magnetic field was calculated to 22.4 s. As shown in Fig. 5.8, the maximum magnetic field at the center of the HTS magnet A is 1.02 T at 540 A of the input current. And the maximum magnetic flux density at the center between two HTS magnets is 0.69 T at the same current.

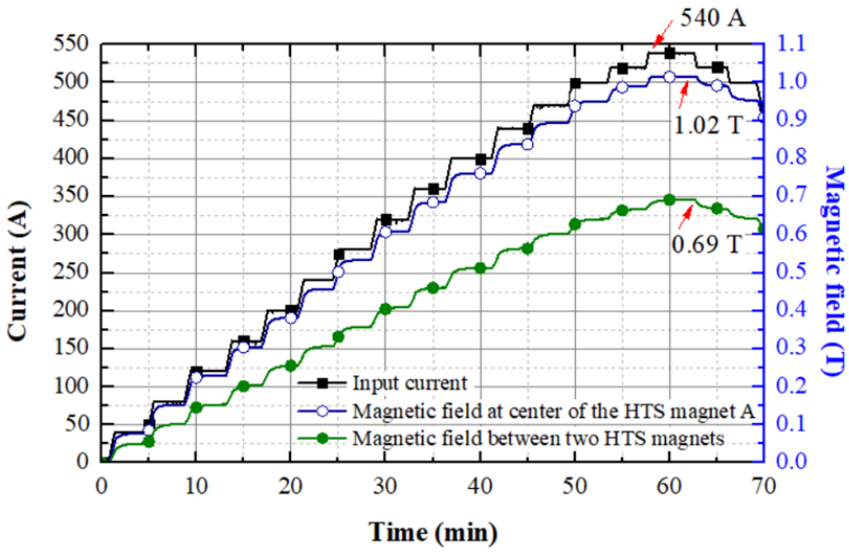

Fig. 5.7 Magnetic field and excitation current curves of the superconducting magnets without iron cores

Second, the excitation test was performed with iron cores installed on the SIH. When the current was supplied into the magnets with a 0.3 A/s ramping rate up to 440A, the magnetic field increased as the magnetization characteristics of the iron yokes. The magnetic flux density at the center between two HTS magnets was measured as 0.75 T at the input current of 140 A. And the maximum magnetic flux density was measured as 1.3 T. All the magnet temperatures are stable during the operation. The terminal voltages increased with inductive voltage and the magnetic field at the center between the two HTS magnets like Fig. 5.9 was saturated every ramps as shown in Fig. 5.10.

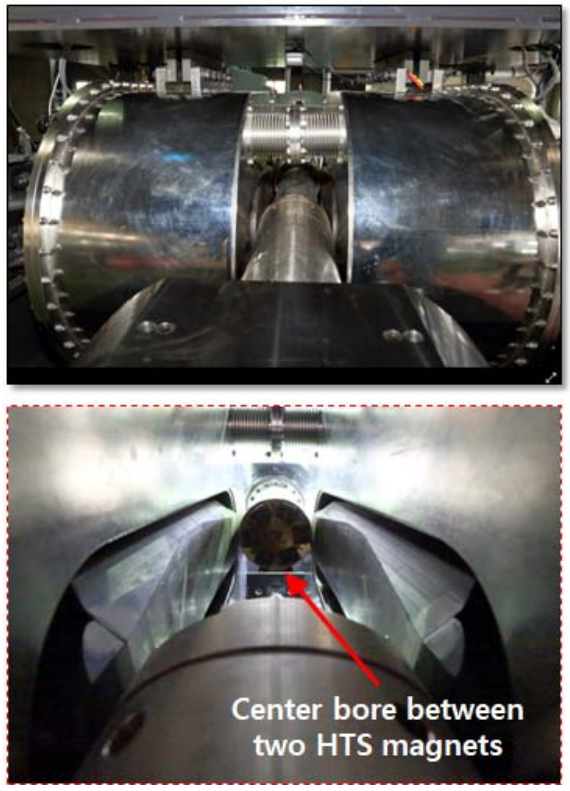

Fig. 5.9 The HTS magnets with iron cores and the metal billet located at the target position

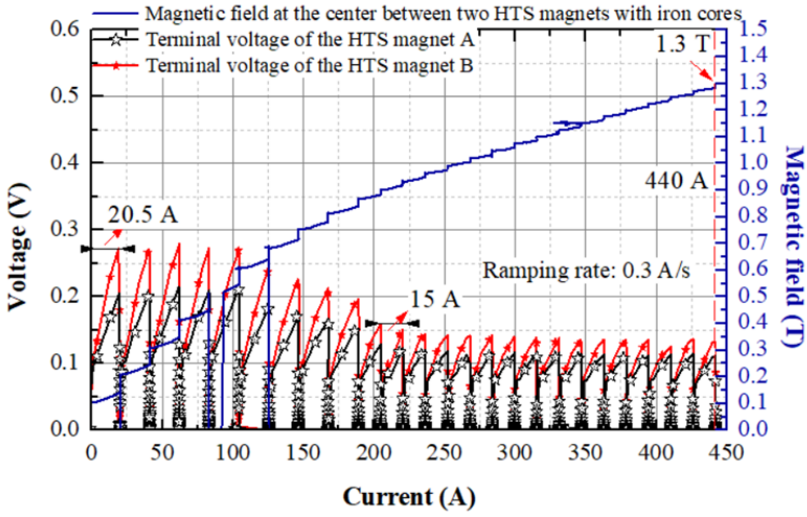

Fig. 5.10 Magnetic field and terminal voltage curves of the superconducting magnets with iron cores

The terminal voltages of two HTS magnet with iron cores was measured according the time as shown in Fig. 5.11. The excitation current ramps up with 0.1 A/s up to 200 A. The inductive terminal voltage of the two magnets were presented, too. The magnetic flux density at the center of two HTS magnets was measured and presented in Fig. 5.12.

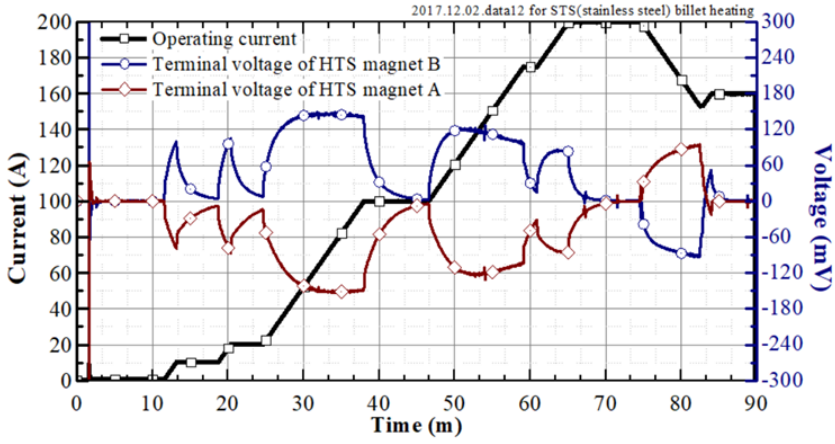

Fig. 5.11 Terminal voltage and excitation current curves of two HTS magnets with iron cores according to operation time

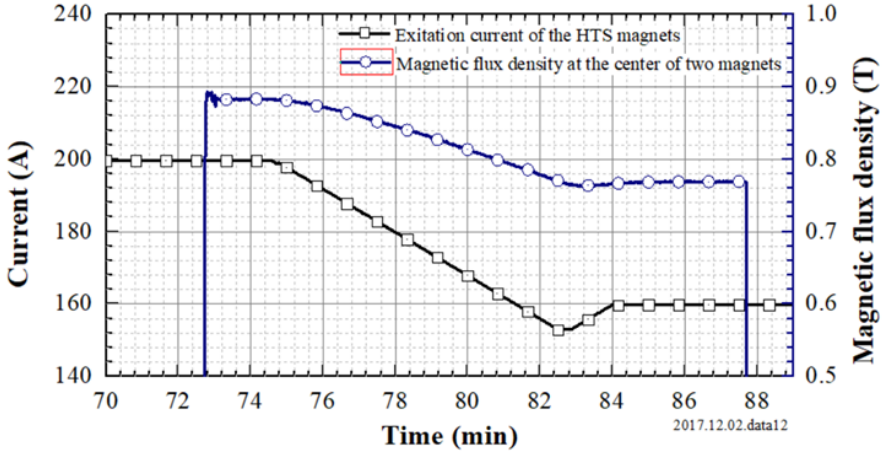

Fig. 5.12 Magnetic flux density at the center of two magnets with the excitation current according to operation time

The terminal voltages of two HTS magnets with iron cores was measured according the time as shown in Fig. 5.13, when the excitation current ramped up with 0.1 A/s until 160 A. At the time, the temperature of the magnet A was indicated, too. As shown in Fig. 5.14, the magnet temperatures, the temperature of the 1st and 2nd stages and the current lead temperatures were presented. The temperatures are all stable after the ramping was finished.

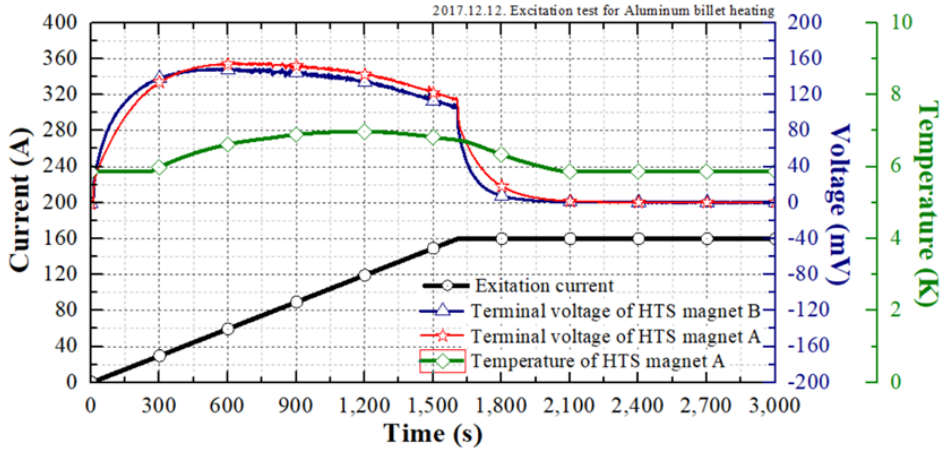

Fig. 5.13 Terminal voltages of two HTS magnets with the magnet A's temperature and the excitation current according to the time

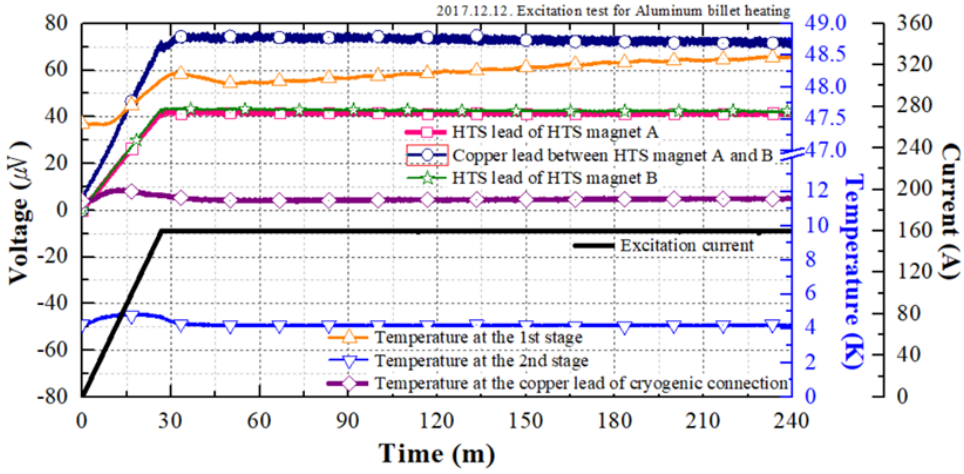

Fig. 5.14 Temperature and other curves of the 1st stage and the 2nd stage during the excitation process

5.1.4 Over-current test and results

To secure the operational reliability of the high-Tc superconducting magnets in the metal industries, the excitation test was performed by inputting current to the magnet, even though the quench occurs as shown in Fig. 5.15. The HTS magnets were excited with the current ramping rate of 0.05 A/s.

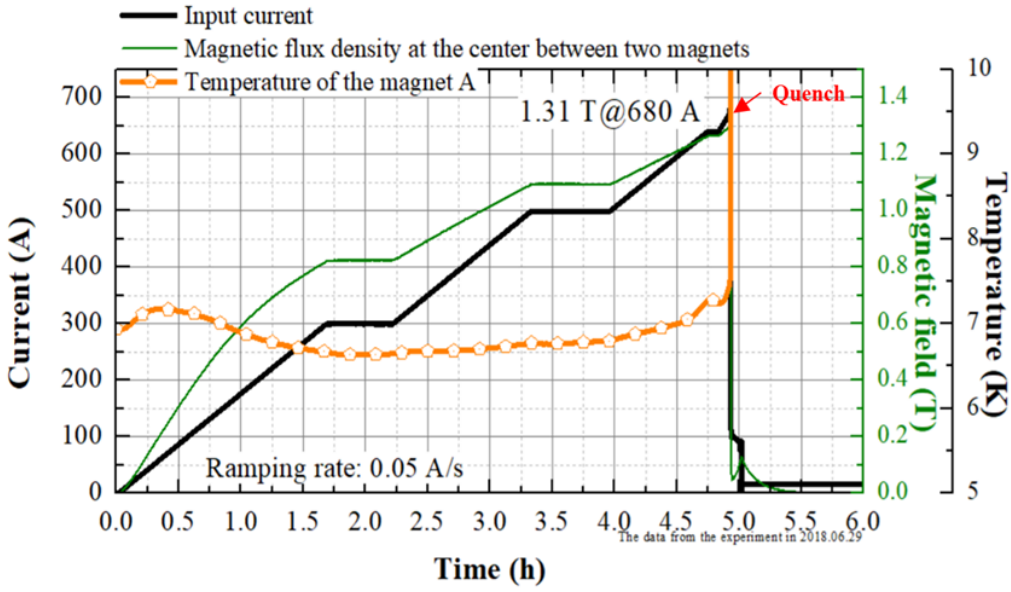

Fig. 5.15 The excitation current and magnetic flux density curves of the HTS magnet A

During the excitation test, the magnetic flux density at the center between two magnets was measured. The temperature of the HTS magnet A was monitored. When the quench occurred, the magnet A's temperature increased sharply up to 42 K owing to discharging the magnetic energy of the magnets, but the 1st stage temperature decreased as shown in Fig. 5.16, because the excitation current decreased to 20 A, suddenly.

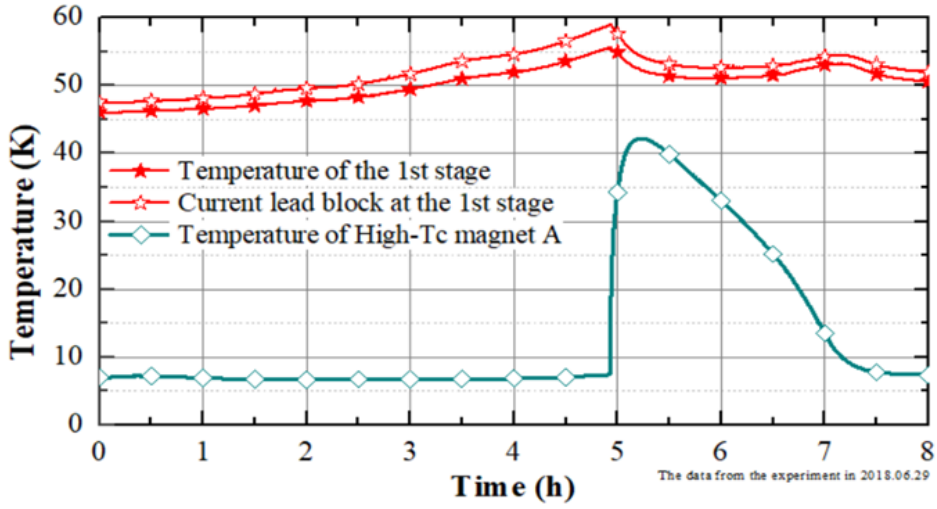

Fig. 5.16 Temperature curves of the magnets under the conduction cooling system before and after the quench

Terminal voltages of the HTS magnets were measured in real time while the input current of 300 A was excited. When the excitation current is to 50 A, the total inductance has the highest value of 1.6 H because of the magnetization characteristics of iron cores. The maximum magnetic flux density at the center between two HTS magnets was recorded to 1.31 T at the current of 680 A. When the excitation current passed through 600 A, the terminal voltage of the HTS magnet A is unstable and then, the quench was occurred at 680 A of the current. The magnetic energy was discharged in full flood as shown in Fig. 5.17. At that time, the magnet cover temperature increased to 42 K, but, the HTS wire temperature increased to more higher temperature. The insulation material is a stainless steel tape. The temperature change is slow because of the low thermal conductivity. The two HTS magnet was not damaged and returned to normal state after the recovery of the cooling temperature, because the magnet was fabricated with metal insulated winding method.

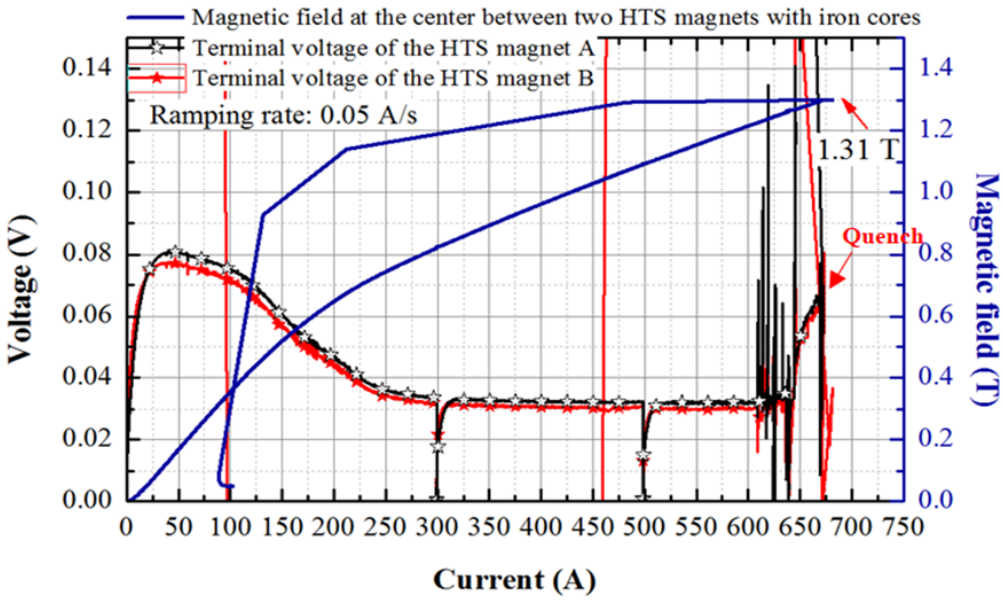

Fig. 5.17 Terminal voltages curves of two magnets before and after the quench

5.2 Heating test of the performance evaluation 1; the aluminum billet

Fig. 5.18 The SIH for test of the performance analysis of various metal billets

The 300 kW SIH as shown in Fig. 5.18, called as a preheating furnace, heats a round metal billet for forging and extruding products. In this operation test, the aluminium billet (AL6061) was used. The billet length is 700 mm and the diameter is 228.6 mm; 9 inch, and the weight is 77.6 kg. To calculate the machine efficiency, the final temperature of the aluminium billet and the total input electrical energy from the source should be measured.

Fig. 5.19 A picture of an heated aluminum billet of a SIH operation at specific time

Two thermocouples were installed at the center hole of the aluminium billet and at the loading jig for measuring the surface temperature of the aluminium billet, respectively. The aluminium billet was heated up for 180 seconds after the motor starting as shown in Fig. 5.19. It takes 25 seconds for the induction motor to reach the rated speed of 592 rpm. After 180 seconds including motor starting time, the motor was terminated within 20 seconds. The pictures of the aluminium billet taken by thermo-graphic camera during heating process were shown in Fig. 5.20.

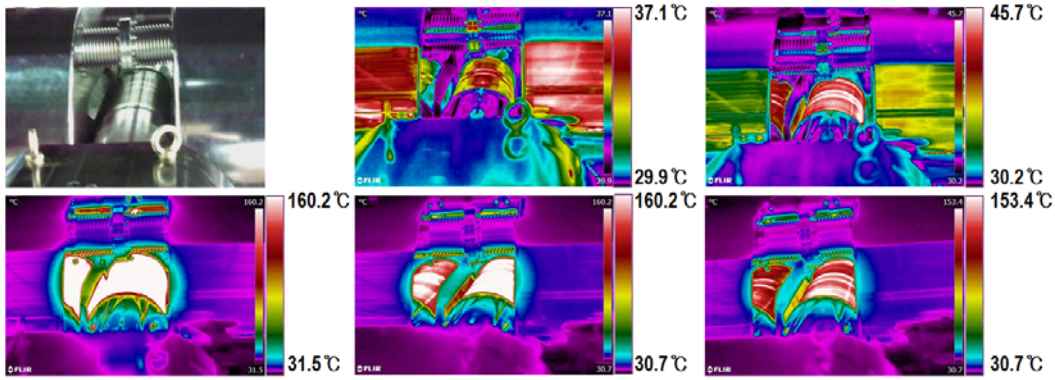

Fig. 5.20 Photos taken by a thermo-graphic camera in aluminum heating phase at a specific time

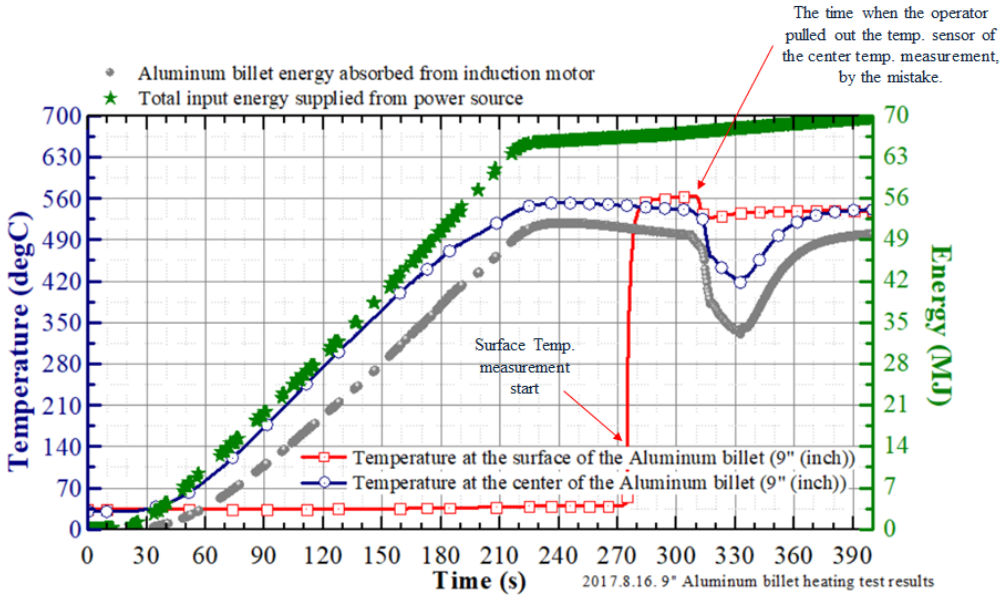

Fig. 5.21 A calculated aluminum billet energy curve absorbed from the induction motor of a SIH in the real-time

The aluminium billet was heated up to 558 Celsius degree of the average temperature between surface and center temperature. The maximum temperature at the surface of the billet was measured to 564 Celsius degree after the billet was completely stopped. The maximum temperature at the center hole of the billet was measured to be 552 Celsius degree through the real time measurement, as shown in the Fig. 5.21. Heating energy in the aluminium

billet was calculated to be 54,240 kJ by considering the average temperature, heat capacity and weight.

The total input electrical energy including all components such as electrical devices, measurement units, invertor, cryogenic and hydraulic system etc. was measured to be 16.8 kWh for heating time. Namely, the total input energy was estimated to be 60,480 kJ. The total efficiency of the heater was calculated to 89.7 %. This result was very successful.

5.3 Heating test of the performance evaluation 2; STS billet

The heating process of the STS billet was started at 954 s as shown in Fig. 5.22 and the rotating process was terminated at 1,260 s. Total heating time was calculated to 306 s and the maximum STS billet temperature of the center hole reached to 410 Celsius degree, and the surface temperature of the billet was measured to 430 Celsius degree as the highest value. A STS billet has low thermal conductivity of about 20 W/m and the temperature deviation at the surface and center of the STS billet is almost 200 Celsius degree when the heating process was terminated. Eventually, the two temperatures of the billet had same temperature after about 200 seconds passed

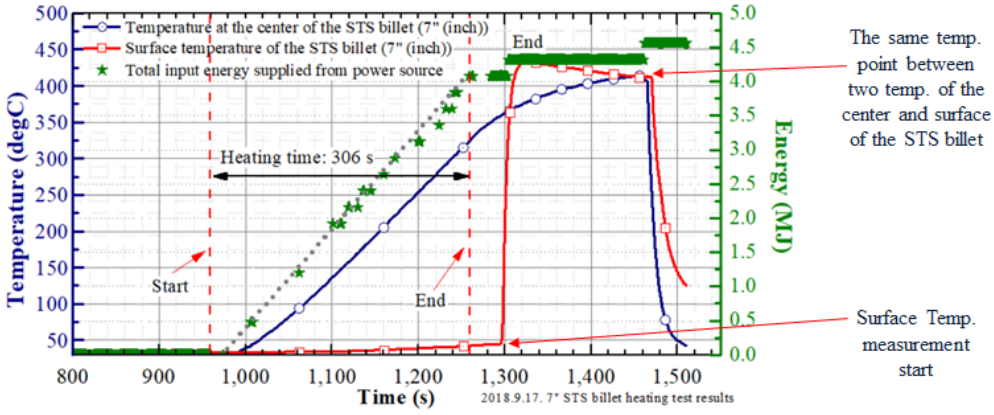

Fig. 5.22 Heating test results of 7 inch stainless steel billet

(a) (b)

Fig. 5.23. (a) A picture of the STS billet on the specific position to be heated; (b) after finishing the heating process of the STS billet

5.4 Heating quality analysis and evaluations

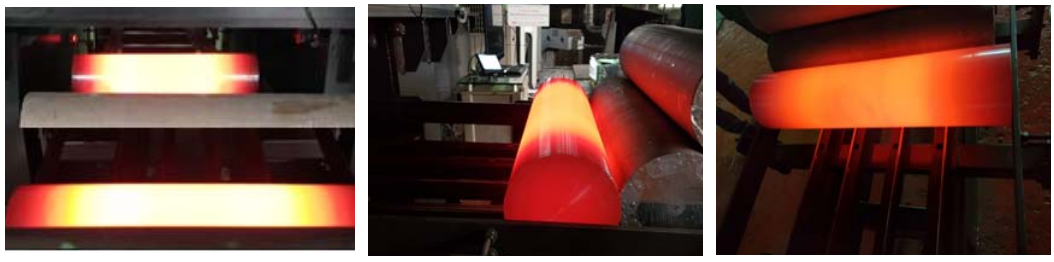

(a) (b) (c)

Fig. 5.24. A STS billet after finishing the heating process of the SIH

The SIH has a heating characteristic depended on the magnetic field along the longitudinal direction of the metal billet. Actually, the STS and iron billet was tested to heat by the SIH as shown in Fig. 5.24. However, the heating quality along the longitudinal direction of the STS billet was not uniform. To extrude the STS billet, the temperature uniformity of the longitudinal direction is very important. The first version SIH has the straight shape in the front of the iron cores as shown in Fig. 5.25. The magnetic field along the longitudinal direction of the billet is not uniform. The magnetic field is high at the center of the billet, but the magnetic field at the edge of the billet is lower than that at the center of the billet as indicated in Fig. 5.26.

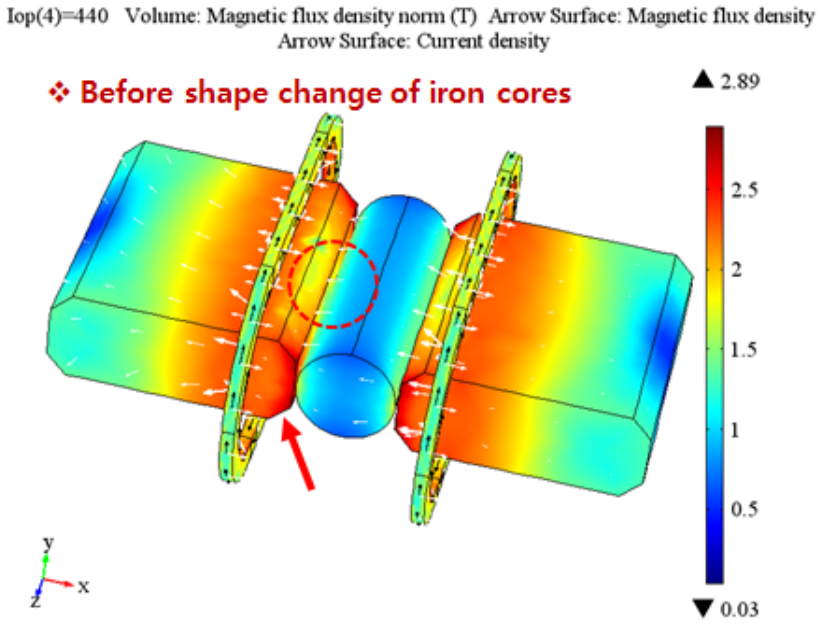

Fig. 5.25. A magnetic flux density distribution of the FEM simulation results before the front shape change of iron cores

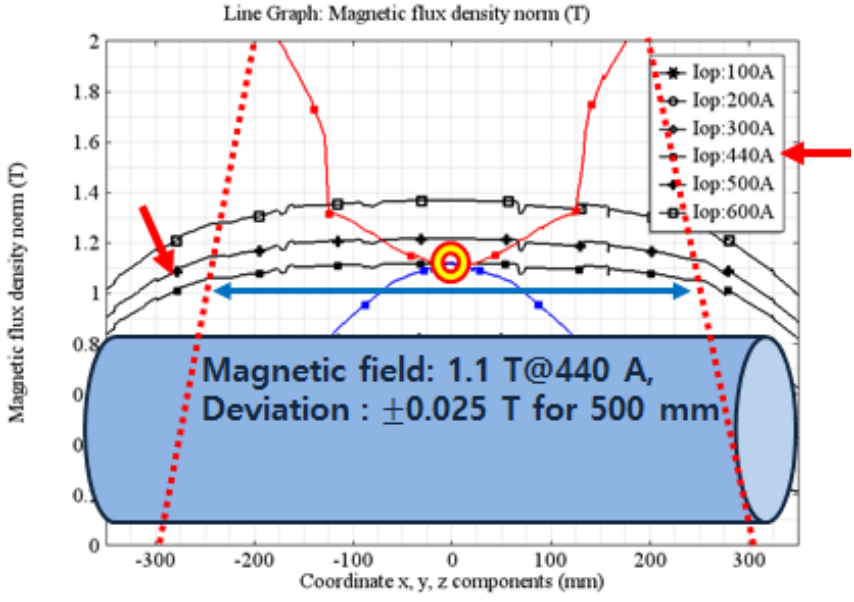

Fig. 5.26 Magnetic flux density curves along the longitudinal direction of the metal billet according to the excitation current increment in the FEM simulation before the front shape change of iron cores

The front shape of the iron yokes were reprocessed to get uniform the magnetic field along the longitudinal direction of the billet. The angle of the iron yoke was changed through the FEM simulation model as shown in Fig. 5.27. After the shape change of the iron yoke, the magnetic field along the longitudinal direction of the metal billet was changed as shown in Fig. 5.28.

In the 600 mm of the length of the billet, the magnetic field deviation is below ± 2.5%. The value is 0.025 T. The target magnetic field is 1.0 T.

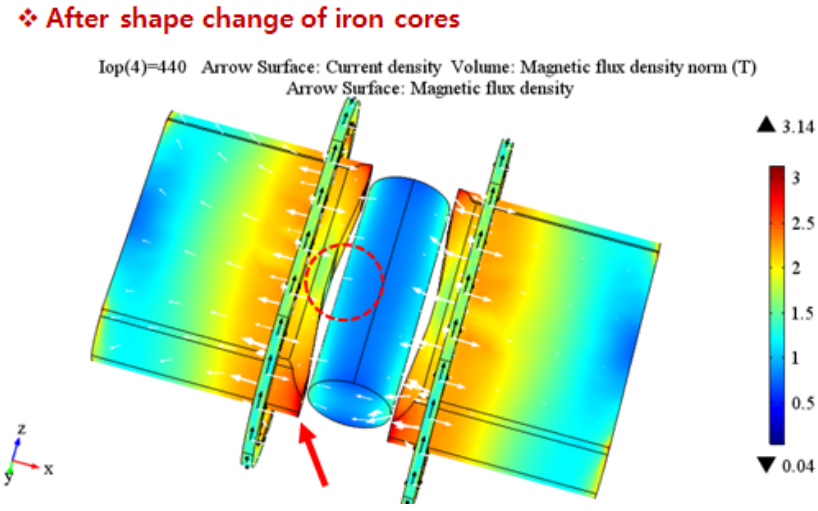

Fig. 5.27 A magnetic flux density distribution of the FEM simulation results after the front shape change of iron cores

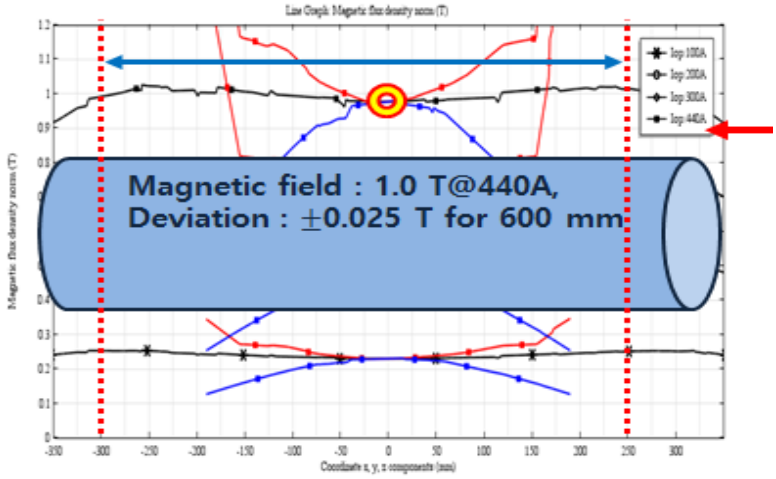

Fig. 5.28 Magnetic flux density curves along the longitudinal direction of the metal billet according to the excitation current increment in the FEM simulation after the front shape change of iron cores

After the shape change of the iron yokes, the magnetic flux density were measured by a hall sensor along the longitudinal direction of the metal billet according to the excitation current increment as shown in Fig. 5.24. As the excitation current increases, the magnetic field deviation is higher.

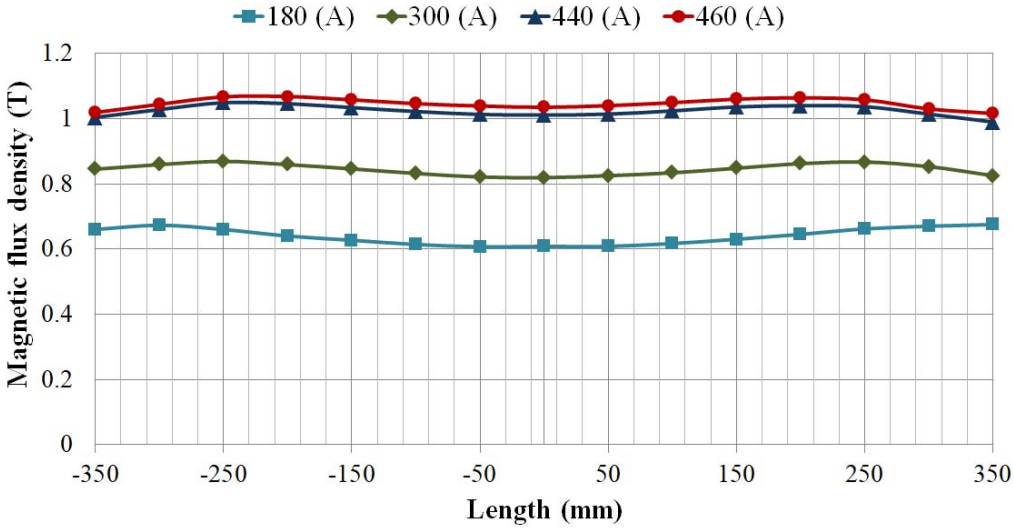

Fig. 5.29 Magnetic flux density measured by a hall sensor along the longitudinal direction of the metal billet according to the excitation current increment after the shape change of the iron yokes

After the front shape change of the iron cores, the excitation test of the HTS magnets was tested again as shown in Fig. 5.30 and 5.31. The magnetic flux density and temperature characteristics were analyzed. The input current reached at 450 A and the magnetic flux density at the center of the two iron cores was measured 1.05 T. The value decreased compared to the magnetic flux density before the front shape change. As shown in Fig. 5.32, the temperatures of the 1st and 2nd stage were presented and is stable after the magnets were excited.

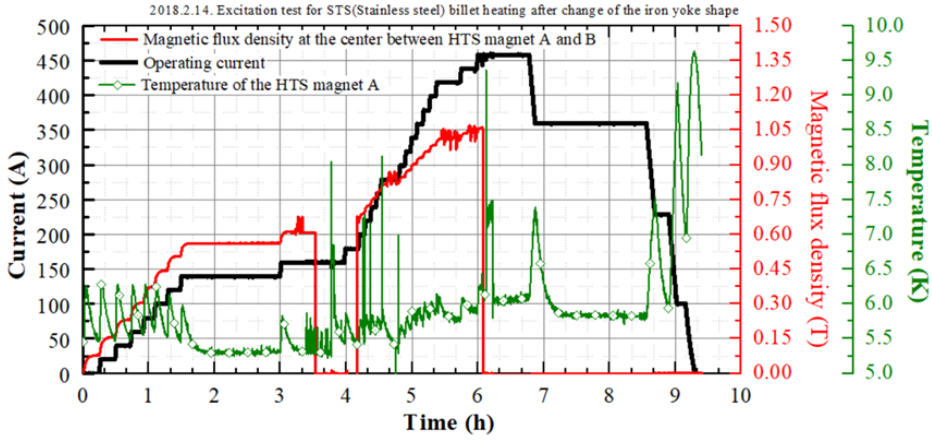

Fig. 5.30 Magnetic flux density curve at the center between two HTS magnets and input current curve of two HTS magnets and the 2nd stage temperature curve according to the time after the front shape change of iron cores

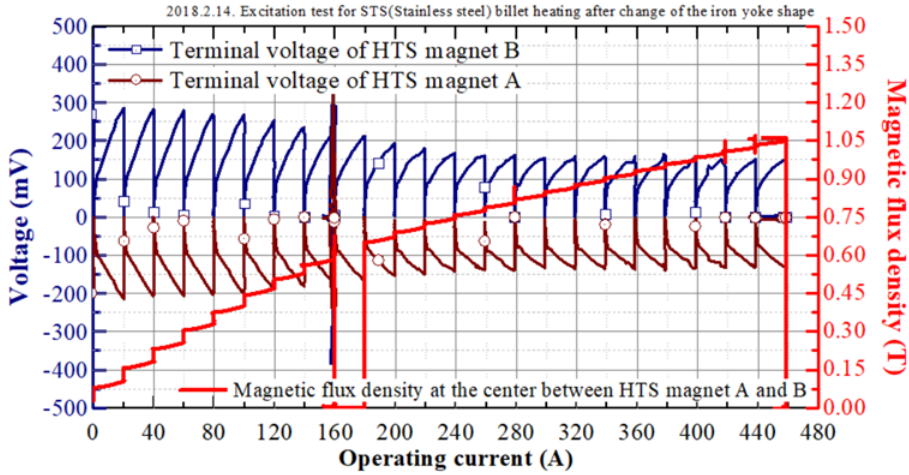

Fig. 5.31 Magnetic flux density curve at the center between two HTS magnets and terminal voltage curves of two HTS magnets according to the time after the front shape change of iron cores

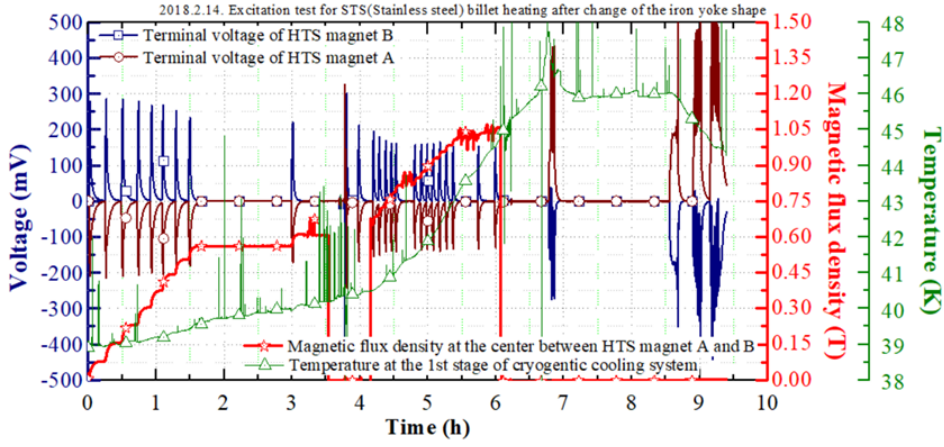

Fig. 5.32 Magnetic flux density curve at the center between two HTS magnets and terminal voltage curves of two HTS magnets and the 1st stage temperature curve according to the time after the front shape change of iron cores

The SIH was tested to heat the STS billet. The results of two heating tests were compared each other. In the case of the straight shape in front of the iron yoke, the temperature at the center of the STS billet was higher than that at the edge of the STS billet as shown in Fig. 5.33. The other hands, the temperature at the center of the STS billet was lower than that at the edge of

the STS billet after the shape change of the iron yokes as shown in Fig. 5.34. The temperature profile of the billet is dependent to the magnet field profile at the center of the billet. Through this heating quality improvement test, the temperature distribution of the metal billet could be controlled by the magnetic field at the center of the metal billet.

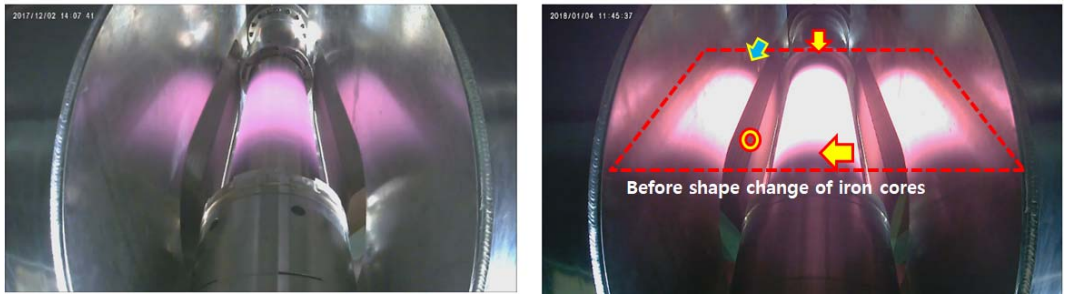

Fig. 5.33 Heating test results of a carbon steel and STS billet before the front shape change of iron cores

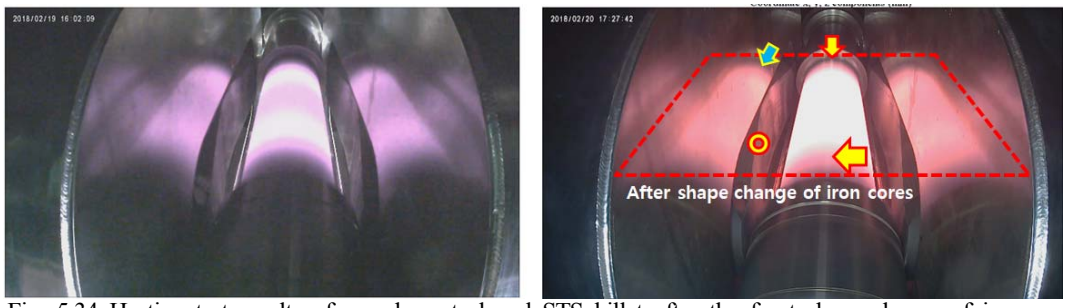

Fig. 5.34 Heating test results of a carbon steel and STS billet after the front shape change of iron cores

CHAPTER 6

CONCLUSIONS AND CONTRIBUTIONS

In the case of the SIH, most energy transfers to the metal billet with high efficiency. There were many countries to develop the superconducting induction heater. There are two countries such as Germany and China as shown in Fig. 6.1.

The SIH, the magnetic billet heater, which Bultmann developed with Zenergy in Germany, was introduced in 2008. The metal billet type is aluminum. The billet size is the length of 1000 mm and the diameter of 200 mm. The superconducting magnet was manufactured by a BSCCO wire. The Shanghai Superconductor developed the SIH in 2017 and they used 2G HTS wire for the superconducting magnet. The capacity of the SIH is 1 MW-class and the target metal billet was aluminum.

In Korea, Supercoil Co., Ltd. had developed and commercialized the SIH. The company got transferred the patent and know how related to the SIH and HTS magnets from TECHSTEEL Co., Ltd. and Changwon National University. The heating capacity is 300 kW class and 2G HTS wire was used for the superconducting magnet. And the target metal billet was aluminum and STS.

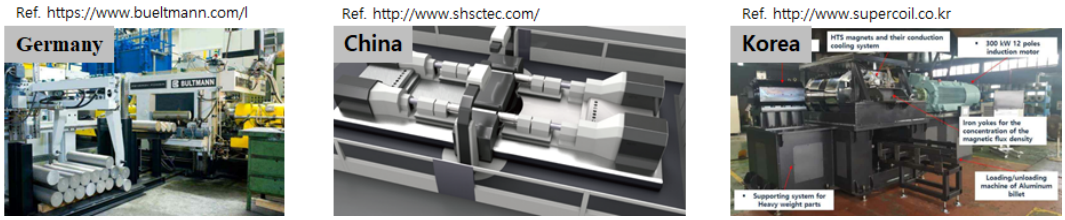

Fig. 6.1 There are three types of the Superconducting induction heaters in the world

Table 6.1 Comparison charts of the developed Superconducting induction heaters in the world [40-43]

Item	Germany	China	Korea
Subject	Bultmann (Zenergy-Bultmann)	Shanghai Superconductor (Shanghai Jiao Tong University)	Supercoil (Changwon Natonal Unviersity, Techsteel)
Year	2008	2017	2017
Heating Power	260 kW, 1MW class	1 MW class	300 kW class
Superconductor	BSCCO(1G)	REBCO (2G)	**REBCO (2G)**
Efficiency	Over 80%	Over 95%	~90%
Operating current	125A@25 K	260A@30 K	**480A@5.9 K**
Billet types	Aluminum, Copper billets	Aluminum billets	**Stainless steel and aluminium billets**
Billet size	D200mm x L1000mm	D200~450mm x L800~1500mm	D180mm x L700mm (STS) D230mm x L700mm (Al)

Item	HTS-High temp. supercon.)			LTS-Low temp. supercon.	Copper
	Ceramic		Metalic		
	Coated conductor	BSCCO	MgB_2		
Period	1987	1988	2001	1957	-
Material	Y,Ba,Cu,O	Bi,Sr,Ca,O	Mg,B	NbTi Nb_3Sn	Cu
Temperature	~ 77 K (-196℃)	~ 77 K (-196℃)	~ 25 K (-253℃)	~ 4 K (-269℃)	-
Stability	GOOD	GOOD	NOT Bad	Bad	-
Operating range	~ 20 T ~	~ 20 T ~	~ 5 T	~ 20 T	~ 0.5 T
Lamination	Copper, brass, STS	Siver	Copper	Copper	-
Manufacturing method	Coating 박막선재	PIT (extruding)	PIT (extruding)	PIT (extruding)	(extruding)
Maker	SuNam (한국) AMSC (미국) SuperPower (일본) 등 다수	Fujikura (일본) Sumitomo (일본) Bruker (유럽)	Columbus (유럽) KAT, 삼동 (한국) Hitachi, Hypertec (일본)	KAT (한국) Jastec(일본) WST (중국) BEAS(유럽) OST(미국) 등 다수	-
Cost	60~120$/m	120 $/m	5~10$/m	1~20$/m	~ 1$/m

Fig. 6.2 There are many kinds of superconducting wires to apply superconducting induction heater in the world

The SIH is using superconducting magnets to generate the magnet field. Actually, there are many kinds of superconducting wires in the world. The low temperature superconductor (LTS) was developed in 1957 and the materials are NbTi and Nb_3Sn through a powder in tube (PIT) extruding method. There are many companies to produce the wire in the world. The HTS wire is made by a ceramic materials like Yttrium and Barium through the coating method.

A MgB_2 superconducting wire was developed in 2001 and the manufacturing cost minimized by the PIT manufacturing method. Nowadays, the various application machineries are researching and developing by using these superconducting wires including the SIH.

In this dissertation, the excitation test of the HTS magnet and performance test of the SIH were performed and the results were analyzed. The components on the 300 kW SIH were described in detail. The operation characteristics including terminal voltages, magnetic flux density of the magnets and temperatures of the cryogenic cooling system were analyzed. The heating operation for the aluminum billet was tested for 180 seconds to reach the 564 Celsius degree of the billet temperature. The pictures taken by thermo-graphic camera were proved the heating performance. The machine energy efficiency was evaluated to be almost 90 % through accumulated electrical energy and the final average temperatures of the aluminum billet.

The commercial SIH was manufactured by Supercoil Co. Ltd. in the end of 2017. The excitation test of the High-Tc based magnets with iron cores was performed and the results were analyzed. The detailed specification on the 300 kW SIH were explained. The operational characteristics including terminal voltages, magnetic flux density of the magnets and temperatures of the cryogenic cooling system were analyzed and proved before and after the quench. The heating operational results for the various metal billets were simulated and the results were presented. The STS billet heating profile was presented and verified with real time measurement data.

These test process will be helpful for heating characteristics analysis of the various metals such as stainless steel, copper and titanium alloys for

commercialization of the SIH system. The metal industries can get the reference information of the SIH.

REFERENCES

[1] M. G. Lozinskii, Industrial Applications of Induction Heating, 1st ed. New York, NY, USA: Pergamon, 1969.

[2] Moreland, W. C. "The induction range: Its performance and its development problems." IEEE Transactions on Industry Applications 1.IA-9 (1973): 81-85.

[3] Stauffer, Paul R., Thomas C. Cetas, and Roger C. Jones. "Magnetic induction heating of ferromagnetic implants for inducing localized hyperthermia in deep-seated tumors." IEEE Transactions on Biomedical Engineering 2 (1984): 235-251.

[4] "Heat treating," ASM Metals HandBook, vol. 4, Novelty, OH, USA: ASM International 1991.

[5] V. Rudnev, D. Loveless, R. Cook, and M. Black, Handbook of Induction Heating. New York, NY, USA: Marcel Dekker, 2003

[6] Davies, E. J., and P. G. Simpson. "Induction heating for industry." Electronics and Power 25.7 (1979): 508-515.

[7] S.Zinn, S. L. Seminatin, ASM International, Elements of Indction heating Design, Control, and Aplications: Ana Nikolic, 2011.

[8] Richard E. Haimbaugh, ASM International, Practical induction heat treating: ASM International Technical Books Committee, 2001.

[9] Stanistaw Grundas, INTECH, Advances in induction and microwave heating of mineral and organic materials: Ana Nikolic, 2011.

[10] M. Runde and N. Magnusson, "Design, building and testing of a 10 kW Superconducting induction heater," IEEE Trans. Appl. Supercond., vol. 13, no. 2, pp. 1612 – 1615, Jun. 2003.

[11] N. Magnusson, R. Bersås, and M. Runde, "Induction heating of aluminum billets using HTS DC coils," in Proc. Inst. Phys., Conf. Ser., Sep. 2004, vol. 181, pp. 1104 – 1109

[12] M. Fabbri and A. Morandi, "DC induction heating of aluminum billets using superconducting magnets," COMPEL – Int. J. Comput. Math. Electr. Electron. Eng., vol. 27, no. 2, pp. 480 – 490, 2008.

[13] A. Morandi, M. Fabbri, and P. L. Ribani, "Design of a superconducting

saddle magnet for DC induction heating of aluminum billets," IEEE Trans. Appl. Supercond., vol. 18, no. 2, pp. 816 – 819, Jun. 2008.

[14] M. Runde, N. Magnusson, C. Fulbier, and C. Buhrer, "Commercial induction heaters with high-temperature superconductor coils," IEEE Trans. Appl. Supercond., vol. 21, no. 3, pp. 1379 – 1383, Jun. 2011

[15] A. Stenvall, N. Magnusson, "Electromagnetic viewpoints on a 200 kW MgB2 induction heater,"Elsevier, Physica C 468 (2008) 487 – 491.

[16] Thierry Lubin, Denis Netter, "Induction Heating of Aluminum Billets Subjected to a Strong Rotating Magnetic Field Produced by Superconducting Windings," IEEE TRANSACTIONS ON MAGNETICS, VOL. 45, NO. 5, MAY 2009. p2118-2127.

[17] M. Fabbri, M. Forzan, S. Lupi, "Experimental and Numerical Analysis of DC Induction Heating of Aluminum Billets," IEEE Trans. Vol.45, no.1, 2009, pp192-200.

[18] N. Magnusson, R. Bersås, and M. Runde, "Induction heating of aluminium billets using HTS dc coils," in Inst. Physics Conf. Series, Sep. 2004, no. 181, pp. 1104 – 1109.

[19] Magnusson, N.: Efficiency analysis of a high-temperature Superconducting induction heater. IEEE Trans. App. Super. 13(2), 1616 – 1619 (2003)

[20] Magnusson, N.: A 200kW MgB2 induction heater project. Inst. Phys. J. Physics Conf. Series 43, 1019 – 1022 (2006)

[21] Runde, Magne, et al. "MgB2 coils for a DC Superconducting induction heater." Journal of Physics: Conference Series. Vol. 97. No. 1. IOP Publishing, 2008.

[22] Sætre, F., et al. "Winding, cooling and initial testing of a 10 H superconducting MgB2 coil for an induction heater." Superconductor Science and Technology 24.3 (2010): 035010.

[23] Dughiero, F., et al. "A new high efficiency technology for the induction heating of non magnetic billets." COMPEL-The international journal for computation and mathematics in electrical and electronic engineering 30.5 (2011): 1528-1538..

[24] Semiconductor, Fairchild. "Induction Heating System Topology Review." (2000).

[25] Zlobina, M., B. Nacke, and A. Nikanorov. "Adaptive induction system for heating of aluminium billet by rotation in DC magnetic field." International Scientific Colloquium Modelling for Electromagnetic Processing. 2008..

[26] Karban, Pavel, Ivo Dolezel, and Pavel Šolín. "Computation of general nonstationary 2D eddy currents in linear moving arrangements using integrodifferential approach." COMPEL-The international journal for computation and mathematics in electrical and electronic engineering 25.3 (2006): 635-641..

[27] Araneo, R., et al. "Electromagnetic and thermal analysis of the induction heating of aluminum billets rotating in DC magnetic field." COMPEL-The international journal for computation and mathematics in electrical and electronic engineering 27.2 (2008): 467-479..

[28] Fabbri, Massimo, Antonio Morandi, and Francesco Negrini. "Temperature distribution in aluminum billets heated by rotation in static magnetic field produced by superconducting magnets." COMPEL-The international journal for computation and mathematics in electrical and electronic engineering 24.1 (2005): 281-290..

[29] Bensaidane, Hakim, et al. "Induction heating of aluminum billets with linear motion in a strong DC magnetic field: magnetothermal analysis in two-dimensional." IEEE Transactions on Applied Superconductivity 21.4 (2011): 3479-3487..

[30] Lubin, Thierry, et al. "Induction heating of aluminum billets subjected to a strong rotating magnetic field produced by superconducting windings." IEEE Transactions on Magnetics 45.5 (2009): 2118-2127.

[31] Wheaton, William C. "A comparative static analysis of urban spatial structure." Journal of Economic Theory 9.2, pp.223-237, 1974.

[32] Phlips, Louis, “Applied Consumption Analysis: Advanced Textbooks in Economics,” Vol. 5. Elsevier, 2014.

[33] Aoki, Masanao, “ed. Dynamic analysis of open economies,” Elsevier, 2014.

[34] Kamien, Morton I., and Nancy Lou Schwartz, “Dynamic optimization: the calculus of variations and optimal control in economics and management,” Courier Corporation, 2012.

[35] Ayyub, Bilal M, “Risk analysis in engineering and economics,” CRC Press, 2014.

[36] Short, Walter, Daniel J. Packey, and Thomas Holt, “A manual for the economic evaluation of energy efficiency and renewable energy technologies,” University Press of the Pacific, 2005.

[37] Mourmouris, J. C., and C. Potolias, “A multi-criteria methodology for energy planning and developing renewable energy sources at a regional level: A case study Thassos, Greece,” Energy Policy 52, pp.522-530, 2013.

[38] Hauk, Sebastian, Thomas Knoke, and Stefan Wittkopf, “Economic evaluation of short rotation coppice systems for energy from biomass－a review,” Renewable and Sustainable Energy Reviews 29, pp.435-448, 2014.

[39] El-Emam, Rami Salah, Hasan Ozcan, and Ibrahim Dincer, “Comparative cost evaluation of nuclear hydrogen production methods with the Hydrogen Economy Evaluation Program (HEEP),” International Journal of Hydrogen Energy, 2015

[40] M. Runde, N. Magnusson, C. Fulbier, and C. Buhrer, "Commercial Induction Heaters With High-Temperature Superconductor Coils," (in English), Ieee Transactions on Applied Superconductivity, vol. 21, no. 3, pp. 1379-1383, Jun 2011.

[41] Y. Wang et al., "Analysis and Comparison Between No-Insulation and Metallic Insulation REBCO Magnet for the Engineering Design of a 1-MW DC Induction Heater," IEEE Transactions on Applied Superconductivity, vol. 27, no. 4, pp. 1-5, 2017.

[42] P. Yang et al., "Design and Fabrication of a 1-MW High-Temperature Superconductor DC Induction Heater," IEEE Transactions on Applied Superconductivity, vol. 28, no. 4, pp. 1-5, 2018.

[43] Z. Y. Li et al., "Design and Test Performance of 2G Pancake Coils for HTS DC Induction Heater Prototype," (in English), Ieee Transactions on Applied Superconductivity, Article vol. 25, no. 3, p. 5, Jun 2015, Art. no. 4601205.

[44] Choi, Jongho, et al. "Practical design and operating characteristic analysis of a 10kW HTS DC induction heating machine." Physica C: Superconductivity 504 (2014): 120-126.

[45] Choi, Jongho, et al. "Fabrication and testing of a prototype 10-kW class HTS DC induction heating machine." Journal of Superconductivity and Novel Magnetism 28.2 (2015): 657-661.

[46] Choi, Jongho, et al. "Design and Performance Analysis of an Iron Core-based No-Insulation HTS Magnet for HTS DC Induction Heating Machine." Physics Procedia 81 (2016): 149-153.

[47] Choi, J., et al. "Characteristic Analysis of a Sample HTS Magnet for Design of a 300 kW HTS DC Induction Furnace." IEEE Transactions on Applied Superconductivity 26.3 (2016): 1-5.

[48] Kurose, Hiroaki, et al. "3-D eddy current analysis of induction heating apparatus considering heat emission, heat conduction, and temperature dependence of magnetic characteristics." IEEE Transactions on magnetics 45.3 (2009): 1847-1850.

[49] Fireteanu, Virgilin, et al. "Finite Element Analysis of Aluminum Billet Heating by Rotation in DC Magnetic Fields." Przegląd Elektrotechniczny 84 (2008): 115-119.

[50] Stiglitz, Martin. "Field and Wave Electromagnetics." Microwave Journal 34.9 (1991): 206-207.

[51] Jin, Jian-Ming. The finite element method in electromagnetics. John Wiley & Sons, 2014.

[52] Ida, Nathan. Engineering electromagnetics. Vol. 2. New York etc: Springer, 2000.

[53] Kovetz, Attay. The principles of electromagnetic theory. CUP Archive, 1990.

[54] Van Bladel, Jean G. Electromagnetic fields. Vol. 19. John Wiley & Sons, 2007..

[55] Zienkiewicz, O. C., C. Emson, and P. Bettess. "A novel boundary infinite element." International Journal for Numerical Methods in Engineering 19.3 (1983): 393-404.

[56] Magnusson, N., and M. Runde. "A 200 kW MgB2 induction heater project." Journal of Physics: Conference Series. Vol. 43. No. 1. IOP Publishing, 2006.

[57] F.P. Incropera, D.P. DeWitt, T.L. Bergman and A.S. Lavine, Fundamentals of Heat and Mass Transfer, John Wiley & Sons, 6th ed., 2006.

[58] R. Codina, “Comparison of Some Finite Element Methods for Solving the Diffusion-Convection-Reaction Equation,” Comp. Meth.Appl. Mech. Engrg, vol.156, pp. 185 – 210, 1998.

[59] A. Bejan, Heat Transfer, John Wiley & Sons, 1993.

[60] G.K. Batchelor, An Introduction to Fluid Dynamics, Cambridge University Press, 2000.

[61] R.L. Panton, Incompressible Flow, 2nd ed., John Wiley & Sons, 1996.

[62] M. Kaviany, Principles of Convective Heat Transfer, 2nd ed., Springer, 2001.

[63] T. Poinsot and D. Veynante, Theoretical and Numerical Combustion, 2nd ed., Edwards, 2005.

[64] R.B. Bird, W.E. Stewart and E.N. Lightfoot, Transport Phenomena, 2nd ed., John Wiley & Sons, 2007.

[65] W. Wagner, and H-J Kretzschmar, International Steam Tables, 2nd ed., Springer, 2008.

[66] J. Zhang, A. Gupta, and J. Bakera, “Effect of Relative Humidity on the Prediction of Natural Convection Heat Transfer Coefficients,” Heat Transfer Engineering, vol.28, no. 4, pp. 335 - 342, 2007.

[67] P.T. Tsilingiris, “Thermophysical and Transport Properties of Humid Air at Temperature Range Between 0 and 100 °C,” Energy Conversion and Management, vol. 29, no. 2008, pp. 1098 - 1110, 2007.

[68] A. Bejan et al., Heat Transfer Handbook, John Wiley & Sons, 2003.

[69] F. Charron, Partage de la chaleur entre deux corps frottants, Publication Scientifique et Technique du Ministère de l'Air, no. 182, 1943.

[70] Tomchev, Peter Ivanov, Nikolay Hristov Nenov, and Rayna Georgieva Ivanova. "Installation For Induction Heating For Testing Thermo Sensors." Environment. Technology. Resources. Proceedings of the International Scientific and Practical Conference. Vol. 2. 2015.

[71] Ma, Hongting, et al. "Investigation on the mechanism of convective mass transfer from a horizontal rotating cylinder without air jet flow." Heat and Mass Transfer 48.10 (2012): 1687-1695.

[72] Bergman, Theodore L., et al. Fundamentals of heat and mass transfer. John Wiley & Sons, 2011.

[73] Monteith, John, and Mike Unsworth. Principles of environmental physics. Academic Press, 2007.

[74] Howell, John R., M. Pinar Menguc, and Robert Siegel. Thermal radiation heat transfer. CRC press, 2010.

[75]ZIENKIEWICZ, Olek C.; TAYLOR, Robert L. The finite element method for

solid and structural mechanics. Elsevier, 2005.

[76] NAYFEH, Ali H.; PAI, P. Frank. Linear and nonlinear structural mechanics. John Wiley & Sons, 2008.

[77] Hahn, Seungyong, et al. "HTS pancake coils without turn-to-turn insulation." IEEE transactions on applied superconductivity 21.3 (2011): 1592-1595.

[78] Wang, Xudong, et al. "Turn-to-turn contact characteristics for an equivalent circuit model of no-insulation ReBCO pancake coil." Superconductor Science and Technology 26.3 (2013): 035012.

[79] Hahn, Seungyong, et al. "No-insulation multi-width winding technique for high temperature superconducting magnet." Applied physics letters 103.17 (2013): 173511.

[80] Hahn, Seungyong, et al. "No-insulation coil under time-varying condition: magnetic coupling with external coil." IEEE Transactions on Applied Superconductivity 23.3 (2013): 4601705-4601705.

[81] Han, Peng, et al. "Structural Design and Analysis of a 150 kJ HTS SMES Cryogenic System." Physics Procedia 67 (2015): 360-366.

[82] Yeom, Han-Kil. "Test of the Conduction Cooling System for HTS SMES." Progress in Superconductivity and Cryogenics 10.1 (2008): 62-66.

[83] Kim, Seokho, et al. "Thermal characteristics of conduction cooled 600kJ HTS SMES system." Cryogenics 49.6 (2009): 294-298.

[84] Kim, Kwang-Min, et al. "Design and Mechanical Stress Analysis of a Toroidal-Type SMES Magnet." IEEE Transactions on Applied Superconductivity 20.3 (2010): 1900-1903.

[85] Yeom, H. K., et al. "Study of cryogenic conduction cooling systems for an HTS SMES." IEEE Transactions on Applied Superconductivity 17.2 (2007): 1955-1958.

APPENDIX A

The excitation ceremony of the HTS magnets for 300kW HTS DC Induction Furnace was successfully held at TECHSTEEL on the 9th of August in 2016.

Fig. A.1. Picture taken in the excitation ceremony on the 9th of August in 2016

SUPERCOIL®

Fig. A.2. Picture taken in a SIH operating ceremony on the 28th of September in 2017

Fig. A.3. Picture taken in a SIH operating ceremony on the 28th of September in 2017

Fig. A.4. Picture taken in a SIH operating ceremony on the 28th of September in 2017

PATENT LISTS

[1] J. Choi, S.H. Cho, M. Park, "Spindle and gripping apparatus for high torque and low speed and superconducting DC induction heating apparatus using the same", registration no. 10-1888057, 2018.08.07.

[2] J. Choi, S.H. Cho, M. Park, "Co-winding device, cowinding method based multi-differential layers, supercoinducting magnet manufactured by the same, and superconducting DC induction heating apparatus", registration no. 10-1883711, 2018.07.25.

[3] J. Choi, M. Park, I.K. Yu, "Superconducting DC induction heating apparatus using magnetic field displacement", registration no. 10-1877118, 2018.07.04.

[4] J. Choi, M. Park, I.K. Yu, "Single structure type superconducting dc induction heating apparatus", registration no. 10-1823763, 2018.01.24.

[5] J. Choi, M. Park, I.K. Yu, K.M. Kim, "Superconductor coil and Induction heating machine thereof", registration no. 10-1468312, 2014.11.26.

[6] J. Choi, M. Park, I.K. Yu, "Superconducting magnet apparatus using movement and Induction heating apparatus thereof", registration no. 10-1658727, 2016.09.12, PCT no. PCT/KR2015/012074, 2015.11.10.

[7] J. Choi, S.H. Cho, M. Park, "DC induction heating apparatus capable of rotating the superconducting magnet", registration no. 10-1922688, 2018.11.21.

PAPER LISTS

[1] Choi, Jongho, et al. "Commercial design and Operating Characteristic Analysis of HTS Magnets based a 300 kW Superconducting Induction Heater." IEEE Transactions on Applied Superconductivity it was submitted in ASC conference.

[2] Choi, Jongho, et al. "Recent development and research activities of induction heater with high-T C superconducting magnets for commercialization." SN Applied Sciences 1.1 (2019): 59.

[3] Choi, Jongho, et al. "Design and Operational Test of Large-sized HTS Magnets with Conduction Cooling System for a 300 kW-class Superconducting Induction Heater." MRS Advances (2018): 1-12..

[4] Choi, Jongho, et al. "An Effective Cryostat Design of Conduction-Cooled HTS Magnets for a 300-kW-Class Superconducting Induction Heater." IEEE Transactions on Applied Superconductivity 28.3 (2018): 1-5.

감사의 글 (Acknowledgement)

이 논문을 완성하는데 까지 진심어린 조언과 함께 지도해주신 이와쿠마 교수님과 박민원 교수님, 두 분 교수님께 진심으로 감사드립니다.

I'm really appreciated with Prof. Iwakuma and Minwon Park for their kind comments and theoretical supports for this doctoral dissertation.

그리고, 지난 7년 동안 항상 곁에서 연구자의 길을 지지해주고, 믿어준 나의 사랑하는 아내, 이향냥에게 진심으로 고맙다는 말을 이 기회를 빌어 전하고자 합니다. 이 논문이 완성되기까지 큰 버팀목이 되어주었고, 사랑하는 우리의 두 아들, 태현이, 유준이에게도 엄마와 아빠가 함께 이룬 성과라고 기쁨 마음으로 전해주고자 합니다.

본 논문이 있기까지 도와주신 모든 분들을 일일이 찾아뵙고 감사인사를 드려야 마땅하나, 본 논문의 마지막 페이지를 빌어 이렇게 감사인사를 대신합니다. 감사합니다.